Functionalization and Application of Ion Track-Etched Nanochannels in Polymer Membranes

Vom Fachbereich Chemie
der Technischen Universität Darmstadt

zur Erlangung des akademischen Grades eines

Doctor rerum naturalium (Dr. rer. nat.)

genehmigte
Dissertation

eingereicht von

Mubarak Ali, M.Phil.
aus Narowal (Pakistan)

Referent:	**Prof. Dr. Wolfgang Ensinger**
Korreferent:	**Prof. Dr. Jörg J. Schneider**
Tag der Einreichung:	20. Juli 2009
Tag der mündlichen Prüfung:	26. Oktober 2009

Darmstadt (2009)
D17

Functionalization and Application of Ion Track-Etched Nanochannels in Polymer Membranes

Vom Fachbereich Chemie
der Technischen Universität Darmstadt

zur Erlangung des akademischen Grades eines

Doctor rerum naturalium (Dr. rer. nat.)

genehmigte
Dissertation

eingereicht von

Mubarak Ali, M.Phil.
aus Narowal (Pakistan)

Referent:	**Prof. Dr. Wolfgang Ensinger**
Korreferent:	**Prof. Dr. Jörg J. Schneider**
Tag der Einreichung:	20. Juli 2009
Tag der mündlichen Prüfung:	26. Oktober 2009

Darmstadt (2009)
D17

Dedicated to,

My loving parents,
&
My life! Saima & Zeeshan

Acknowledgement

I express my sincere gratitude to the followings;

- **Prof. Dr. Wolfgang Ensinger** for giving me place in his group and for his kind formal supervision. He was always available to discuss obstacles and progress associated with my research. I especially thank to him for his every effort to support me.
- **Prof. Dr. Reinhard Neumann** for providing me the opportunity to perform PhD research work at the GSI Material Research Department. Every work in this thesis was greatly influenced by his scientific curiosity, encouragement, and guidance.
- **Prof. Dr. Jörg J. Schneider** for accepting to be the second referee of this work.
- Dr. Birgitta Schiedt for initially introducing me in the field of nanochannels and for her always availability to discuss any problem related to research work.
- Dr. T. W. Cornelius, O. Picht, and M. Rauber for their support to use FESEM.
- V. Bayer and Q. H. Nguyen for their assistance in etching experiments.
- I also had the great pleasure to work with a number of enthusiastic collaborators at the MPIP, Mainz, and Universitat de València, Spain. Thanks to Dr. Basit Yameen and Dr. Omar Azzaroni for their fruitful discussions about the use of macromolecules. I am also thankful to Dr. Patricio Ramírez and Prof. Dr. Salvador Mafé for the theoretical simulations of our experimental results.
- Dr. S. Karim for the nice company during his stay at GSI, Darmstadt, Germany.
- Dr. M. Nawaz Tahir for the valuable discussions and suggestions.
- All members of materials research for a very pleasant and friendly working atmosphere.
- My first cusion **Nayyar Iqbal,** for every thing which he did for me. I have no words to say him thanks.
- My parents, brothers and sisters for their prayers and good wishes for my success.
- My parents-in-law for their constant well wishes for me.
- My nice and beloved wife, Saima Nasir! I am thankful to you for bearing “hours of mindlessness” during which i was thinking research problems while physically being at home. All the fun and happiness my cute prince **Zeeshan Ali** brings to me, credited to my wife.
- For all my friends and fellows who pray for my success.

- Last but not the least many thanks to Federal Ministry of Hessen for the financial support via Technische Universität Darmstadt and also to Higher Education Commission of Pakistan for providing the partial financial support during the last year of my research work.

ABSTRACT

Nanochannels fabricated in ion-tracked polymer membranes have a great range of applications in biotechnology, where they are suitable for sensing biomolecules, and act as stimuli-responsive devices and molecular filters of high selectivity. For all these applications, it is highly desirable to control the channel-surface properties, i.e. to functionalize the surface in order to match specific requirements concerning hydrophobicity, selectivity, and interaction with molecules passing through the channel. In ion-tracked polymer membranes, single conical nanochannels were fabricated by selective chemical etching of the damage trails caused by the ions along their trajectories, resulting in the generation of carboxylate groups on the channel surface. These groups were functionalized with molecules having variable polarity and chemical groups that act as binding sites for different analytes. As is well-known, the negatively or positively charged conical nanochannels selectively transport cations or anions, respectively. This rectifies ionic current flowing through the channel. The success of functionalization procedure was examined and proven by measuring the asymmetric current-voltage (*I-V*) curves and permselectivity of the channel. The functionalized single conical nanochannels were successfully used for the electrochemical interaction of bovine serum albumin. The work presented here also includes the fabrication and characterization, both experimentally and theoretically of a single amphoteric nanochannel, functionalized with lysine and histidine chains, whose positive and negative charges are very sensitive to external pH. This nanofluidic diode with amphoteric chains attached to the channel surface allows for a broad set of rectification properties supported by a single nanodevice. A new facile approach was also introduced to incorporate biosensing elements into nanochannels by using electrostatic self-assembly of bifunctional macromolecular ligands which were used for the biospecific recognition of protein analytes. This approach also enables the creation of supramolecular multilayered structures inside the nanochannels that are stabilized by strong ligand-receptor interactions. The integration of “smart” polymer brushes, constituted of zwitterionic monomers in polyimide conical nanochannels, to obtain a new highly functional signal-responsive chemical nanodevice, has been reported for the first time. This strategy enables a higher degree of control over rectification properties, when compared with charged monolayer assemblies. Moreover, nanochannels were also functionalized with poly-*N*-isopropylacrylamide and poly(4-vinyl pyridine) brushes to display temperature and pH controlled gating properties, respectively.

ZUSAMMENFASSUNG

Nanokanäle in Ionenspur-geätzten Polymermembranen haben ein breites Spektrum von Anwendungen in der Biotechnologie. Sie sind geeignet zur Detektion von Biomolekülen, wirken als gezielt ansprechbare Nanostrukturen und stellen hochselektive molekulare Filter dar. Für all diese Anwendungen ist es sehr wichtig, Kontrolle über die Eigenschaften der Kanalwände auszuüben, also deren Oberfläche so zu funktionalisieren, dass spezifische Anforderungen bezüglich der Hydrophobizität, Selektivität und Wechselwirkung mit durch den Kanal durchtretenden Molekülen erfüllt werden. Einzelne konische Nanokanäle wurden durch gezieltes chemisches Ätzen der geschädigten Bereiche entlang Ionenspuren in Polymermembranen erzeugt. Diese Behandlung resultierte in der Erzeugung von Carboxyl-Gruppen auf der Oberfläche der Kanalwände. Diese Gruppen wurden sowohl mit Molekülen mit variabler Polarität als auch mit chemischen Gruppen, die als Bindungsstellen für verschiedene Analyte dienen, funktionalisiert. Es ist wohlbekannt, dass durch negativ oder positiv geladene konische Nanokanäle entweder Kationen oder Anionen bevorzugt hindurchtreten können. Dadurch wird der Ionenstrom durch den Kanal gleichgerichtet. Das Gelingen des Verfahrens zur Funktionalisierung wurde durch die Messung der asymmetrischen Strom-Spannungs (I-V) Kurven und der Permselektivität der Kanäle geprüft und nachgewiesen. Die funktionalisierten konischen Einzelkanäle wurden erfolgreich für die elektrochemische Wechselwirkung mit bovinem Serumalbumin verwendet. Die hier präsentierte Arbeit beinhaltet auch die Herstellung und die, sowohl experimentelle als auch theoretische, Charakterisierung eines amphoteren einzelnen Nanokanals, der mit Lysin- und Histidin-Ketten funktionalisiert wurde und dessen Ladungszustand somit sehr empfindlich auf den äußeren pH-Wert reagiert. Diese nanofluide Diode, die durch die Anlagerung amphoterer Ketten auf der Oberfläche eines Nanokanals entsteht, vereint eine große Bandbreite an Gleichrichtungseigenschaften in einer einzelnen Nanostruktur. Des Weiteren wurde ein neuer, einfacher Ansatz zur Integration biosensorischer Elemente in Nanokanäle eingeführt, bei dem elektrostatische Selbstanordnung bifunktioneller makromolekularer Liganden auf den Kanalwänden ausgenutzt wurde. Diese Liganden wurden wiederum zur spezifischen Detektion von Protein-Analyten verwendet. Der hier gezeigte Ansatz ermöglicht auch die Herstellung supramolekularer, mehrlagiger Strukturen innerhalb der Nanokanäle, welche von starken Ligand-Rezeptor-Wechselwirkungen stabilisiert werden. Die

Integration „intelligenter“ Polymer-Bürsten, bestehend aus zwitterionischen Monomeren in konischen Polyimid-Nanokanälen, durch die eine neue, hochfunktionelle, gezielt über Signale ansprechbare chemische Nanostruktur entsteht, wurde zum ersten Mal berichtet. Verglichen mit anderen Anordnungen aus geladenen Monolagen ermöglicht die hier gezeigte Strategie einen höheren Grad an Kontrolle über die Gleichrichtungseigenschaften. Zusätzlich wurden Nanokanäle mit Poly-N-Iospropylacrylamid und Poly(4-Vinylpyridin) Bürsten funktionalisiert, um die Durchfluss-Eigenschaften auch thermisch oder über den pH-Wert kontrollieren zu können.

Die Übereinstimmung mit der englischen Zusammenfassung wird bestätigt.

19. Juli 2009 Darmstadt

Table of Content

Abbreviations

ATRP	Atom transfer radical polymerization
BSA	Bovine serum albumin
b-PAH	Biotinylated poly(allylamine) hydrochloride
$CuCl_2 \cdot 2H_2O$	Copper(II) chloride dihydrate
DMF	*N,N*-Dimethylforamide
EDA	Ethylenediamine
EDC	*N*-(3-dimethylaminopropyl)-*N′*-ethylcarbodiimide HCl
EDTA	Ethylenediaminetetraacetic acid
FESEM	Field emission scanning electron microscopy
pI	Isoelectric point
I-V	Current-voltage
KCl	Potassium chloride
LCST	Lower critical solubility temperature
NaOH	Sodium hydroxide
NaOCl	Sodium hypochlorite
NHS	*N*-Hydroxysuccinimide
PA	Propylamine
PAH	poly(allylamine hydrochloride)
PBS	Phosphate-buffered saline
PC	Polycarbonate
PET	Polyethylene terephthalate
PFP	Pentafluorophenol
PI	Polyimide
PNP model	Poisson-Nernst-Planck model
PNIPAM	Poly(*N*-isopropylacrylamide)
PVP	Polyvinyl pyridine
SA	Succinic anhydride
SAv	Fluorescein (FITC)-conjugated streptavidin

1. GENERAL INTRODUCTION

Nanochannels (frequently also known as nanopores) have at least one dimension in the range of one to some tens of nanometres. In all living cells, nanochannels which are formed by membrane proteins are present in the cellular membranes. The living cells communicate with each other by means of ion transport which is necessary for performing proper cellular and biological processes.[1,2] The protein ion channels can selectively transport ions[3] or particular analytes across the cell membranes, and they open (ions are allowed to pass) and close (ion transport is blocked) by a gated mechanism which occurs in response to external stimuli, e.g. the presence of ligand molecules, deformation in the cell membrane, and change in potential across the membrane. Therefore, these channels form the molecular basis of many processes, including the propagation of neural impulses,[4] muscle activity,[5] and protein translocation across cell membranes.[6,7] Presently, nanodevices have proven their ability to be compact and robust chemical sensors.

Protein ion channels (α-hemolysin), embedded within a lipid bilayer support either in their wild or chemically engineered form, have been used experimentally for the detection of DNA,[8-14] metal ions[15,16] and enantiomer of drug molecules,[17] proteins[18,19] and small organic molecules.[20,21] These ion channels offer precisely controlled structures and interfacial chemistry. However, in biological membranes, channels and their embedding lipid bilayer are susceptible to changes in external parameters such as pH, salt concentration, temperature, mechanical stress, etc. To overcome these difficulties, solid-state synthetic nanochannels emerged as "abiotic" analogues to protein pores / channels with the ability to mimic the function of biological ion channels and, consequently, act as extremely sensitive sensor. However, the sensing capabilities of these channels depend sensitively on the surface functionalities. The chemical groups present of channels surface and walls act as binding sites for different analytes as well as interact with molecules passing through the channels. In this context, different methods have been developed to manipulate the surface properties of these nanochannels for the detection and selective binding of specific analyte molecules.

1.1 Solid-State Nanochannel Fabrication

Solid-state nanochannels were fabricated in a variety of substrates, e.g. alumina, silicon, silicon oxide, silicon nitride, glass, and polymer membranes. A variety of different methods have been developed in recent years to fabricate such nanochannels. Currently, the most popular class of methods starts with first fabricating a relatively large channel (several tens of nanometers) in thin (a few tens of nanometers) SiO_2 or Si_3N_4 membranes using an ion-beam. Then the large channel was subsequently narrowed with a diffuse beam or the electron beam of a transmission electron microscope (TEM).[22,23] A similar shrinking effect was also found while fabricating a nanochannel in silicon membranes using a field-emission SEM,[24] and applying laser in thermoplastic membranes.[25] Another way to reduce the size of a relatively large channel drilled by focused ion beam, followed by subsequent material deposition, as done by Danelon *et al.*[26] using silicon dioxide membrane. Recently, focused ion[27] and electron beams[24] have also been used to directly create channels of a few nanometers in diameter in SiC and Si_3N_4 membranes, respectively. In the methods which induce shrinking of larger channels, the channel size development can be observed online by either collecting or counting the transmitted ions in the case of ion-beam sculpting, or obtaining a direct image of the channel in the TEM approach. Also the channels created directly by ion or electron beams can be monitored by TEM; in the case of the ion beam method, the position of the channel is marked by a cross, which is created by slightly thinning the material also with the ion beam. Pipette-based and nanochannel quartz electrodes[28,29] have also been fabricated having tip diameter down to 20 nm, used for sensing experiments. Solid-state nanochannels were also successfully fabricated in ion tracked polymer membranes via chemical etching. In this method, polymer foils were first irradiated with heavy ions. During irradiation, local damaged zones (latent tracks) were created which were chemically etched to obtain nanochannels. By using asymmetric track-etching technique, it is also possible to prepare single conical nanochannels in polymer membranes.[30-33] These nanochannels have been employed for the template synthesis of gold nanotubes, embedded with in polymer membranes which can be subsequently functionalized by thiol-terminated molecules for sensing applications.[34-38] The main potential advantage is probably the material they are made of, since polymers open the possibility to directly chemically modify the channel surface properties and thereby influence their interaction with different analytes.

1.2 Functionalized Nanochannels

By a suitable chemical modification, the surface chemistry (charge and hydrophilicity) and size of the nanochannel can be changed to enable more selective detection and separation of molecules. These surface modification approaches are inspired by nature, where biological nanochannels are formed in cell membranes by proteins. The lumen of these nanochannels is composed of different amino acids which assemble to create channels and also regulate the flow of certain chemical species, such as ions, into and out of cells.

The functionalization of biological nanochannels (α-hemolysin) with molecular recognition agents has made possible their use for detecting a variety of target species (e.g., ions, proteins, and organic compounds). Biological nanochannels were modified via mutagenesis, targeted chemical reactions, and formation of non-covalent supramolecular structures. Mutagenesis helps to introduce various amino acids with side chains varying in size, shape, polarity and reactivity into the lumen of the channel.[39,40] Through targeted modification,[41] short oligonucleotides were selectively attached with the single cysteine residue located in the interior of a protein channel.

Molecular recognition agents were also covalently attached to α-hemolysin through single polyethylene-glycol chains[19] for the sensing of protein analytes which was not possible with unmodified α-hemolysin nanochannels. Other than mutagenesis and covalent modification, it is also possible to modify the channel through non-covalent modification. This helps to introduce host molecules like cyclodextrin, non-covalently within the lumen of α-hemolysin channel.[20,42] The host molecules were capable of binding guests through the formation of host-guest type supramolecular aggregates.

Concerning the applications and chemical modification, the solid-state synthetic nanochannels offer greater flexibility in terms of shape, size, and surface properties and are also resistent to harsh experimental conditions. Therefore, physical and chemical properties can be tuned selectively by chemically modifying the nanochannel surface charge.

The solid-state nanochannels were modified by using a variety of strategies (covalent or non covalent) depending upon the substrate material. The molecules attached covalently show higher stability as compared to that adsorbed electrostatically on the charged nanochannel surface. Although, there has been advantage in strong physisorption of different species like ions[43] and polyelectrolytes.[44] The formations of self-assembled monolayers (SAMs) from the molecules

with proper functionality have also been used for the surface modification.[45,46] With silane chemistry, nanochannels in silica and glass or alumina membranes with a layer of metal oxide can also be functionalized by using a variety of silane derivatives.[47-51] Wang et al. described the chemical modification of glass nanochannel electrodes to import photochemical control and transport selectivity based on electrostatic forces at the channel orifice.[29] A control on nanochannel wetting by light was also achieved via modification of nanoporous alumina membranes with photochromic spiropyran and hydrophobic molecules.[49] Similarly, immobilization of DNA fragments has also been achieved on the surface of nanochannel in a variety of substrates.[52,53]

The tethering of biomolecules either directly or through bifunctional cross-linkers on gold (Au) coated nanoporous membranes was achieved by using thiol-chemistry. This results in the formation of S–Au bonds between molecules possessing SH or S–S groups. In track-etched polymer membranes, nanochannel walls were coated with a layer of Au by electroless plating and the surface properties of these Au-nanotubes were subsequently changed, e.g., by chemisorption of variety of thiols that vary in size, shape, and polarity.[34-38,54] Similarly, the surface charge of single conical Au nanotubes, embedded in polymer membranes, was changed by modification with thiols, terminated with carboxylate (anion) and ammonium (cation) groups, respectively. The inner walls of single conical nanotubes were also functionalized with molecular recognition agents for the detection of specific protein analytes.[38] The Au-plated conical nanotubes were also successfully used for the immobilization of thiol-terminated DNA fragments with variable chain length.[34,54]

The diameter and selectivity of nanochannels in polycarbonate membranes can be tuned by first adhering a thin coating of Sn^{2+} ions followed by the chemical adsorption of polymers with variable size and chemical composition inside the channel walls.[55] This creates polymer nanotubes inside the nanochannels which can separate chemical and biochemical molecules based on size, charge and relative hydrophobicity.

The carboxyl groups on the surface of track-etched polymer nanochannels can be directly modified using standard chemistry by a variety of methods, such as alkylation, methylation or amidation. For example, alkylation of these groups was carried out with alkyl bromide in the presence of KF as a catalyst,[56-58] methylation was accomplished by treating with diazomethane[59] and amidation was achieved by first activating the carboxyl groups with carbodiimide and subsequent reaction with amine.[60] Recently, single conical nanochannels in PET membranes were

modified by activating the carboxyl groups by using EDC or EDC / NHS coupling chemistry into amine-reactive esters.[61-64] The active esters were selectively coupled with ethylenediamine, and the resulting nanochannel behaves like a diode.[61,63] Similarly, single conical PET nanochannels modified with ethanolamine were successfully used for the detection of dsDNAs analytes via the resistive-pulse method.[62] Similarly, carboxyl groups on the surface of conical nanochannel were functionalized with DNA motor, the conformation of the immobilized DNA motor changes with the change of pH of the external environment.[64]

1.3 Aims and Motivation

The aims and motivation of the present work is to develop new strategies for the fabrication and chemical functionalization of abiotic (synthetic) nanochannels in polymer membranes. This in turn may provide a basis for the systematic development of new functionalized nanochannel surfaces for a variety of applications. In the present work, the surface modification of single conical nanochannels in polymer membranes can be achieved via covalent attachment of different small organic and macromolecules having variable polarity or electrostatical self-assembly of bifunctional macromolecular ligands, respectively. These functionalized channels are further studied for various applications like thermo-responsiveness, antifouling, bio-sensing, ion channelling, and nanofluidic diodes. The work presented here is divided into two parts, the first part dealing with the improvement of nanochannel fabrication techniques, and the second part dealing with nanochannel surface modification.

In the first part, fabrication of nanochannels by asymmetric as well as surfactant-controlled etching techniques have been employed, with the aim to influence the geometry of the channels via the choice of various etching parameters. The shape of the etched channels was determined using different techniques, namely, scanning electron microscopy of multi-channel membrane cross-sections or of metal deposited inside the channels, and conduction measurements of single channels were applied. Experiments with surfactant-controlled etching of PET foils led to surprisingly high rectification ratios (the ratio of positive to negative current at a given voltage). Furthermore, the etching procedure seems to be stabilized by the surfactant, so that the process becomes more reproducible than the asymmetrical etching with the etchant applied on one side of the membrane, which was so far performed at GSI. Hence, a new approach for surfactant-enhanced etching under asymmetrical conditions in a conductivity cell was found.

The second part of the work focuses on the chemical functionalization for tuning the surface chemistry of nanochannels. Polyimide and polyethylene terephthalate membranes containing track-etched single nanochannels are the two investigated substrates. The specific organic as well as polymeric macromolecules were tethered covalently or electrostatically onto the surface of nanochannels leading to a change of surface charge, artificial proton conducting channels, thermally nanoactuated macromolecular gates, biosensors by supramolecular bioconjugation and pH-tunable nanofluidic diodes.

1.4 Materials of Relevance

For a long time already, mimicking the processes of nature has been an inspiration for many researchers. In this context, the importance of biological channels in many physiological processes of a living organism has stimulated the interest in artificially fabricated functional nanochannels. Although biological channels have proved to be very useful for a range of interesting translocation experiments,[65] they do exhibit a number of disadvantages including the limited stability. Fabrication of nanochannels from solid-state materials (polymeric or ceramic membranes) presents advantages over their biological counterpart such as high stability, control of diameter, channel length and the potential for integration into devices and arrays. Various routes have been explored to meet the challenge of fabricating channels with true nanometer dimensions.[66,67] Synthetic solid-state nanochannels, fabricated in track-etched polymer membranes, being investigated in the present work, are introduced here.

The polymer membranes, polyethylene terephthalate (Hostaphan RN12, Hoechst) and Polyimide (Kapton 50HN, DuPont), both 12 μm in thickness are mainly used for the fabrication of solid-state track-etched nanochannels. In these membranes, the fabrication of nanochannels is based on the following: Firstly, a swift heavy ion passes through the membrane, deposits its energy along its trajectory, and thus creates a cylindrical damage zone called a *latent track*. By a suitable wet chemical etching, the damaged material along the track can be removed faster than the bulk material, thus developing the ion tracks into nanochannels[30-33,61] (Figure 1.1). The number of channels formed in this way is equal to the number of ions penetrated through the membrane. By reducing the number of impinging ions to one, it is possible to prepare a membrane sample containing one single channel.

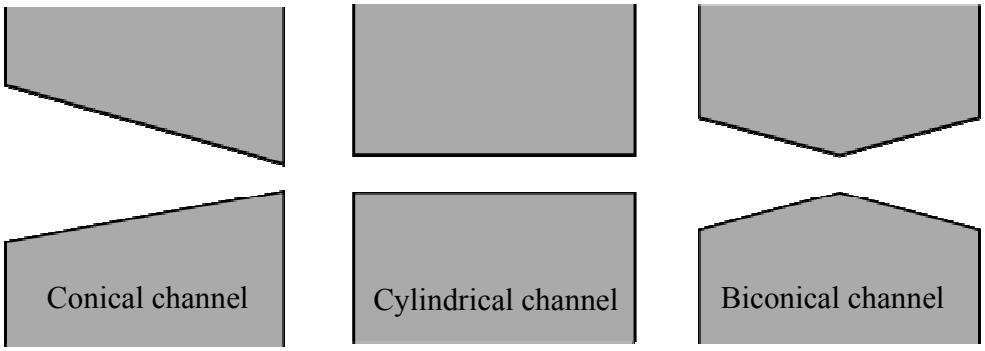

Figure 1.1: A Schematic illustration of ion track-etched nanochannels with different shapes.

The single conical nanochannels are of special interest as they are able to rectify the ion current. This behavior is called "*rectifying*", because these nanochannel preferentially transports cations / anions from the narrow entrance towards the wide opening of the channel. It has been proved, both experimentally[30,33,68,69] and theoretically,[70-74] that the rectifying characteristics of the nanochannels emerge because of the channel asymmetry and the electrostatic effects due to the fixed charges created on the channel wall. Experimentally, by applying a transmembrane potential across the membrane, an electric diode-like current rectification is obtained which is in close resemblance to the voltage-gated biological ion channels. The rectification property is visualized by measuring current–voltage (*I-V*) curves under symmetrical electrolyte conditions.

Ion channels with asymmetric *I-V* characteristics are also found in nature. Their behavior is also called 'rectifying'. It can be found in the inwardly rectifying potassium channels,[75,76] which transport potassium effectively into, but not out of the cell. Such analogies of artificially fabricated solid-state conical nanochannels with naturally occurring systems have triggered the interest of the scientific community related to diverse research fields, including life sciences, chemistry, and applied biophysics.

Although the physical and chemical surface properties of these nanochannels are yet to be fully exploited separation techniques, biological sensing, and fabrication of nano-actuators are the research areas actively considering these materials.

2. EXPERIMENTAL

Ion track technology uses to a great extent the irradiation of polymer membranes with swift heavy ions, leading to the formation of damaged zones known as latent tracks. In this work, these ion tracks were transformed into channels by chemical etching. The resulting channels were characterized by using a suitable method. Finally, the chemical species (mainly carboxyl groups) generated on the channel surface were chemically functionalized with a variety of molecules for manipulating the surface charge, biosensing of protein analytes, and providing stimuli-responsive and nanofluidic diodes.

2.1 Swift Heavy-Ion Irradiation

The UNILAC linear accelerator at GSI accelerates swift heavy ions of specific kinetic energies up to 12 MeV/u. When these charged particles penetrate through a material, they lose their energy mainly by

(a) Excitation of target electrons and ionization (electronic energy loss),

(b) Elastic collisions with target atoms (nuclear energy loss).

The other modes of energy loss, like Bremsstrahlung and Cherenkov effect (electromagnetic radiation) play no role at these kinetic energies.[77]

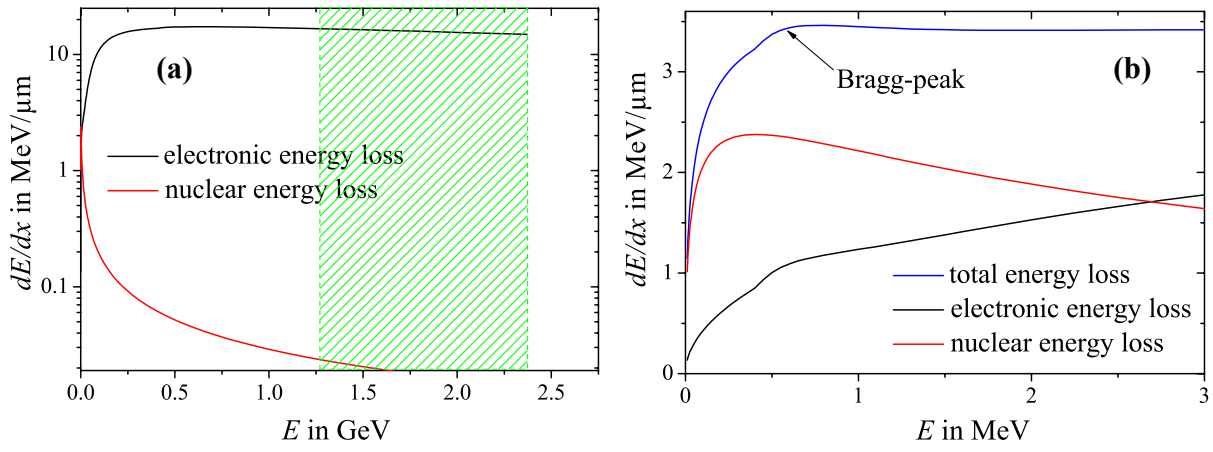

Figure 2.1: SRIM calculations for a Pb^{92+} ion in PET. (a) Energy loss of the ion (b) Energy loss at low ion energies.

As shown in Figure 2.1 b, the electronic energy loss dominates at energies higher than 2.6 MeV for Pb ions, corresponding to approximately 0.01 MeV/nucleon. Here, the total energy loss has a plateau. At lower energies the dominating effect is the nuclear energy loss. Shortly before the ion is stopped completely, the so-called Bragg-peak is visible in the total energy loss. This peak is rather broad and shallow for heavy ions such as lead or uranium, but can become very pronounced for lighter ions such as carbon. If the target is thick enough, the incoming ion can deposit all its energy and is eventually stopped in the material.

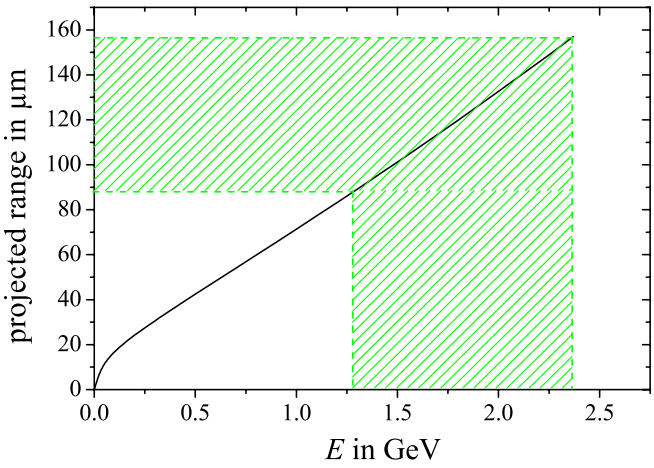

Figure 2.2: Projected range of a Pb^{92+} ion in PET, calculated with the SRIM program.

The range R an ion can penetrate in a material before it stopped is given by the integral over the inverse energy loss conducted from zero to the initial projectile energy E_0:

$$R = \int_o^{Eo} \left(\frac{dE}{dx} \right)^{-1} dE \qquad 2.1$$

This range is called the "projected range" of the ion. The energy loss and projected range of an ion can be calculated with the SRIM code.[78] The result is shown in Figures 2.2, and 2.1 for lead ions penetrating a PET target.

After the initial projectile ion is stopped completely, which in Figure 2.1b is the case on the left-hand side at $E = 0$, a "tail" can be formed in the energy loss curve. This tail is not calculated by the SRIM program, but can be taken into account by a more detailed approach in the TRIM program. It is caused by secondary particles such as knocked-on and scattered target atoms or lighter nuclei produced from projectile ions via nuclear reactions. The electronic energy loss (dE/dx) can be described by the Bethe-Bloch formula:

$$\frac{dE}{dx} = 4\pi \frac{Z_{eff}^2 n_e e^4}{m_e c^2 \beta^2} \left(\ln \left(\frac{2 m_e c^2 \beta^2}{I\left(1-\beta^2\right)} \right) - \beta^2 \right) \qquad 2.2$$

where

Z_{eff} : effective charge of the projectile ion, see eq. 2.3

n_e : electron density of the target material: $n_e = Z_t n_t$

Z_t and n_t denote atomic number and number density of target atoms, respectively

m_e : free electron mass

e : elementary charge

β : v/c where v denotes the velocity of the projectile

I : ionization energy

The effective charge of the projectile depends on its velocity. If the ion hits a target, the electrons with orbital velocities lower than the velocity of the projectile itself will be stripped off and the ion increases its charge state. Thereby, Z_{eff} increases with the kinetic energy of the projectile. Ions with low kinetic energies keep some of their electrons, whereas swift ions with high kinetic energies are almost completely stripped of electrons. This relation is expressed by the Barkas formula

$$Z_{eff} = Z_t \left(1 - \exp\left(-\frac{130\beta}{Z_t^{2/3}}\right)\right) \qquad 2.3$$

The polymer membranes used here for nanochannel fabrication are 12 μm thick. These membranes are usually irradiated in stacks of 6 pieces by swift heavy ions (^{238}U, ^{206}Pb, ^{197}Au) of energy 11.4 MeV/u from the UNILAC. This makes sure, that the energy loss throughout the whole stack of foils is in the region of the plateau in the energy loss diagram (Figure 2.1a), and thereby approximately constant. The region of about 72 μm, which corresponds to the thickness of a stack of 6 PET membranes with 12 μm each, is marked in Figures 2.2 and 2.1a with the green lines.

The lower limit for the energy loss, at which an ion track in a polymer material is still etchable, is 2 − 5 keV/nm. Tracks formed with too little energy deposition are either not etchable at all or etch discontinuously, so that the size distribution of the channels can become too broad and the longitudinal cross-section may become rugged.[79] Only a sufficiently high energy deposition, which is homogeneous over the whole latent track, ensures a good etchability. Therefore, it is desirable to obtain an energy loss as high as possible. Regarding equations 2.2 and 2.3, this can be realized by the choice of a high atomic number.

In order to vary the density of ion tracks in the material, the applied ion fluence can be changed. For nanochannel fabrication, usually fluences of maximally 10^7 to 10^8 ions cm^{-2} are applied. Higher track densities are not desirable because this would cause a great overlap in the etched

nanochannels. The variation of the fluence can be achieved either by a set of electromagnetic lenses which can widen or focus the incoming ion beam, or by the choice of irradiation time during which the target is exposed to an ion beam with a constant flux. Most commercially available ion track membranes are irradiated by drawing large sheets of polymer foil on reels through the ion beam. Hence, the ion tracks are not aligned, but have an angle distribution with respect to the membrane surface. However, at the UNILAC facility the samples for nanochannel fabrication are placed in a way, that the incident ion beam is oriented perpendicular to the surface. Hence, these membranes contain tracks strictly parallel and perpendicular to the surface. This is of great advantage with regard to the reproducibility of experiments. Even so, the irradiation is still a stochastical process, meaning that the spatial distribution of tracks is random, so that even at relatively low fluences an overlap of two ion tracks can occur.

Single-ion irradiation is performed in the following way: A metal mask with a centered aperture of diameter d = 300 µm is placed in front of the sample, which is then irradiated with a defocused ion beam. The frequency of ions passing through the aperture is lowered thereby to a few ions/s. This makes it possible to switch off the beam by electrostatic deflection as soon as the detector behind the sample registers the first ion, thus avoiding the passage of a second one. The sample holder and experimental setup used for the single-ion irradiation is shown in Figure 2.3.

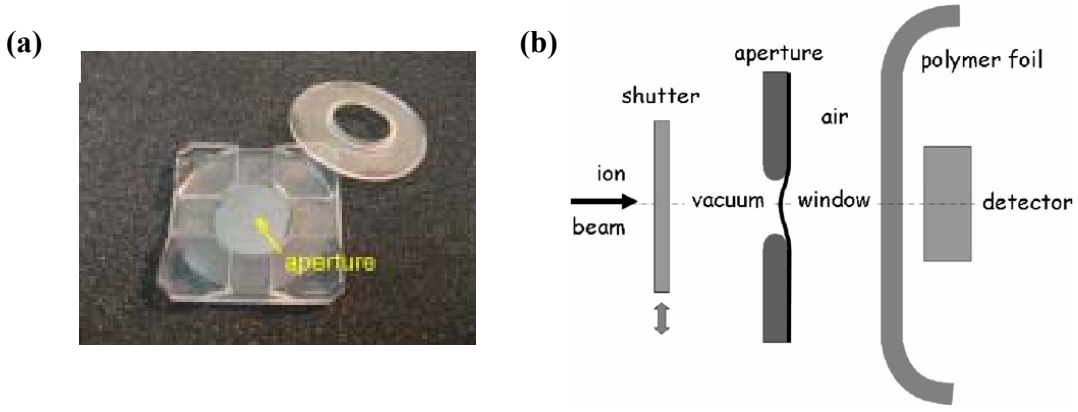

Figure 2.3: (a) Sample holder having a diameter of 30 mm including the metal mask. (b) Principle of single-track irradiation. The shutter closes as soon as one ion is detected.

2.1.1 Origin of Latent Tracks

Latent ion tracks are long lasting memories of the passage of energetic ions through insulating solids (Figure 2.4). A glimpse on the involved processes can be gained by observing the particles emitted from the surface of the solid. The passing ion transfers its energy to the loosely bound electrons of the solid, releasing a cascade of secondary electrons streaming radially outward from the ion path and transferring their energy gradually into atomic motion, thereby heating the solid. The released heat creates a modified zone, the track core, characterized by decreased density and increased chemical reactivity.[80]

The track core is susceptible to selective track etching. In polymers, track etching increases with the deposited energy per unit path length up to a saturation value. Further away from the track core, a track halo is created, characterized by chemical changes such as radicals. The stored effect decreases rapidly with the distance from the ion path. Selective track etching is dominated by etching of the track core.

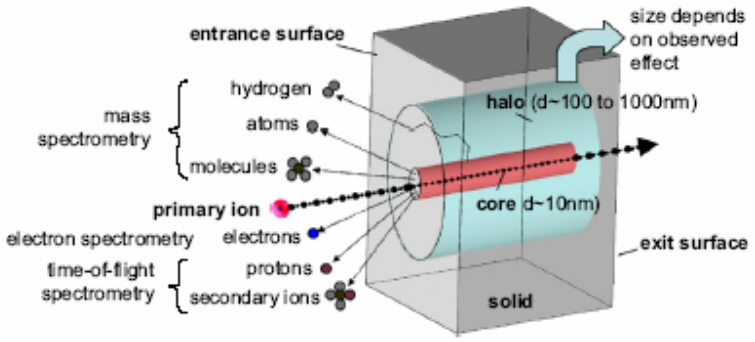

Figure 2.4: Origin of ion tracks, associated processes, and observation techniques.

In polymers the track core consists of polymer fragments. Part of radiolysis products in heavy ion tracks are chemically active species undergoing post-irradiation reactions, such as oxidation, photo-oxidation, etc. For this reason, storage of the irradiated polymers in air leads to a significant increase in the track etch rate. Additionally, the tracks can be sensitized by exposing the samples to UV-light before etching.[81,82] It is presumed that the energy deposited by the UV light breaks additional chemical bonds along the track, thus increasing the track-etch rate v_t and the *selectivity* by a factor of up to 10. Heavy ion tracks in polymer membranes can be effectively sensitized by the treatment with certain organic solvents.[83]

2.2 Fabrication of Nanochannels

The latent tracks produced in the polymer membranes due to the penetration of swift heavy ions can be selectively etched through with a suitable chemical etchant. During chemical etching the damaged zone of a latent track is preferentially removed and transformed into a hollow channel. The etching rate, with which the latent track is dissolved, is known as track etch rate (v_t), and the etching rate of undamaged bulk material is referred to as bulk etch rate (v_b). During the etching process, the track etch rate is higher than the bulk etch rate. Therefore, the geometry of the fabricated nanochannel depends mainly on the ratio of track to bulk etch rate (v_t/v_b) which is further influenced by a) concentration of the etchant, b) additives to the etchant, c) temperature, and d) voltage applied during the etching process. In addition, the sensitization of the polymer membranes with either soft UV light or organic solvent and the energy loss dE/dx of the heavy ion in the material also affect the fabrication of the latent track.

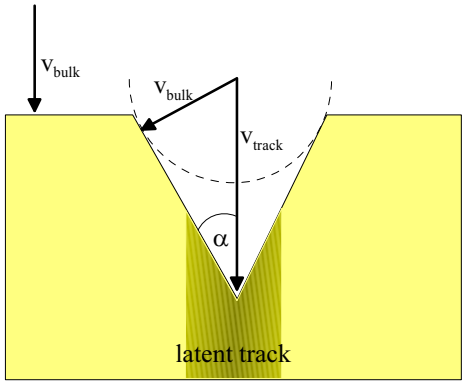

Figure 2.5: Schematic illustration of the etching process.

Figure 2.5 shows schematically the correlation of v_b and v_t. For better visibility, the scaling of the etch cone and the latent track is biased. The etching of bulk material leads to a reduction of the foil thickness as well as a widening of the nanochannel perpendicular to the surface of the "etch-cone". The removal of the track material with speed v_t is responsible for the breakthrough of the membrane. The cone angle α can now be considered as a function of v_b and v_t, so that $\sin \alpha = v_b/v_t$. For very high track etch rates $v_t >> v_b$, the cone angle approaches zero, which leads to a cylindrical geometry of the nanochannels, and for smaller etching velocities conical channels are obtained. Here, the entire latent track, which has an average diameter of approximately 20-30 nm in PI and approximately 10 nm in PET and PC, is etched away very quickly.[84]

2.2.1 Symmetrical Etching

In symmetric etching of latent tracks in polymer foils, etchant can attack from both sides of the membranes. The simplest setup for symmetric etching consists of a beaker filled with a suitable etching solution. The polymer membranes are immersed in etchant in order to etch the ion tracks from both sides. The temperature of the etching solution can be controlled by a circuit of heated or cooled water flowing through the double walls of the beaker. The only way to control the channel size in a certain etching solution is the duration of the etching process. After the etching, the samples are taken out from the etching solution and rinsed several times with deionized water. This technique is most often used for the fabrication of cylindrical channels in polycarbonate or PET membranes and of biconical channels in polyimide.

The symmetric etching in a beaker is simple, easy to handle, and includes also the possibility to stir the etching solution. Thereby, the concentration of the solution and the temperature in the vicinity of the polymer are kept approximately constant throughout the process. Nevertheless, particularly for the fabrication of very narrow channels, it is desirable to monitor the etching process online. This can be done by symmetrical etching in a conductivity cell in which both compartments are filled with etchant (Figure 2.6), and the etching process is monitored by applying a constant voltage between the two halves of the cell and constantly measuring the current with picoampere precision.

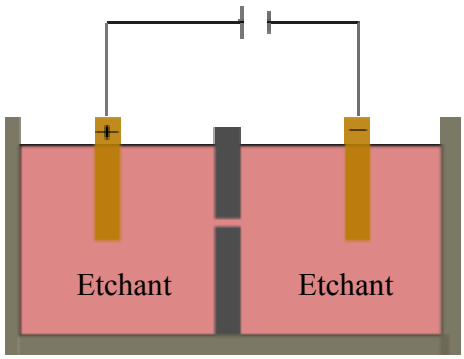

Figure 2.6: Principle of etching a cylindrical channel in a conductivity cell.

2.2.2 Asymmetrical Etching

The conductivity cell used for the etching of ion tracked polymer membranes is shown in Figure 2.7. It consists of three cell compartments made of polychlorotrifluoroethylene (PCTFE), also known as Neoflon, between which two foils with a preset number of ions can be placed and clamped tight. The electro-leakage around the outer surface of the membrane is prevented by the pressurized seal. The metal housing of the cell serves as an electrical as well as a thermal shield. Usually, one single-shot membrane and one membrane irradiated with a higher fluence like e.g. 10^7 ions/cm^2 are placed on both sides of the middle compartment of the cell (Figure 2.7). The middle chamber, having holes on both sides, was filled with etchant while the other two chambers were either filled with etchant or stopping solution in order to obtain cylindrical or conical channels, respectively. By this method, the single-channel membrane can be used for quantitative current-voltage measurements, while the channel size can be easily observed with a scanning electron microscope (SEM) employing the multi-channel membrane.

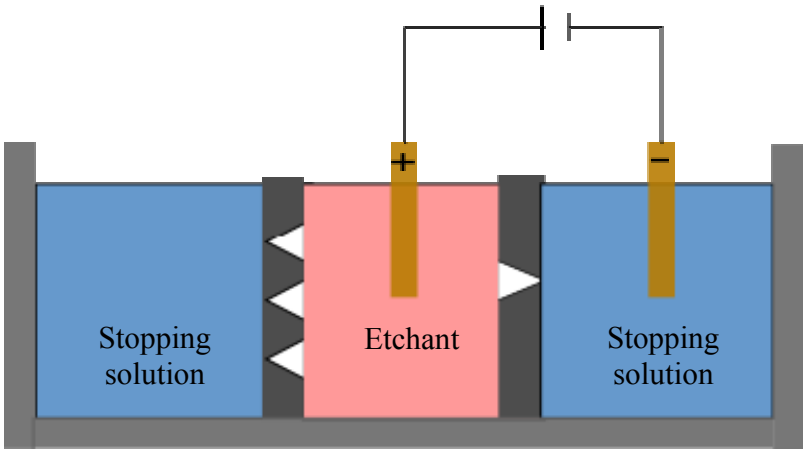

Figure 2.7: Conductivity cell used for the asymmetric fabrication of conical channels in polymer membranes.

For online monitoring of the etching process, two gold electrodes are placed in adjoining compartments, and a voltage of -1V is applied across the membrane. The current transported by the ions in the solutions can be recorded. For better reliability of the measurement, the current flowing through the single-channel membrane is monitored. Because the breakthrough times of the different channels in a membrane can vary, a current signal observed over the multi-channel membrane can indicate a breakthrough even if only one channel is open yet. If the etching would

then be terminated, the single channel in the other membrane need not necessarily be already open.

2.2.2.1 Conical Nanochannels in Polyimide

In order to obtain conical nanochannels, ion-track polyimide membranes were etched asymmetrically in a special type of conductivity cell as explained above. Sodium hypochlorite (13% active chlorine content) is used as the etching solution, while a stopping solution (1 M KI) is placed on the other side of the membrane. The etching process is carried out at 50 ^{o}C. In order to monitor the etching process, a voltage of -1V is applied across the membrane. Initially, the current flowing across the membrane remains zero and after the break-through, continuous increase of ionic current was observed as shown in Figure 2.8. The etching process is being terminated when the quantity of current flowing through the nascent channel reaches a certain value.

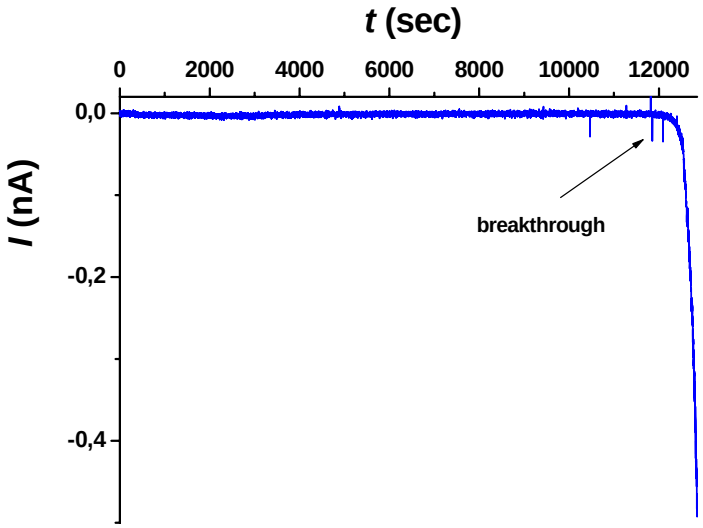

Figure 2.8: Current recorded during the asymmetric etching of an ion-tracked PI membrane.

Here, the stopping solution, acting as reducing agent, is used to reduce OCl^- to Cl^- and oxidize the iodide ions. This process was supported further by applying a potential of +1 V on the side containing the etchant with the other side grounded, so that once the channel opened, the active ClO^- ions were swept back from the channel tip. This provides an additional protection from etching to the other side of the membrane. Shortly after breakthrough the channels were washed

with stopping solution, followed by deionised water. The time required for a complete one-side etching varies from 3 – 4 hours, and the bulk etch rate, calculated from the thickness and weight loss measurements, is ~ 7 nm / minute.[85]

Polyimide (Kapton) films are highly heat-resistant and also resistant to most chemicals. But the ion tracks are susceptible to a chemical attack. The preferential points of etch attack are the ether and imide bonds in the polymer back-bone. The imide functional groups in PI react with strongly basic etchant (NaOCl, pH ~12.5) at high temperature. This resulted in the opening of imide ring into amide and carboxylate salt,[86] as summarized in Figure 2.9. After washing with water, generation of carboxyl groups takes place at the ends of broken polymer chains. Simultaneous action of two factors – oxidation and alkalinity – leads to a complex etching mechanism. Therefore, it is hard to say what point in the molecule is the etch-rate determining one.

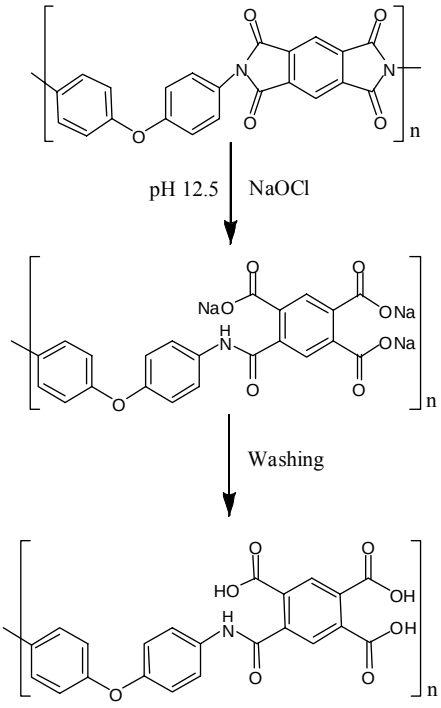

Figure 2.9: Chemical etching of an ion-tracked PI membrane in NaOCl (pH ~ 12.5) solution.

2.2.2.2 Conical Nanochannels in Polyethylene terephthalate

The etching method for the fabrication of conical nanochannels in PET membranes was developed by Apel *et al.*[30] Briefly, the heavy ion-irradiated membrane was placed between the two halves of a conductivity cell in which it served as a dividing wall between the two compartments. An etching solution (9 M NaOH) was added on one side, and the other side of the cell was filled with stopping solution (1M HCOOH + 1M KCl). The etching process was carried out at room temperature. During the etching process, a voltage of -1 V was applied across the membrane in order to observe the flowing current. The current remains zero as long as the channel is not yet etched through. After the break-through, the stopping solution on the other side of the membrane neutralizes the etchant. For PET, the breakthrough usually occurs as a sudden increase in current to typically ~100 pA, followed by a period of time in which the current

fluctuates very strongly (Figure 2.10). If the etching is interrupted during this time, which can last for several minutes, the channels tend to close again. In the following time, the current is more stable but does usually not increase significantly over a time period of tens of minutes. Only then a further increase in current is observed. The etching process was stopped when the current reached a certain value, and the channel was washed first with stopping solution in order to quench the etchant, followed with deionised water. The etched membrane was immersed in deionised water in order to remove the residual salts. About 1 hour is required for the break-through, and the bulk etch rate is ~ 1.7 nm per minute for a 12-µm PET membrane.[85]

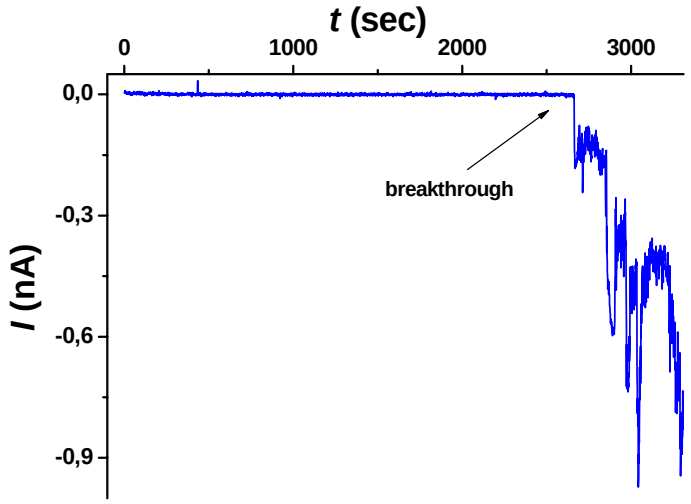

Figure 2.10: Current recorded during the asymmetric etching of an ion-tracked PET membrane.

In PET (commonly also known as polyester), the ester bonds formed by the condensation of terephthalic acid and ethylene glycol are the main points for the chemical attack of an etchant (NaOH). The alkali easily hydrolyses these partially charged ester bonds in the polymer chains. Therefore, during the process of alkaline etching, these weak bonds are broken into terminated carboxyl (–COOH) and hydroxyl (–OH) groups as shown Figure 2.11.

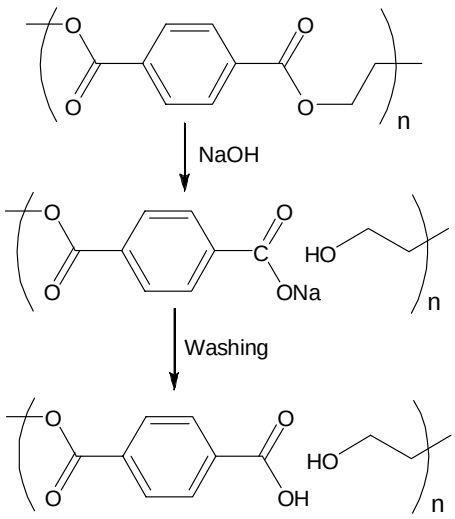

Figure 2.11: Chemical etching of an ion-tracked PET membrane in aqueous NaOH solution.

2.2.3 Surfactant-Controlled Asymmetric Etching

The surfactant-controlled asymmetric fabrication method yields a significantly better reproducibility than the one-side etching. Additionally, the choice of the etching conditions (increased temperature and enhanced surface wetting due to the surfactant) leads to a much faster process (in the order of a few minutes as compared to hours).

A variety of surfactants were added in the etching solution to improve wetting for uniform fabrication of channels in ion tracked polymer membranes. The previous studies showed that the small surfactant molecules were restricted for wetting. Large surfactant molecules behave differently during the fabrication process, which changes the kinetics of channel opening as well as the internal shape of the channel because of the following reasons: Firstly, the adsorbed layer of surfactant molecules on the surface reduces the effectiveness of an etchant for direct chemical attack on the ion tracks. Secondly, the diffusion rate of small etchant molecules in the restricted volume of the etched channel is different from that of large nano-sized surfactant molecules which are also comparable to the radius of the preferentially etched track core.[87]

A surfactant molecule consists of an alkyl chain of about 8-12 carbon atoms referred to as hydrophobic tail, and of a second part containing ionic or non-ionic groups known as hydrophilic head. The polymer surface is hydrophobic in nature; therefore adsorption of surfactant on the surface occurs through their hydrophobic part, while the hydrophilic part remains directed towards the aqueous phase.[88] This results in the formation of a quasi-solid layer of surfactant molecules on the surface, and the existence of such monolayer was also confirmed by measuring the adsorption isotherms on the polymer surface. The adsorbed layer of surfactant molecules partially protects the surface from the direct attack of etchant molecules, which leads to a reduced bulk etch rate of the polymer surface.

An anionic surfactant, Dowfex 2A1 (Figure 2.12), is preferred for the etching of ion tracked PET membranes because of its better solubility in concentrated alkali solution. The major component of this surfactant is sodium dodecyl diphenyl oxide disulphonate.

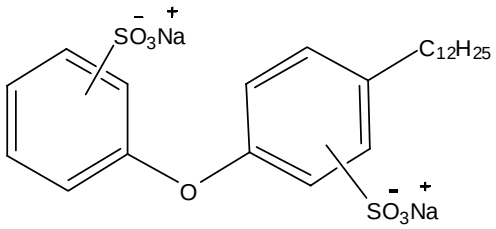

Figure 2.12: Chemical structure of surfactant sodiumdodecyldiphenyloxidedisulphonate (Dowfex 2A1).

Apart from surfactant, sensitization of the polymer membrane with long-time UV light exposure is also helpful to control the geometry of the etched channel. The membranes are irradiated by soft UV light with wavelength of about 320 nm for 15 to 40 hours from one side only.[88] The light is absorbed in the upper membrane layer with a thickness of few hundred nanometres which leads to photo-oxidative degradation of the surface. As a result, the overall polarity on the surface increases due to the formation of polar moieties like aldehydes, ketones, and carboxylate groups. The polarity difference on both sides of the surface affects the adsorption of surfactant molecules, which leads to an asymmetry in the etching process, and as result bullet-shaped channels are produced.

For the fabrication of asymmetric channels in PET, heavy ion-irradiated foils were treated with UV light (320 nm) from one side for 35 hours. Then, each foil was inserted in a conductivity cell, in which it served as a dividing wall between the two compartments. The compartment facing the UV-treated side of the foil was filled with etching solution, while the other half of the cell was filled with surfactant-containing etchant as shown in Figure 2.13a. The etching process was carried out at 60 °C. During etching, a voltage of -1 V was applied across the membrane in order to observe the current flowing through it. The current remains zero as long as the channel is not yet etched through (for about half a minute), and increases continuously after breakthrough as shown in Figure 2.13b. The etching process was terminated at a desired current value corresponding to a certain tip diameter, and 1 M HCl solution was used in order to neutralize the etchant. Finally, the membrane was washed with deionised water.

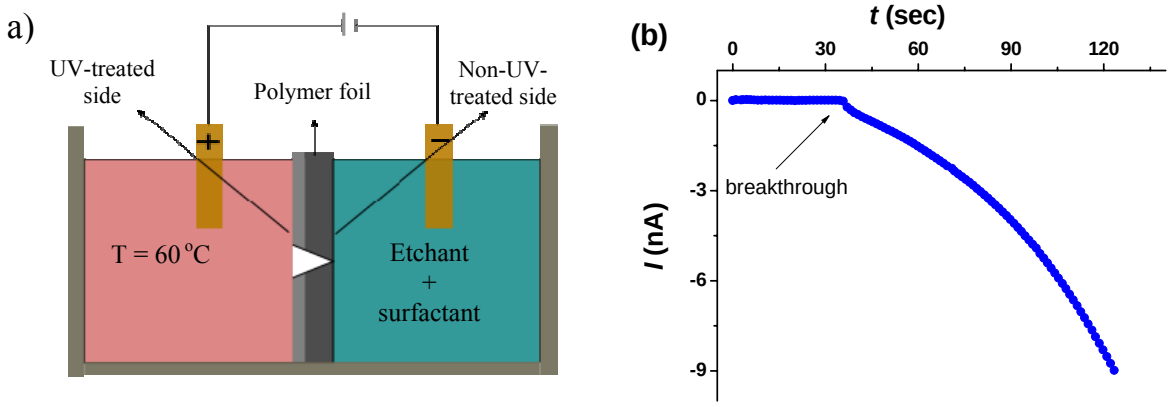

Figure 2.13: (a) Schematic diagram of an etching cell used for asymmetric surfactant-controlled track-etching of PET membranes. (b) Ion current versus time record of the etching process.

However, the etching method described here differs from the previous one in the following way: Firstly, etching of the latent track was performed in a conductivity cell in which the pure etchant was placed on the UV-treated membrane side, while the non-UV-treated side faces the etching solution with surfactant molecules as shown in Figure 2.13a. The etching proceeds much faster on the UV-treated side, whereas the non-UV-sensitized side is protected from direct attack of the etchant by an adsorbed layer of surfactant molecules (Figure 2.14). Additionally, a constant voltage (-1V) was applied across the membrane in order to facilitate the fabrication process, and the etching process was monitored by observing the ion current flowing through the nascent channel. In this way, one is able to fabricate nanochannels with an approximately conical geometry, which was not possible before, using the reported surfactant-controlled fabrication methods.

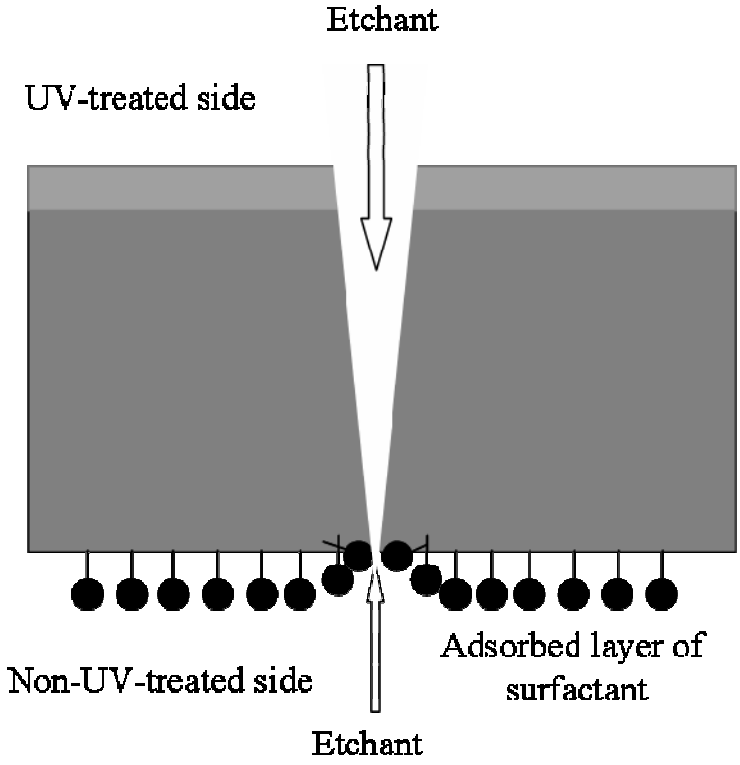

Figure 2.14: Schematic drawing of the chemical etching, with surfactant added to the etching solution on the non-UV-treated side of an ion-tracked PET membrane.

Figure 2.15 shows pictures recorded by field-emission scanning electron microscopy (FESEM) of the tip side (surfactant protected), base side (UV-sensitized), and a side view of the channels of a

polymer membrane irradiated with $1x10^8$ ions cm^{-2}, which was etched under the same conditions as the single-channel sample.

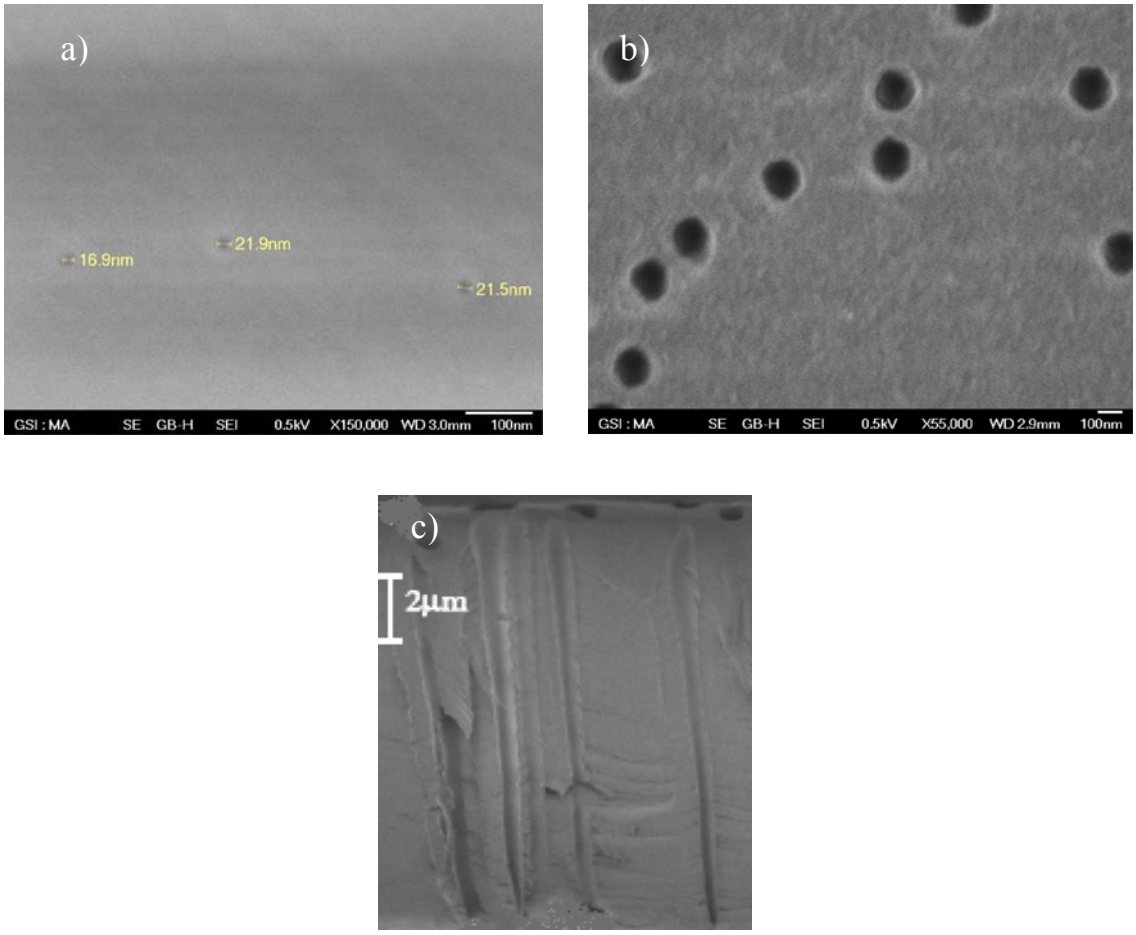

Figure 2.15: FESEM images of (a) the small (surfactant-protected), (b) the large (UV-treated) side, (c) the side view of channels in a polymer membrane, containing $1x10^8$ ion/cm^2 and etched by the surfactant-controlled asmmetric etching method.

2.3 Characterization of Nanochannels

A variety of methods like field emission scanning electron microscopy (FESEM), transmission electron microscopy (TEM), and atomic force microscopy (AFM) are used for the geometrical characterization of track-etched nanochannels. Apart from these methods, conductance measurements, size exclusion techniques, and scattering experiments are applied for the estimation of channel size. The geometry of the internal channel can also be determined by electrochemical deposition of nanowires (replica method) in the channels.

2.3.1 Scanning Electron Microscopy

After track-etching, the geometry of the channels can be characterized directly by SEM. The SEM images provide shape and size of the etched channel. To be imaged with SEM, the sample needs to be at least a little bit electrically conductive. Insulating samples present an imaging challenge because charging of the sample can deflect the scanning beam, which results in a distorted image. As a help in imaging, insulating samples are sputter-coated with a very thin layer of metal, for instance gold. FESEM produces clearer, less electrostatically distorted images with spatial resolution down to 1.5 nm. This resolution is 3 to 6 times higher than reachable with conventional SEM.

A typical FESEM micrograph of the surface of a track-etched PI membrane with single and ~ 10^7 channels cm^{-2} is shown in Figure 2.17. For the lateral view of the channels, track-etched PET membranes were exposed to UV light for about 60 hours from both sides. After this treatment, the membranes become brittle and can be manually broken apart. A cross-sectional view of a membrane, having approximately 10^8 channels cm^{-2}, is shown in Figure 2.15c.

2.3.2 Estimation of Channel Diameter

By assuming a certain geometry, the channel diameter can be calculated by using an electrochemical method.[85] After track-etching, the membrane containing a single channel is washed with distilled water and mounted between the two halves of a conductivity cell. An

electrolytic solution (1 M KCl) with known conductivity is filled into each half, and Ag/AgCl electrodes are used in order to obtain a current-voltage curve (*I-V*) for the channel.

For cylindrical channels, the *I-V* curve is linear, and the slope is a measure of the ionic resistance of the electrolyte-filled channel. The effective channel diameter *d* is calculated by using the following equation,

$$d = \sqrt{\frac{4LI}{\pi\kappa U}} \qquad 2.4$$

where *L* is the channel length corresponding to the foil thickness, *I* is the measured current, U is the applied voltage, and κ is the specific conductivity of the 1 M KCl solution (10 S/m at 20 °C).

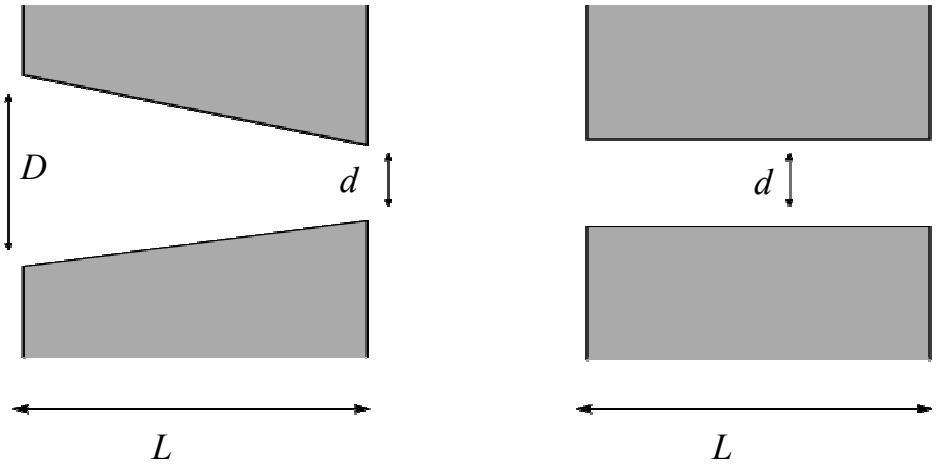

Figure 2.16: Scheme illustrating the geometrical parameters of conical (left) and cylindrical (right) nanochannels.

This method can also be used for the estimation of the small tip opening, with diameter *d*, of a conical nanochannel. Because of the rectifying behaviour of a conical channel, the value of ionic current, measured at a certain positive voltage, is higher than that measured at the same negative voltage. As the bulk conductivity is different from the conductivity of a charged conical nanochannel, the pH value of the electrolyte is adjusted in order to obtain a linear *I-V* curve for an uncharged conical channel. For the calculation of tip opening diameter, the equation 2.4 has to be slightly modified, taking into account the conical geometry with two different diameters on both sides:

$$d = \frac{4LI}{\pi\kappa UD} \qquad 2.5$$

The large opening with so-called base diameter (*D*) of a conical channel was determined independently by FESEM, using a sample containing 10^7 channels/cm^2, which was etched simultaneously with the single-channel membrane under the same conditions as shown in Figure 2.17.

The value of *D* can also be calculated from the bulk etch rate which is 2.13 nm/min for PET at room temperature in 9 M NaOH and 7 nm/min for PI in NaOCl at 60 ^{o}C, respectively.

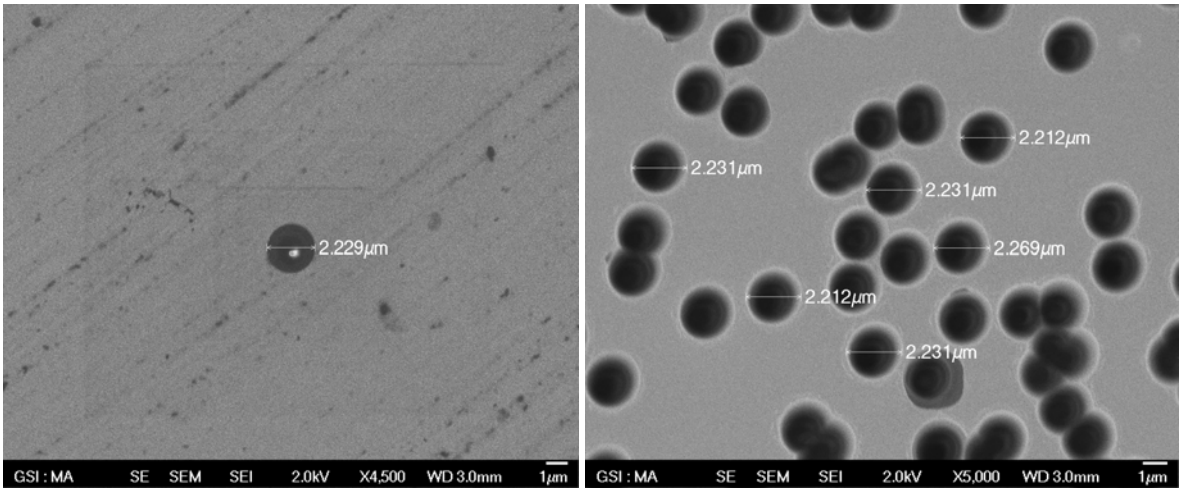

Figure 2.17: FESEM images of base opening of a single conical nanochannel (left) and of 10^7 conical nanochannels cm^{-2} (right) in polyimide foils which were etched simultaneously in a conductivity cell.

2.3.3 Current-Voltage (*I-V*) Characteristics

The current-voltage (*I-V*) measurements were performed in the same conductivity cell used for the fabrication of single conical channels in ion tracked polymer membranes, as explained in Figure 2.7. The membranes containing single conical channels were mounted between the two halves of the conductivity cell, and both halves were filled with electrolyte (1M or 0.1M KCl) solution. The pH of the electrolyte was adjusted by dilute HCl or KOH solutions. A Ag/AgCl electrode was placed into each half-cell solution, and a picoammeter/voltage source (Keithley 6487, Keithley Instruments, Cleveland, OH) was used to apply the desired transmembrane voltage. To measure the resulting ion current flowing through the nanochannel, a scanning triangle voltage with steps of 100 mV between -2 to +2 V on the tip side was applied (the base side of the channel remained connected to the ground electrode). By introducing a time span of at

least 1 second between each step, the system could be assumed to be in a condition of equilibrium all the time.

As it is well-known the conical nanochannels in polymer membranes rectify the ionic current (i.e. transport more ions in one direction than in the other). The rectification of ionic current occurs due to an asymmetry of the electrochemical potential inside the nanochannel. A typical *I-V* measurement with the applied triangle voltage and the current recorded for a single track-etched conical channel in PET is shown in Figure 2.18.

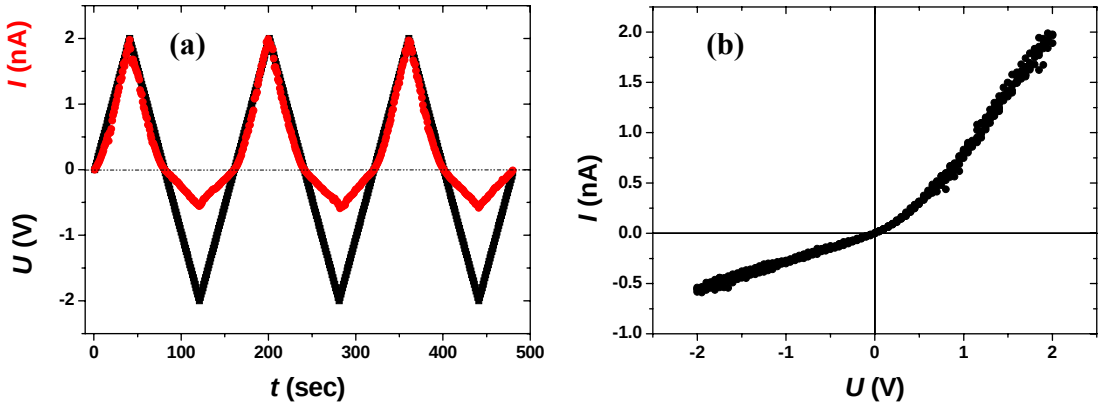

Figure 2.18: *I-V* measurements for a single conical PET channel, (a) triangle sweeps of voltage (black) and current (red), (b) corresponding *I-V* curve.

As a result of track etching, carboxyl groups are generated on the channel surface in polymer membranes (PET or PI). At neutral or basic pH values, the surface negative charge due to the ionized carboxylate ($-COO^-$) groups renders the nanochannels cation selective, and it was found by Siwy et al. that 90% of the ion current signal is due to potassium ions, when using KCl as electrolyte.[89] Neutral channels do not rectify the ion current, whereas positively and negatively charged channels rectify the current in opposite directions. An example of this pH dependence is shown in Figure 2.19 for a

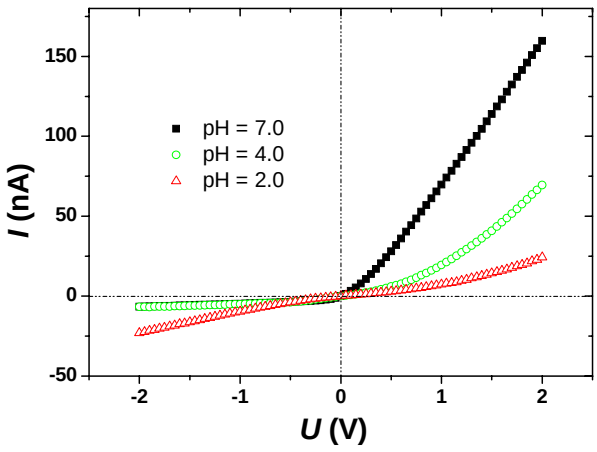

Figure 2.19: pH dependent *I-V* curves of a track-etched single conical nanochannel in polyimide.

conical track-etched channel, whose walls are negatively charged at neutral pH (-COO^-) and become neutral at low pH, where the carboxyl groups are protonated (-COOH). It can be clearly seen that the negatively charged channel rectifies the ionic current while the neutral one at pH 2.0 behaves like an ohmic resistor.

2.4 Functionalization of Nanochannels

2.4.1 Materials and Chemicals

Foils of polyethylene terephthalate (PET) (Hostaphan RN 12, Hoechst) and polyimide (PI) (Kapton 50 HN, DuPont) of 12 μm thickness were irradiated at the linear accelerator UNILAC (GSI, Darmstadt) with single swift heavy ions (Pb, U and Au) having an energy of 11.4 MeV per nucleon.

N-(3-dimethylaminopropyl)-*N*′-ethylcarbodiimide hydrochloride (EDC, 98%), pentafluorophenol (PFP, 99+ %), succinic anhydride (SA, 99%) L-lysine (98 + %), L-histidine (99.5+ %), phosphate-buffered saline (PBS, pH 7.6) 4,4′-Azobis(4-cyanopentanoic acid), (≥98.0%), *N*,*N*′-dicyclohexylcarbodiimide (DCC, ≥99.0%),were obtained from Sigma-Aldrich, Schnelldorf, Germany. Dry *N*,*N*-dimethyl formamide (DMF) and *N*-isopropylacrylamide (99 %)were obtained from Acros Organics, Geel, Belgium. Ethylenediamine (EDA, 99+ %), propylamine (PA, 99+ %), potassium chloride and copper(II) chloride dihydrate (99 %) were obtained from Merck, Germany. The surfactant Dowfax* 2A1 solution was received from Dow Chemical Company, Midland, USA. Sodium hydroxide and ethanol (99%) were obtained from LS Labor-Service, Germany. Fluorescein (FITC)-conjugated streptavidin (SAv) was purchased from Thermo Fisher Scientific Inc. Rockford, USA. All chemicals were used as received without further purification. Biotinylated poly(allylamine) hydrochloride (b-PAH) was synthesized and provided by Dr.Basit Yameen at Max-Planck-Institut für Polymerforschung, Mainz, Germany.

2.4.2 Modification of Carboxyl Groups

The surface of the nanochannels walls contain carboxyl (–COOH) groups which were generated during the irradiation and etching processes (Figure 2.20). Moreover, the surface chemistry of

these nanochannels can be manipulated by covalent or electrostatic attachment of a variety of functional groups with the carboxyl moieties, respectively. The chemical functionalization of these carboxyl groups was achieved by the following procedure: the first step was the activation of these groups into amine-reactive ester via carbodiimide coupling chemistry. Then, these reactive esters were further condensed with a variety of molecules having primary amine ($–NH_2$) groups through the formation of covalent bonds. The chemical functionalization of carboxyl groups was accomplished via EDC/NHS or EDC/PFP activation as described in detail in this section.

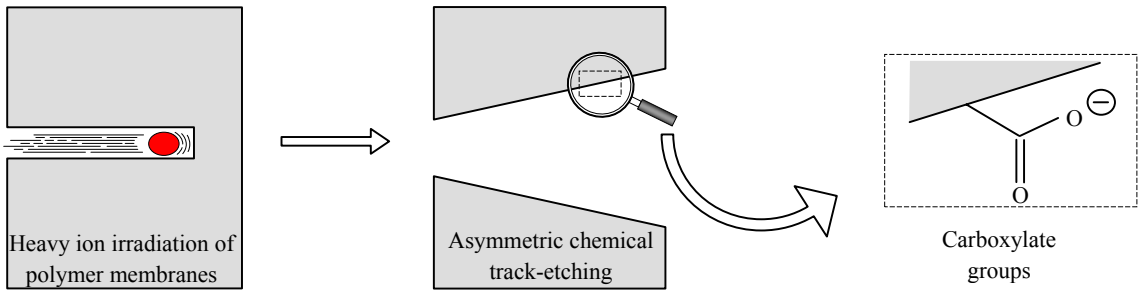

Figure 2.20: Scheme describing the generation of carboxyl species on the channel surface.

2.4.2.1 Modification via EDC/NHS activation

The chemical reaction scheme for the conversion of carboxyl into amine groups, and again conversion of amino groups into terminated carboxyl groups, is given in Figure 2.21. All reactions were carried out in the same cell as used for etching. An aqueous solution of *N*-hydroxysuccinimide (NHS, 400 mM) and *N*-(3-dimethylaminopropyl)-*N*′-ethylcarbodiimide hydrochloride (EDC, 200 mM) was prepared separately. Then, these solutions were mixed in equal volume and the resulting solution contains 200 mM and 100 mM of NHS and EDC, respectively. A membrane having single conical nanochannel was mounted between the two halves of the conductivity cell. For the activation of carboxyl groups into NHS-ester, a solution containing NHS and EDC was filled in both halves of the cell. The activation was carried out for 1 h at room temperature. After washing with distilled water, the samples were further treated with ethylenediamine (EDA, 100 mM) for an overnight time period. Finally, functionalized channels were washed several times with distilled water.

To re-terminate the amino groups with a terminated carboxyl species, the modified channels were further treated with a saturated solution of succinic anhydride (SA) for over night, and afterwards washed with distilled water.

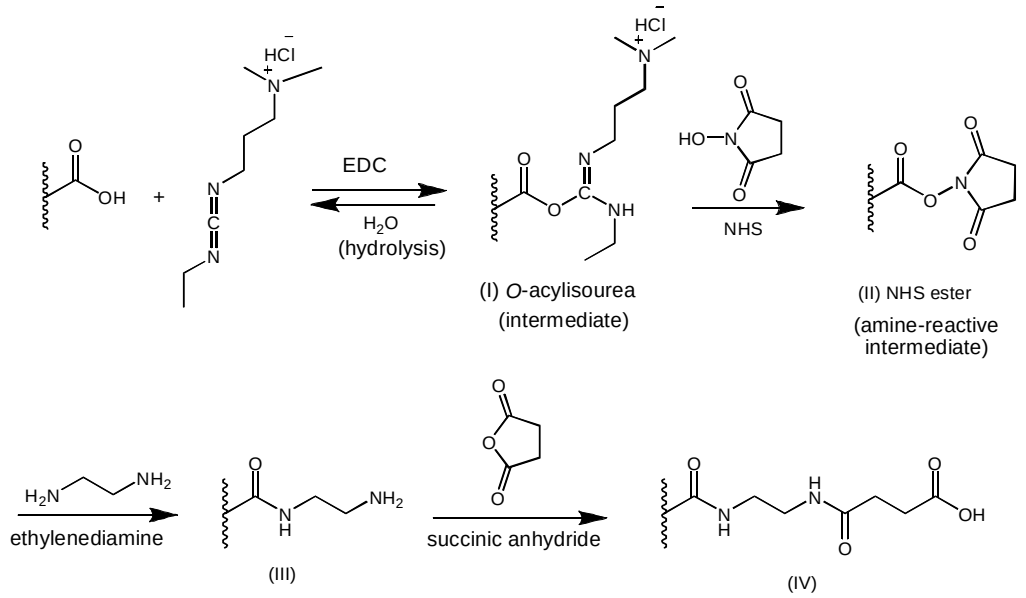

Figure 2.21: Reaction scheme for the attachment of amino-terminators to surface carboxyl groups, and the subsequent attachment of carboxyl-terminated species.

2.4.2.2 Modification via EDC/PFP activation

For the activation of carboxyl groups, pentafluorophenol can also be used instead of *N*-hydroxysuccinimide because pentafluorophenyl esters are ~10 times more active than the corresponding *N*-hydroxysuccinimidyl esters. The chemical reaction scheme for the conversion of carboxyl into amino and alkyl terminated groups (Figure 2.22). For the activation of the carboxyl groups into pentafluorophenyl esters (II), an ethanol solution containing *N*-(3-dimethylaminopropyl)-*N*′-ethylcarbodiimide hydrochloride (EDC, 100 mM) and pentafluorophenol (PFP, 200 mM) was placed on both sides of the track-etched single channel membrane. The reaction was carried out for 60 minutes at room temperature. Then the solution was replaced with ethylendiamine (EDA, 100 mM) or propylamine (PA, 100 mM) on both sides of the membrane for an overnight time period, in order to get amino ($–NH_2$) and alkyl ($–C_3H_7$) terminated groups (Figure 2.22 III and IV), respectively. Finally, the chemically modified membranes were washed first with ethanol and then with distilled water.

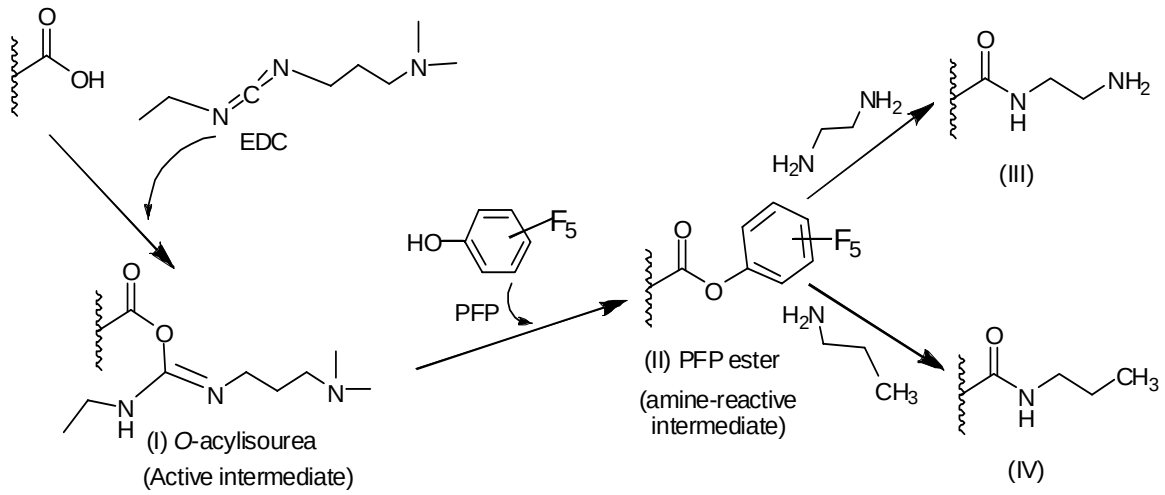

Figure 2.22: Reaction scheme for the conversion of carboxyl groups into terminated amino groups (III) and propyl groups (IV), respectively.

2.4.2.3 Functionalization with Amino Acids

For the functionalization of amino acids having more than one primary amine e.g. L-lysine, it is necessary to protect one of them for the successful coupling of terminated amino group with carboxyl groups. In order to block the α-amino and α-carboxylic groups, a solution of L-lysine (50 mM) was prepared in 60% aqueous ethanol (C_2H_5OH/H_2O, 6:4 by volume), and solid copper chloride (25 mM) was added slowly with continuous stirring. As a result, blue colored Cu(II) chelate complex of L-lysine was prepared containing a free amino group at the terminus of the chain, as shown Figure 2.23a. All chemical reactions were carried out in the conductivity cell used for etching of tracked polymer foils. The carboxyl (-COOH) groups generated on the channel surface during the track-etching process were modified by the following procedure. First, these groups were converted into pentafluorophenyl esters by using ethanolic solution of *N*-(3-dimethylaminopropyl)-*N′*-ethylcarbodiimide hydrochloride (EDC, 100 mM) and pentafluorophenol (PFP, 200 mM) for one hour. Second, the amine-reactive PFP esters were covalently coupled with the ε-amino group of the copper complex of lysine for overnight. After washing with distilled water, the modified channels were exposed to ethylenediaminetetraacetic acid (EDTA, 100 mM) for two hours in order to remove the copper ions from the surface of the channel. Finally, the modified channel was washed thoroughly with distilled water.

Functionalization of L-histidine on the channel surface was done by first activating the carboxylic groups into PFP-esters following the same procedure described for lysine. After activation, reactive esters were condensed with the α-amino groups of an L-histidine (50 mM) solution prepared in 60% aqueous ethanol, and allowed to react overnight at room temperature. Finally, the functionalized membranes were washed with distilled water several times.

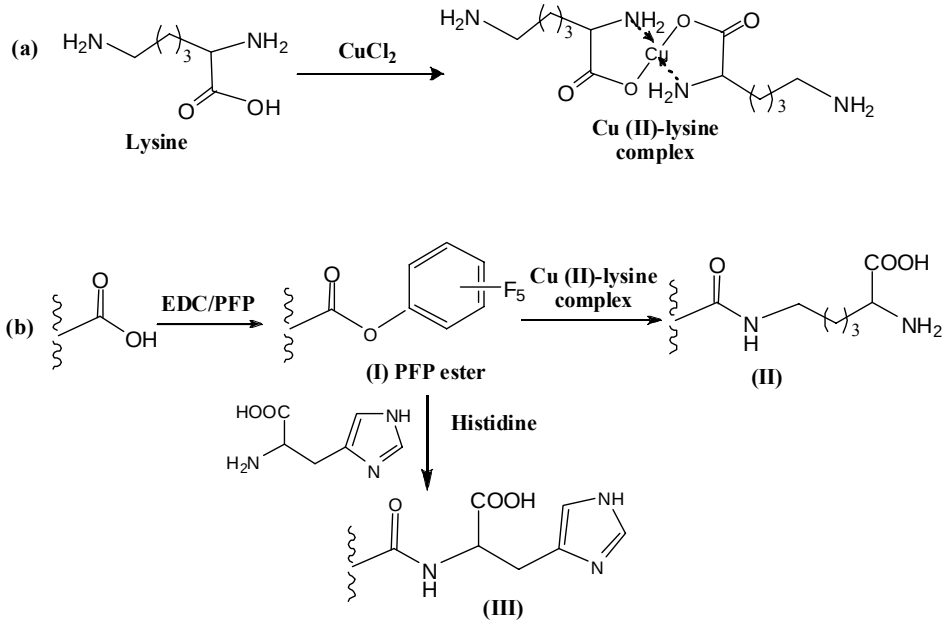

Figure 2.23: Functionalization of the channel surface with L-lysine (II) and L-histidine (III), respectively.

2.4.3 Electrostatic Self-Assembly of Bifunctional Macromolecules

As a result of track etching, negatively charged carboxylate moieties appear on the surface of the PET nanochannel. These functionalities are further used for electrostatical self-assembly of bifunctional polyelectrolytes as discussed below.

2.4.3.1 Electrostatic Self-Assembly of Biotinylated Poly(allylamine HCl)

The polycations, biotinylated poly(allylamine hydrochloride) a bifunctional polyvalent ligand (b-PAH), were electrostatically self-assembled on the negatively charged surface of the conical nanochannel, while the membrane was still mounted on the electrochemical cell used for *I-V* measurements. For this purpose, aqueous solution of b-PAH (1 mg/mL) was placed on both sides

of the track-etched membrane and allowed to self-assemble overnight. Then, the membrane was washed three times with Milli-Q water and three times with PBS buffer (pH 7.6) solution prior to biosensing experiments. The current-voltage curves of biotinylated nanochannels were measured with 0.1 M KCl as electrolyte (buffered with PBS, pH 7.6). The various concentrations of streptavidin prepared in the same electrolyte were used for the respective *I-V* measurements.

2.4.3.2 Formation of Multilayered Supramolecular Bioconjugates

The SAv solution (1 nM) was placed on both sides of the b-PAH-functionalized nanochannel for 4 h, and aftre washing, *I-V* curve was measured. Then the solution of b-PAH was introduced on both sides and allowed to self-assemble on the SAv layer overnight. After washing three times with Milli-Q water and three times with PBS solution, 1 nM SAv was introduced again on both sides of the nanochannel for 4 h, and a new *I-V* curve was measured.

2.4.4 Covalent Functionalization of Macromolecules*

For the covalent tethering of macromolecules, the surface of single conical nanochannels fabricated in ion track-etched PI membranes was first aminated by the coupling of EDA with the surface carboxyl groups via EDC/PFP activation as described above in 2.4.2. Subsequently, these aminated channels were then successfully functionalized with zwitterionic poly(methylacryloyl-l-lysine), thermo-responsive poly(*N*-isopropylacrylamide) and pH-responsive poly(4-vinyl pyridine) brushes, respectively.

2.4.4.1 Functionalization with Poly(methylacryloyl-L-lysine)

2.4.4.1.1 Anchoring of 4,4′-azobis(4-cyanopentanoic acid)

Briefly, 0.5g (1.78 mmole) of 4,4′-azobis(4-cyanopentanoic acid) and 0.92g (4.5 mmole) of DCC were added to a single neck Schlenk flask and closed with a rubber septum. The reactants were degassed under vacuum for 15 minutes followed by back filling with N_2 (g). 40 mL of dry DMF was added to the flask through the septum with the help of a syringe, and the reactants were

* The polymerization reactions were performed at Max Plank Institute for Polymer Research, Mainz, Germany.

allowed to dissolve. After complete dissolution, 0.13 mL of dry pyridine was added. A membrane with a single conical aminated nanochannel was sealed in a Schlenk tube and degassed (4 × high vacuum pump/ N_2 refill cycles). Then, the reaction mixture was syringed into the Schlenk flask containing the azo-modified membrane and left overnight under N_2 (g) at room temperature. Finally, the membrane was removed from the reaction mixture and immersed in a beaker containing DMF. The beaker was gently shaken over a period of 2h. The membrane was then washed twice with DMF followed by washing with water and ethanol. The initiator functionalized membrane was stored under nitrogen below 4 °C until further use.

2.4.4.1.2 Poly(methacryloyl-L-lysine) brush growth

In a 50 mL Schlenk flask, 2.5 g of the monomer methacryloyl-L-lysine was dissolved in 36 mL of aqueous HCl solution (pH 2.5). The solution was degassed by N_2 (g) bubbling for 1h. The initiator-functionalized membrane was sealed in a Schlenk flask and degassed (4 × high-vacuum pump/ N_2 refill cycles). The monomer solution was syringed into the Schlenk flask containing the membrane. Then, the flask was immersed in an oil bath preheated at 65 °C and the polymerization was carried out during 45 min. The PI membrane was then removed from the polymerization solution and left overnight in aqueous HCl solution with pH of 2.5. The following day, the membrane was gently rinsed with abundant deionized water. The poly(methacryloyl-L-lysine) brush-modified membrane was stored in water at room temperature until further use.

2.4.4.2 Functionalization with Poly(*N*-isopropylacrylamide)

2.4.4.2.1 Immobilization of ATRP initiator

A solution of 2-bromoisobutyryl bromide (BIBr) (0.185 mL, 3 mmol) and triethylamine (0.205 mL, 3 mmol) in dry dichloromethane (30 mL) was injected over membrane with surface -NH_2 groups under N_2 at room temperature and left for 2h. The membrane was washed with dichloromethane followed by absolute ethanol, and dried under a stream of N_2.

2.4.4.2.2 Poly(*N*-isopropylacrylamide) brush growth

The polymerization was carried out using aqueous ATRP as reported in literature with slight modifications. Briefly, NIPAAM (2.5 g, 22.1 mmole) was dissolved by stirring in 5 mL of methanol and 5 mL of water at room temperature. To this solution pentamethyldiethylenetriamine (0.138 g, 0.8 mmole) was added. The mixture was stirred and degassed by N_2(g) bubbling for an hour before Cu(I)Br (0.032 g, 0.22 mmole) was added. The mixture was degassed with N_2(g) bubbling for another 15 minutes. The membrane was sealed in a Schlenk tube and degassed by four high-vacuum pump/N_2(g) refill cycles. The reaction mixture was syringed into this Schlenk tube, adding enough to cover the membrane completely, and the mixture was left overnight under N_2(g). The samples were removed and thoroughly rinsed with deionized methanol and water.

2.4.4.3 Functionalization with Poly(4-vinyl pyridine)

2.4.4.3.1 Anchoring of 4,4′-azobis(4-cyanopentanoic acid)

PET membranes containing single cylindrical aminated nanochannels were first functionalized with initiator by following the same procedure as described above (section 2.4.4.1).

2.4.4.3.2 Poly(*4-vinyl pyridine*) brush growth

In a 50 mL Schlenk flask, 8 g of the 4-vinylpyridine (previously passed through basic alumina) was dissolved in 10 mL of ethanol. The solution was degassed by N_2(g) bubbling for 1h. The initiator functionalized single cylindrical-nanochannel membrane was sealed in a Schlenk tube and degassed (4 × high vacuum pump/N_2 refill cycles). The monomer solution was syringed into this Schlenk flask adding enough liquid to fully cover the membrane. The flask was immersed in an oil bath preheated to 65 °C. The polymerization was carried out at 65 °C for 45 min. The PVP modified nanochannel membrane was then removed from the polymerization solution and thoroughly rinsed with ethanol. The poly-4-vinylpyridine brush grafted membrane was stored in water till further use.

3. RESULTS AND DISCUSSION

3.1 Modifying the Surface Charge of Single Track-Etched Conical Nanochannels in Polyimide

3.1.1 Introduction

Synthetic nanochannels are currently considered as promising candidates for a variety of applications, including separation techniques and biological sensing. The latter includes electrical or optical detection and analysis of single molecules passing through an individual channel (DNA analysis has been the most explored application to date, reviewed in,[90] but there is ongoing work on other biomolecules also),[18,38,91-93] as well as exploring changes in the channel's transport properties due to specific interactions of analytes with the channel's surface (to avoid confusion, here we use "channel surface" to mean the surface within the channel, as opposed to the surface of the membrane in which the channel is contained). The properties of these surfaces are crucial for all the above mentioned applications, since they influence the channel's transport properties (e.g. hydrophobicity, permselectivity), and chemical groups on the inner channel walls may serve as binding sites for analytes[38] as well as interact with molecules passing through the channel and thereby influence their translocation.[16,94,95] Therefore, it is of highest interest to be able to control the channel wall properties, i.e., to functionalize the walls to achieve desired interactions with molecules of interest, which is still a challenge for current nanochannel production techniques.[96]
A variety of different substrate-specific methods have been published to modify the surface of track-etched nanochannels.[28,29,37,38,47,51,63,97] One method applicable for track-etched polymer membranes is to cover the surface and channel walls with gold by electroless plating[98] and subsequently change the surface properties of these nanotubes, e.g., by chemisorption of thiols.[34, 37] Thus, molecular recognition agents can be attached to the inner surfaces of these nanotubes, which, e.g., allow the binding of specific proteins[38] to be detected by the changes they cause to the tubes' ionic transport characteristics.

However, this gold plating step can be eliminated by directly chemically modifying the functional groups on the channel surface, which in addition allows more stable covalent attachment of the desired molecules. In polyimide (PI), these functional groups are mainly carboxyl (-COOH) moieties, created during the track-etching process.[69] They can be modified using standard chemistry by a variety of methods, such as alkylation, methylation or amidation. Up to now, work concerning the chemical functionalization of track-etched channels focused mainly on polyethylene terephthalate (PET), which also possesses carboxyl groups on the surface. For example, alkylation[56-58] of these groups was carried out with alkyl bromide in the presence of KF as a catalyst. Methylation[99] was accomplished by treating the track-etched membranes with diazomethane, and the amidation[60,100] was achieved by first activating the carboxyl groups with carbodiimide and subsequent reaction with amine. However, many of these methods involve the use of organic solvents, which might affect the polymer and therefore the geometry of the channel. This is of minor importance for relatively large channels, but becomes crucial when going down to nanometer sizes, where it is necessary to use only water and ethanol soluble reagents. Vlassiouk and Siwy[63] recently used this approach to selectively amidate the carboxyl groups in ~2.5 nm diameter PET nanochannels, creating an ionic diode. Our work involved similar amidation of PI nanochannels by using EDC/NHS coupling chemistry.

The single conical nanochannels studied here were prepared in PI foils, with an opening of only a few nanometers on one side, similar to those which have recently been used successfully for the detection of DNA molecules.[101,102] These channels are characterized by asymmetric *I-V* curves, which originate from electrostatic interaction of the channels charged surfaces with the ions passing through them.[71,73,103,104] As explained in the cited articles, at neutral and basic pH, the channel walls are negatively charged due to ionized carboxyl groups ($-COO^-$), which in combination with the conical shape of the channel leads to an asymmetric intrinsic electrostatic potential along the channel axis. The latter process causes different dependences of the anion and cation concentrations within the channel on the applied voltage and therefore rectify the ionic current passing through them. At acidic pH, the carboxyl groups become protonated (-COOH) and the channel walls become neutral, resulting in the loss of rectification. The presence of surface charge at a particular pH is therefore indicated by a rectifying *I-V* curve.[32]

3.1.2 Results and discussion

The single conical nanochannels were fabricated in 12 μm thick polyimide membranes, following the etching procedure described in chapter 2 (section 2.2.2). As a result of asymmetric chemical etching, carboxyl groups were generated on the surface of these nanochannels (3.1.1a). These carboxyl groups were converted into *N*-hydroxysuccinimidyl esters by reacting with an aqueous solution containing *N*-(3-dimethylaminopropyl)-*N*-ethylcarbodiimide (EDC) and *N*-hydroxysuccinimide (NHS) as an activating agents.

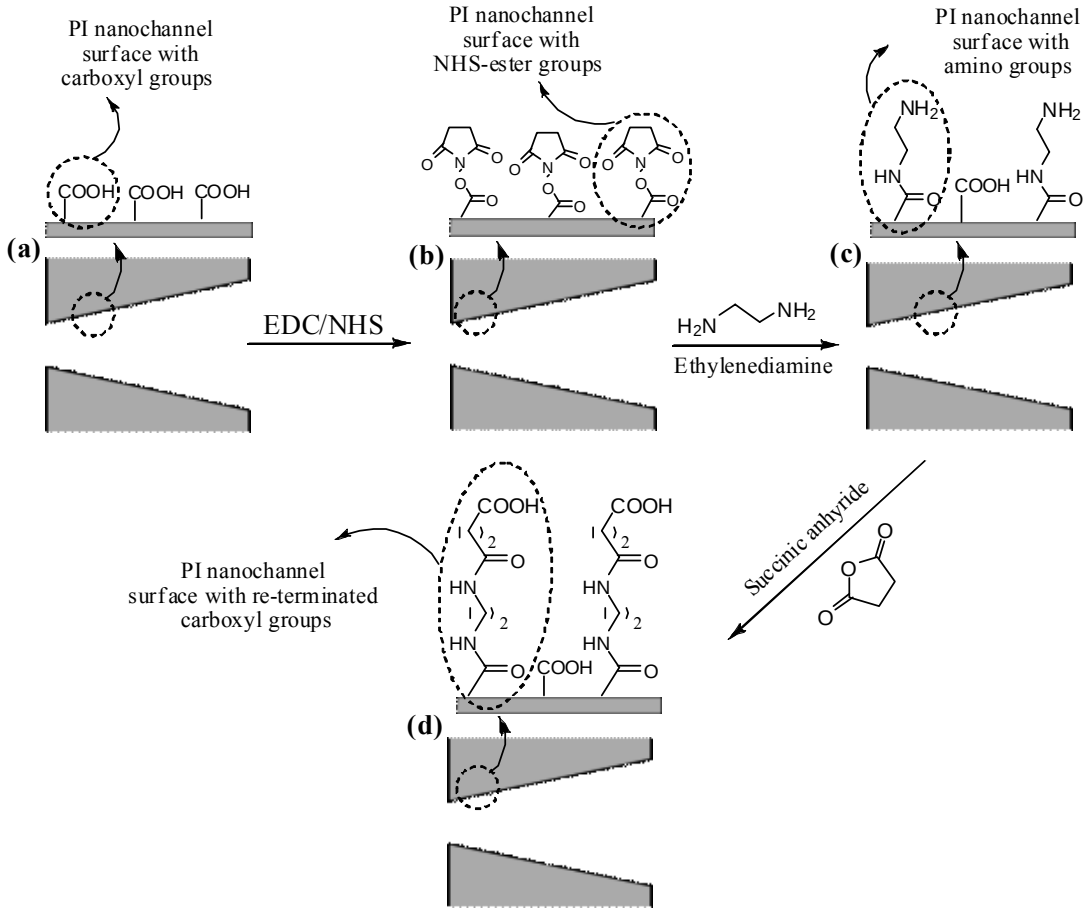

Figure 3.1.1: Schematic representation of chemical modification of the channel surface (a) carboxyl groups into (b) amine- reactive NHS-esters, (c) terminated amino groups, and (d) re-termination of amino groups into carboxyl moieties.

The carboxyl groups were first reacted with EDC, forming an amine-reactive *O*-acylisourea intermediate. This intermediate is susceptible to hydrolysis, making it unstable and short-lived in aqueous solutions. Therefore, these activated intermediate esters were subsequently replaced by

NHS-esters. The use of NHS is the main difference between the method described here and that of Vlassiouk and Siwy,[63] and its addition stabilizes the intermediate by converting it to more stable amine-reactive NHS-ester (Figure 3.1.1b**)**, which would thus be expected to increase the efficiency of EDC-mediated coupling reactions. These NHS-esters have sufficient stability and subsequently react with ethylenediamine to yield amide bonds with surface carboxyl groups.[105, 106] This results in the modified channel surface with terminated amino groups (Figure 3.1.1c). In addition, NHS allows controlled two-step modifications where the molecule to be attached containing both carboxyl and amino groups, not possible otherwise as EDC, would link those molecules into chains. The terminal $-NH_2$ groups were later treated with a saturated solution of succinic anhydride (SA)[63,107] in order to attach carboxyl-terminated groups (Figure 3.1.1d). The detailed reaction procedure was described in chapter 2 (section 2.4.2).

To verify the success of the procedure, *I-V* curves of unmodified and channels modified with ethylenediamine and succinic anhydride were recorded in 0.1 M KCl at pH 7 and pH 2. The pH was adjusted by addition of HCl or NaOH. It has been shown experimentally and theoretically for conical polymer channels as well as for asymmetric nanopipettes that reversing the surface charge of these systems results in the reversal of the preferential direction of ionic transport, i.e., the rectification.[28,37,72,108] Therefore, the direction of rectification is an indicator of the polarity of the charges on the channel walls, and its magnitude depends on the surface charge density (i.e. more highly-charged channels rectify the ionic current more). Therefore, measuring the *I-V* characteristics before and after modification allows the success of the modification reaction to be confirmed.

At pH 7, before modification, the conical channels with fixed negative surface charge due to the ionized carboxylate ($-COO^-$) anions, rectifies the ionic current with the preferential direction of the cation flow from the small opening towards the wide opening of the channel. At pH 2, the carboxyl (-COOH) groups become protonated and diminish the charge on the surface of the channel. The neutral channel is no more selective for ions. The cations and anions flow equally from both sides, and as a result, a linear current-voltage curve was observed as shown in Figure 3.1.2a.

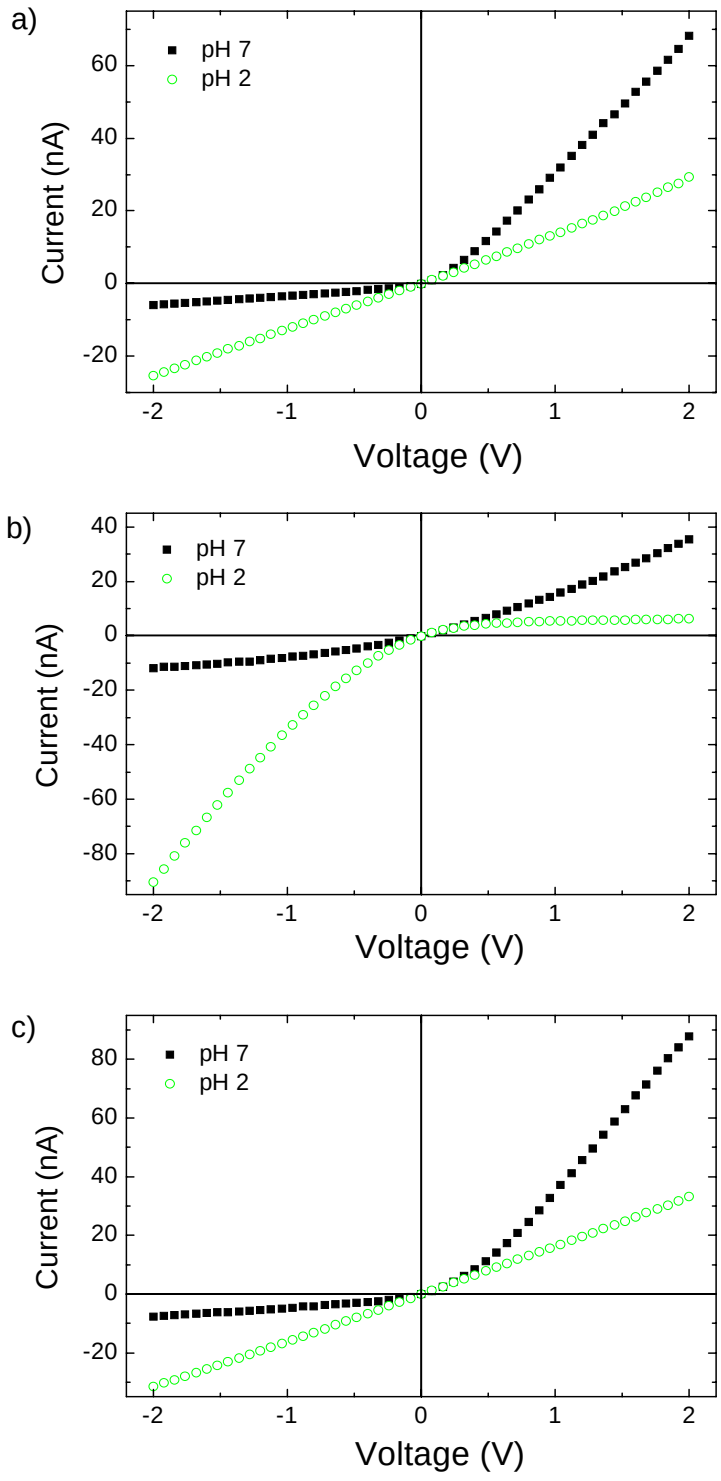

Figure 3.1.2: pH dependence of the *I-V* curve with 0.1 M KCl of a polyimide channel with $d \sim 64$ nm and $D \sim 1.57$ µm, where d and D are the diameters of the small and large openings of the conical channel, respectively. (a) Before and (b) after the modification with ethylenediamine, and (c) after the modification with succinic anhydride.

At acidic pH, the direction of rectification reverses for the modified channels due to the protonated amino groups and the un-reacted carboxyl groups becomes neutral. This renders the surface and channel walls positively charged. As a result, the channel now becomes anion selective and inversion of rectification has occurred (Figures 3.1.2b and 3.1.3b). This is expected in the case of a successful modification reaction, since at acidic pH the channel becomes positively charged due to protonation of the amino ($-NH_3^+$) groups.

Regeneration of terminal carboxyl groups (-COOH) on the channel surface was then achieved by reacting the amino groups with succinic anhydride. This restored the behaviour of the conical nanochannel, observed before modifying the surface charge (Figure 3.1.2c and 3.1.3a, b).

After modification with ethylenediamine, the channels still rectify the ion current at neutral pH, but to a much lower degree, presumably due to some carboxyl groups remaining unmodified. As shown in Figure 3.1.3, the degree of rectification is quantified as the ratio of positive to negative current at a given voltage, symbolized by *V*.

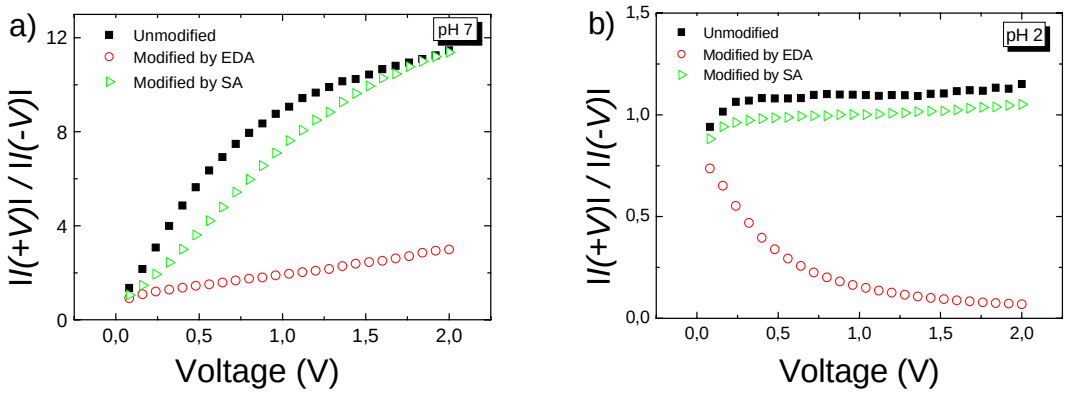

Figure 3.1.3: Degree of rectification calculated from the data shown in Figure 3.1.2. After modification with EDA, the channel shows a much lower degree of rectification for pH 7 (a) and reverse rectification (values below 1) at pH 2 (b). Treatment with succinic anhydride essentially restored the initial behaviour.

In addition to this study of *I-V* characteristics, selectivity measurements were also performed to further verify the success of the modification reactions. Nanometer-sized charged channels are permselective, i.e. they preferentially transport ions of opposite charge to those on the channel walls.[109] The higher the surface charge density for a given geometry, the higher the so-called transference number t_i , which is defined as

$$t_i = \frac{I_i}{I_{tot}}, i = +,- \qquad 3.1.1$$

where I_i is the current carried by the ionic species i, and I_{tot} is the total measured current.
This transference number can be determined experimentally by exposing the membrane to an electrolytic concentration gradient and measuring the resulting reversal potential V_{rev}, i.e. the potential required to balance the ionic flow driven by the concentration gradient. The channel's transference number, in this case for cations, is given by[110]

$$t_+ = \frac{1}{2}\left[1 + \frac{F}{RT}\frac{V_{rev}}{\ln(c_1/c_2)}\right] \qquad 3.1.2$$

where c_1 and c_2 are the concentrations on either side of the membrane, and R, T and F are the universal gas constant, the temperature in Kelvin and the Faraday constant. Therefore, the higher the measured potential, the higher will be the channel's transference number and so also its charge density. The reversal potential can be obtained by recording I-V curves under asymmetric electrolyte conditions, where it is the potential for zero current.
It is known from previous studies[70,74] that the selectivity of conical nanochannels in polymers depends not only on the degree but also on the direction of an applied concentration gradient. The selectivity and therefore the reversal potential is higher when the lower concentration is applied on the side facing the channel tip, because the observed transport properties are dominated by what happens at the channel tip, since the transported ions have the greatest interactions with the surface there, and at lower concentration the screening effect of solution cations on the surface charges is reduced, so these interactions are stronger. Therefore, a configuration where the lower concentration is facing the tip side of the channel was used here, which leads to higher reversal potentials and thus facilitates measurements. Concentrations of 0.01 and 0.1 M KCl at pH 7 and pH 2 were used, creating a tenfold concentration gradient. The results of these measurements are shown in Figure 3.1.4.

The reversal potential for the unmodified channel was 47 ± 3 mV at pH 7, indicating a strong cation selectivity (the theoretical value for a completely selective channel is given by the Nernst equation[1]

$$V_{rev} = \frac{RT}{zF}\ln\frac{c_1}{c_2} \qquad 3.1.3$$

as 59 mV for a tenfold concentration gradient). After modification, this value was reduced to 18 mV, in agreement with the observed reduced rectification, both indicating a lower surface charge density. For pH 2, the channel does not show any selectivity, as expected from the linear *I-V* curves measured under these conditions. After treatment with EDA, the sign of the reversal potential was reversed, indicating that indeed the surface charge was modified. The fact that the absolute value of V_{rev} is much lower than that for the initially unmodified channel could result from the fact, that not all carboxyl groups have been converted in this case.

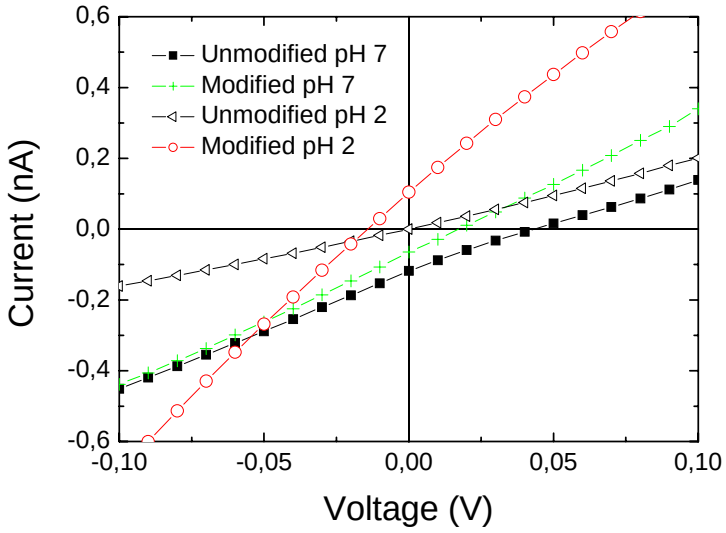

Figure 3.1.4: Sections of *I-V* curves recorded under a tenfold concentration gradient with 0.1 M KCl on the large and 0.01 M KCl on the small side of the channel, before and after modification with EDA, for pH 7 and pH 2. The dimensions of the channel were $d \sim 30$ nm and $D \sim 1.4$ µm. The reversal potential (potential for zero current) is reduced by the modification from 45 to 18 mV for pH 7 and changed its sign after the modification for pH 2 (-14 mV), indicating a significant change in the surface charge, which is now slightly positive.

It has to be noted that the high degree of rectification observed here for channels with several tens of nanometers in diameter is not explained by any of the existing theoretical models and was not observed for PET channels with small opening greater than 15 nm in diameter.[73] However, a similar effect has been observed for asymmetric channels in PET produced by surfactant-controlled etching which hindered etching close to the surface of the foil.[88] There, it was speculated that swelling of the polymer in the wet state may have reduced the channel diameter, which was determined in the dry state. This can be ruled out in our case, since the diameter was

determined in the wet state, however, it could be possible that the channel shape deviates from an ideal cone and therefore the real diameter is smaller than the one given here. On the other hand, the current models may not be fully describing the experiments and therefore possibly need to be extended.

3.1.3 Conclusion

The aim of this study was to directly chemically modify the functional groups on the walls of track-etched PI nanochannels. This modification was accomplished by activating those carboxyl groups with EDC and NHS, followed by covalent coupling of ethylenediamine. The resulting amino terminal groups could be further reacted with succinic anhydride in order to attach terminated carboxyl groups (-COOH), restoring the original behaviour. The success of this reaction was confirmed by current-voltage (*I-V*) measurements as well as measurements of the channel's permselectivity. Both methods indicate a negative surface charge before modification, which becomes positive afterwards.This successful study is an important step towards the ability to modify track-etched nanochannel surface properties at will. The method presented here extends the previous approach to provide more efficient modification, and also allows controlled attachment of molecules containing carboxyl groups, not possible previously. Potentially, any molecule containing primary amino groups can be attached to the surfaces of these channels, for example to cause strong interactions with specific molecules, as will be necessary for many types of nanopore-based biosensors.

3.2 Fabrication and Functionalization of Single Asymmetric Nanochannels for Electrostatic/Hydrophobic Association of Protein Molecules

3.2.1 Introduction

Synthetic nanochannels have a large potential in biotechnology, where they can be applied, e.g., as sensors for biomolecules,[54,111-114] detectors and analyzers of DNA analytes,[67,90,94,96,97,101,115-120] and for the separation of molecules.[55,121] For all these applications, it is important to understand the channels' ionic transport characteristics and to be able to influence them at will, depending on the desired application. In this context it is highly desirable to control the channel-surface properties, i.e. to functionalize the surface in order to match specific requirements concerning hydrophobicity, selectivity, and interactions with various biomolecules.

Track-etched channels are a type of synthetic nanochannels that are produced by heavy-ion irradiation and subsequent track etching of polymer membranes. These channels are produced in a variety of polymer films, allow the control of size and shape, and are stable as well as easy to handle. Recently, conical track-etched channels[30,32] have been used successfully for the detection of biomolecules.[96,101] Previous studies also showed that thiol-functionalized gold nanotubes, prepared in track-etched nanochannels, have been employed for the detection and analysis of a variety of biomolecules.[34,38,68,122] Moreover, the surface charge of these nanochannels has been manipulated by the direct covalent coupling of diamine with the carboxyl groups present on the channel surface after chemical etching.[63,123] The nanochannels have been functionalized selectively with specific polymers for the separation of small molecules on the basis of their size, charge, and hydrophobicity.[55]

Bovine serum albumin (BSA), isoelectric point (*pI* 4.7),[124] has become the subject of intensive research activities during recent years because of its structure, which undergoes conformational changes very easily by altering the pH value.[125] There exists also some studies, where nanochannels have been used for the sensing and characterization of BSA protein molecules.[112, 113,122]

Single conical track-etched nanochannels in polymer foils are a well-studied system suitable for sensing experiments and can be used as biomimetic sensors. For this purpose it is important to be able to control the channel shape as precisely as possible. These channels are usually produced by etching in a conductivity cell from one side, while the other side is exposed to a neutralizing solution. During the etching process the current is constantly monitored, so that as soon as current is flowing, which corresponds to the opening of the channel, the etching process can be interrupted. Longer etching leads to an increase in the current, corresponding to an enlargement of the channel. This method has been refined recently to control the tip diameter of PET channels even more precisely by applying a two-step etching process: first etching is stopped shortly before the breakthrough. Subsequently, the process is finished by inserting an etching solution on both sides of the membrane.[126] This avoids problems in precisely determining the ionic current that arise from mixing of the etchant and stopping solutions.

Another method for the fabrication of nanochannels was developed by Apel *et al*.[88] It consists of sensitizing one side of the polymer membrane by long-time UV irradiation and adding a surfactant to the etching solution which is placed on both sides of the polymer membrane. The surfactant protects the channel opening on the non-UV-treated side from the direct attack of etchant, and hence bullet-shaped channels can be produced while etching from both sides. These channels, which have either slightly or highly tapered geometry, exhibit diode-like current-voltage characteristics similar to those produced by the one-side etching method.[33] Recently, P. Ramírez *et al.* have presented a theoretical model to explain the influence of tip shape on the rectification properties of the synthetic nanochannels having fixed charges on their surface.[127]

Here, an additional approach to reproducibly fabricate asymmetric channels in PET membranes is reported. It employs also a long-time UV irradiation from one side but, in contrast to the method developed by Apel *et al*., the surfactant is employed only on the non UV treated side, while the UV-sensitized side is in contact with the pure etchant. This method yields a significantly better reproducibility than the one-side etching. Additionally, the choice of the etching conditions (increased temperature and enhanced surface wetting due to the surfactant) leads to a much faster process (in the order of a few minutes as compared to hours).

The surface charges and hydrophilicity of these channels were manipulated by the selective functionalization of the carboxyl groups, present on the channel surface after etching, using EDC/PFP coupling chemistry.[128,129] The unmodified carboxylated (negatively charged), amino functionalized (positively charged) and alkyl functionalized (hydrophobic) nanochannels were

used for the electrochemical sensing of bovine serum albumin (BSA) protein. The BSA molecule, isoelectric point (*pI* 4.7), is negatively charged at neutral and positively charged at lower acidic pH values. Therefore, we investigated the effect of electrostatic/hydrophobic association of BSA on the channel wall as a function of rectifying characteristics of the channels by variation of the pH value.

3.2.2 Results and Discussion

Single asymmetric nanochannels studied here were produced in 12 µm thick polyethylene terephthalate (PET) membranes by the surfactant-controlled track-etching technique described in chapter 2 (section 2.2.3). While the *I-V* curves of the channels produced here resemble those of conical channels etched conventionally with a stopping solution, they show however different characteristics during the etching and in time-resolved current traces. Traditional conical channels in PET are known to show current fluctuations at different stages: First, the current signal recorded during the etching usually exhibits a sudden height increase followed by a period with no further growth but a lot of fluctuations instead of an ideal quadratic rise for longer etch times. Second, the current-time traces of these PET channels exhibit current fluctuations similar to those of biological ion channels.

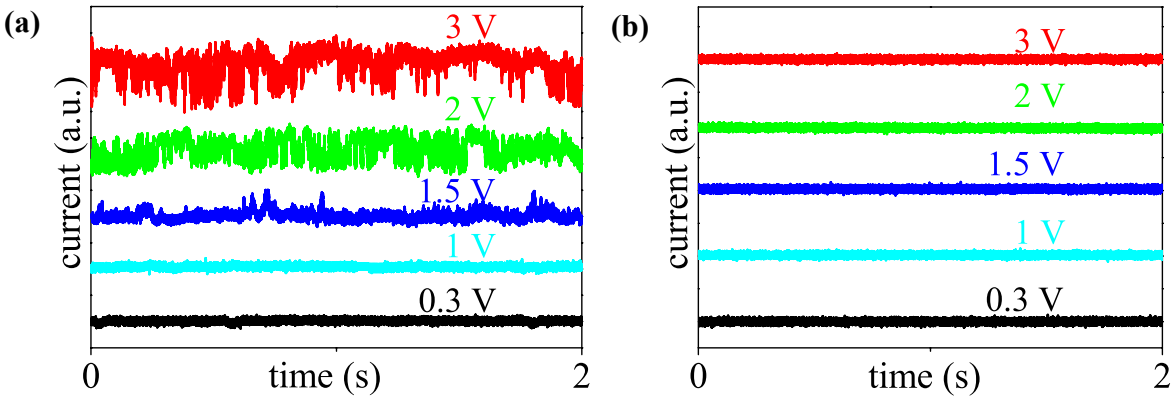

Figure 3.2.1: Current fluctuations in a single nanochannel in PET in dependence on the applied voltage, measured with 0.1 M KCl (a.u. refers to abitrary units). (a) one-side etching, tip diameter ~ 2 nm, (b) surfactant-controlled etching, tip diameter ~ 8 nm.

In contrast, the channels produced here show none of these fluctuations. Their etch curves (Chapter 2, Figure 2.10b) exhibit the expected quadratic increase and are in general much more reproducible than those of conventional etching. From the graphs it is also obvious that, due to the increased temperature and the chemical attack on the track from both sides, the etching time is drastically reduced. Together, these two facts make the described etching technique much more suitable for routine channel production. A comparison of voltage dependent current-time curves for channels etched from one side only and with the surfactant aided method is presented in Figure 3.2.1.

As presumed already earlier,[30] the fluctuations observed after the breakthrough originate probably from chemical reactions occurring during the neutralization of the etchant by the stopping solution.

The fluctuations taking place in the time-resolved current traces have been attributed to so-called 'dangling ends' – short polymer chains ending in carboxyl groups, which "dangle" from the channel wall, and can shortly block the current by moving in and out of the small tip region.[33]

The fact that by replacing the neutralizing solution, which consists normally of 1 M HCOOH + 1 M KCl, by pure KCl, one can obtain an etching curve with less fluctuations, gives an additional hint towards the above explanation. Also, asymmetric channels in polyimide fabricated by a similar method, show regular etch curves, probably due to less effective chemical reaction between the etchant (12.5 % NaOCl) and stopping solution (1 M KI).

However, channels in polyimide also do not exhibit ion current fluctuations,[69] suggesting that these two phenomena are somehow related. Polyimide has a different chemical structure consisting of aromatic rings, which would not allow the production of dangling polymer chains.

Since, with the other etching technique used for PET, the current fluctuations vanished, a slightly different explanation can be taken into consideration. Moreover, the PET membranes used here consist of a mixture of crystalline and amorphous regions. Therefore, it is conceivable that during the one-side etching the opening of the channel does not progress linearly and smoothly, but sometimes bigger chunks of the material are detached, which can then shortly block the emerging channel before they are removed completely. If such pieces remain in the channel after completion of the etching process, they could also cause fluctuations similar to the dangling polymer chains. By contrast, polyimide is a fully amorphous material where such effects are unlikely.

Consistently with the presumptions stated above, the improved behaviour of the channels etched with surfactant can be attributed to the etchant, being in this case applied from both sides. This might help opening the tip of the channel, where also the removal of etching products and "chunks" of polymer is aided. Furthermore, the solutions in both compartments of the conductivity cell consist basically of the same chemical (the surfactant is negligible) so that chemical reactions can not take place between them.

Figure 3.2.2 showed a typical current-voltage characteristic obtained for a single channel etched by the method described above. *I-V* curves were measured by applying triangular voltage sweeps of low frequency to avoid capacitance effects. It can be seen that the channel exhibits a very stable current signal over several voltage sweeps.

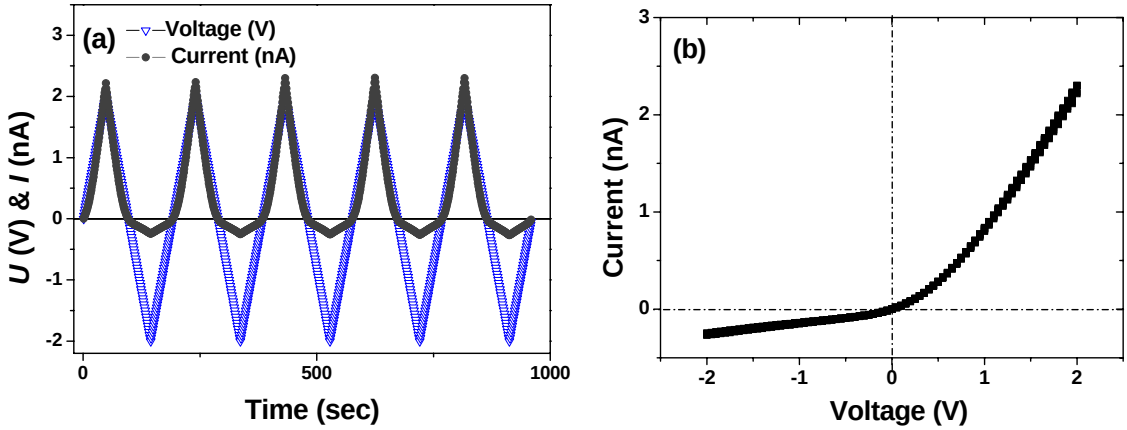

Figure 3.2.2: Representation of (a) applied voltage and ion current record, (b) current-voltage characteristic of a single PET channel with $d \sim 8$ nm and $D \sim 320$ nm in 0.1 M KCl solution.

A change in the surface charge of the channel can be detected by an alternation in the rectification characteristic. A positively charged channel rectifies the current oppositely to a negatively charged one.[63,123]

The carboxyl groups (–COOH), generated on the channel surface, were converted into amine-reactive pentafluorophenyl (PFP) esters by the reaction of pentafluorophenol in the presence of *N*-(3-dimethylaminopropyl)-*N*-ethylcarbodiimide hydrochloride.[129,130] The PFP-esters are ~10 times more active as compared to the amine-reactive NHS-ester.[131] Therefore, the activation of the carboxyl groups was done with PFP-esters which lead to higher efficiency of the modification reactions. These PFP-esters were further covalently coupled with ethylenediamine or

propylamine in order to obtain amine (–NH_2) and alkyl (–C_3H_7) terminated groups on the channel surface, respectively, for the manipulation of surface charge and hydrophilicity (Figure 3.2.3). The detail of the experimental procedure was described in chapter 2 (section 2.4.2)

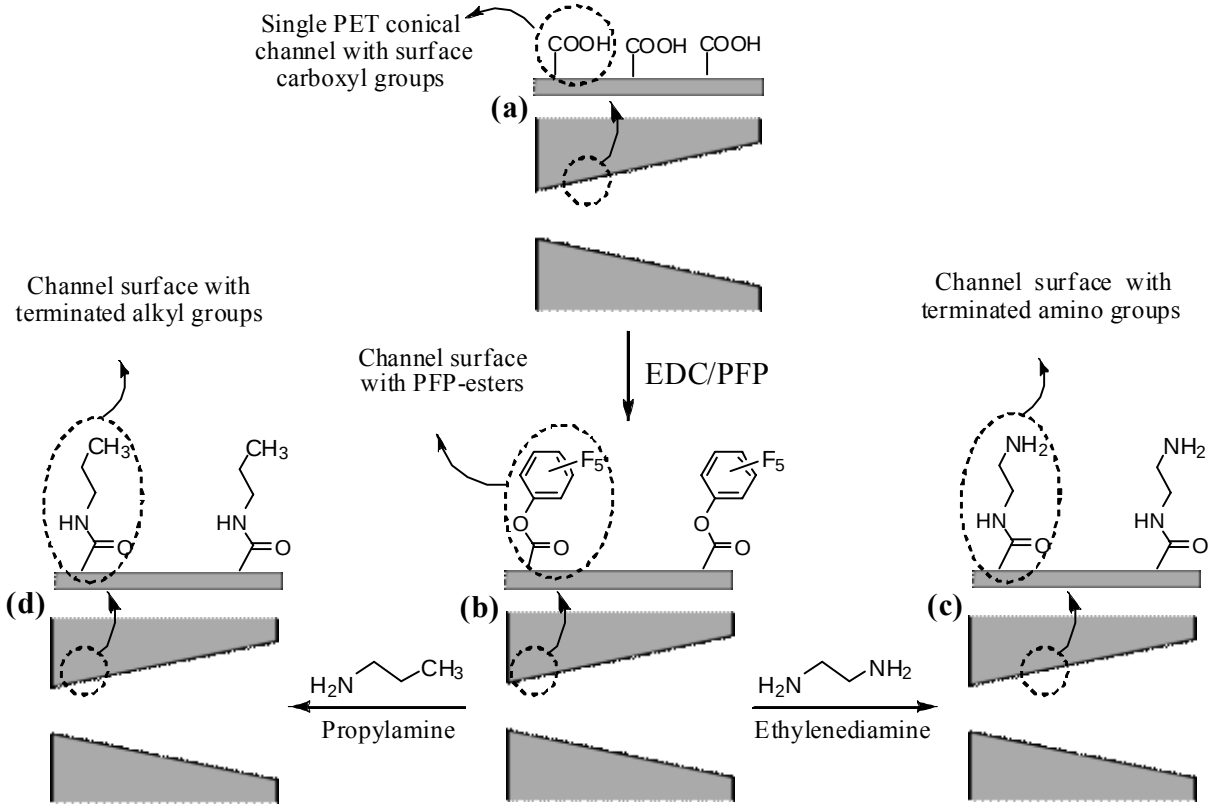

Figure 3.2.3: Schematic representation of the conversion of channel surface carboxyl groups (a) into reactive PFP-esters (b), which were further converted into terminated amino groups (c), and alkyl groups (d).

Before modification at pH 6.5, the channels rectify the ion current, as shown in Figure 3.2.4 (black circles), due to the presence of anionic carboxylate (–COO^-) groups. The rectification behaviour is reversed when the channel was modified with ethylenediamine, because it becomes positively charged due to the protonation of terminal amino (–NH_3^+) groups (Figure 3.2.4a). When the carboxyl groups are coupled with propylamine, the channels exhibit a linear *I-V* characteristic due to terminal nonpolar propyl group (-C_3H_7), as shown in Figure 3.2.4b. In this case, the channel surface becomes neutral and hydrophobic. The success of the modification reactions was also confirmed by selectivity measurements. The unmodified channels are cation selective at neutral pH, as measured by the reversal potentials (+44 mV) for a ten-fold concentration gradient (0.1 M KCl on the base side and 0.01 M KCl on the tip side of the

channel). The channel shows a negative (-22 mV) and zero (0 mV) reversal potential when the channel surface was modified with ethylenediamine and propylamine, respectively.

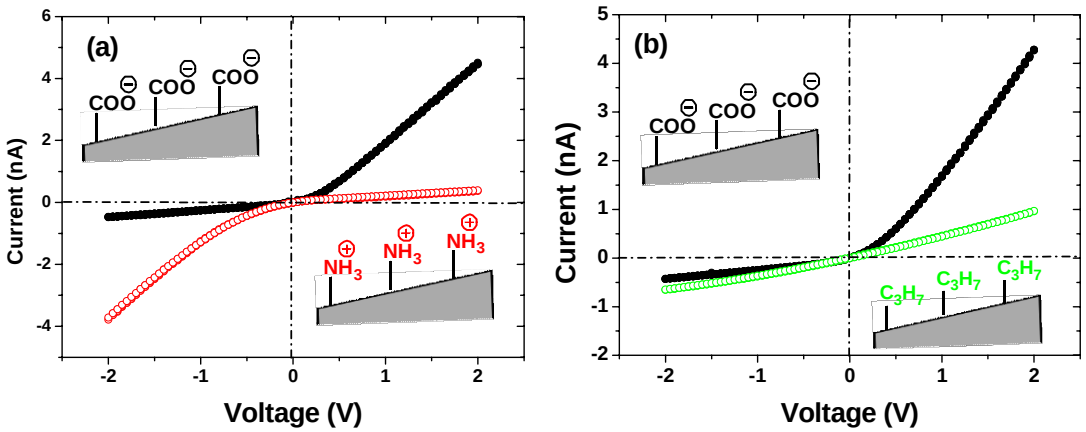

Figure 3.2.4: *I-V* characteristics of PET single asymmetric channels in 0.1 M KCl at pH 6.5, before (●) and after modification, (a) with ethylenediamine (○) having $d \sim 18$ nm, and (b) with propylamine (○) having $d \sim 16$ nm, respectively.

The track-etched PET membranes have an isoelectric point (pI = 3.8),[132] and the nanochannel shows hydrophilic behaviour due to the presence of ionized carboxylate ($-COO^-$) groups at neutral pH.[133] In order to observe the influence of BSA on the rectification behaviour, an electrolyte consisting of 0.1 M KCl and 100 nM BSA was placed on the side, facing the tip opening of the channel at different pH values. At pH 6.5, BSA is negatively charged and does not show any effect on the rectification behaviour of the channel (Figure 3.2.5a). This effect can be explained in the following way: Firstly, there exists an electrostatic repulsion between the channel surface and the BSA molecules because both are negatively charged at pH 6.5. Additionally, these hydrophobic protein molecules did not show any affinity toward the hydrophilic surface of the channel. Therefore, an additional repulsion occurs between them.[134]

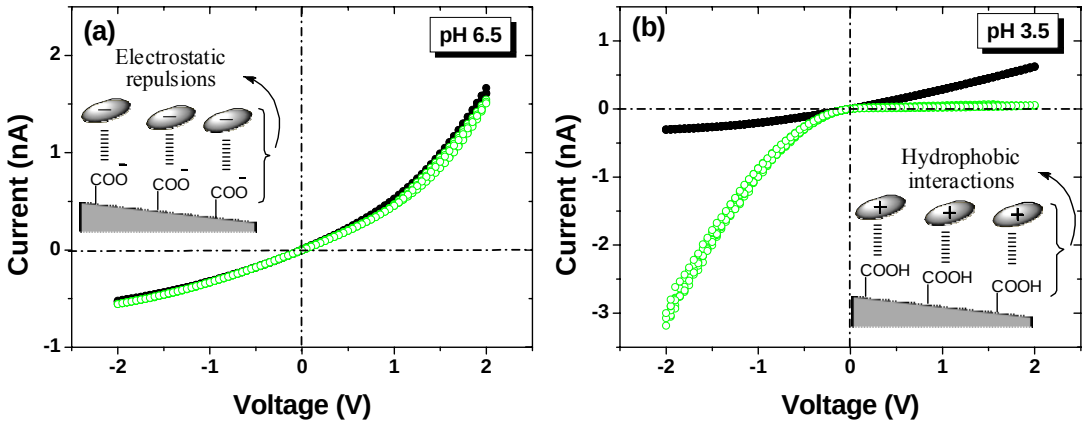

Figure 3.2.5: Current-voltage characteristics of a carboxylated PET channel in 0.1 M KCl having d ~ 10 nm and D ~ 288 nm, prior to (●) and after (○) the addition of 100 nM BSA, (a) at pH 6.5, (b) at pH 3.5.

At pH 3.5, the unmodified channels behave neutral and hydrophobic due to the protonation of the carboxyl groups (–COOH), which results in the loss of rectification and in a linear *I-V* curve. At such an acidic pH, the BSA is positively charged and hydrophobic in nature. Therefore, these protein molecules can readily adsorb on the hydrophobic channel surface[134] and impart positive charge, which leads to the inversion of rectification as expected for a positively charged surface. This is shown in Figure 3.2.5b.

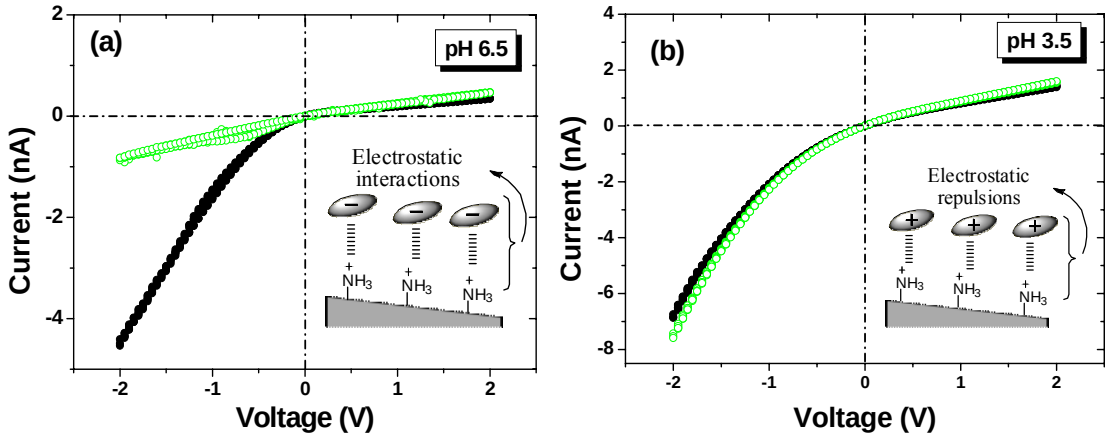

Figure 3.2.6: Current-voltage characteristics of an aminated PET channel in 0.1 M KCl having d ~ 25 nm and D ~ 315 nm, prior to (●) and after (○) the addition of 100 nM BSA, (a) at pH 6.5, (b) at pH 3.5.

A reverse effect of BSA is observed for a channel modified with amino groups. At pH 6.5, the aminated channel surface becomes positively charged (due to the protonated amino groups) and rectifies the ion current in the opposite direction as compared to the negative one. When this

nanochannel is exposed to negatively charged BSA, the protein molecules adsorb electrostatically on the positively charged channel. This effect shields the surface charge and neutralizes the channel surface. The inverse rectifying behaviour of the channel is lost, which results in a linear current-voltage curve as shown in the Figure 3.2.6a. However, at acidic pH 3.5, the BSA molecules are not adsorbed on the channel surface due to electrostatic repulsion. Therefore, the inverse rectification behaviour of the channel was not affected after the introduction of protein molecules as shown in the Figure 3.2.6b.

However, there is another way to confirm the hydrophobic association of BSA, where one can obtain a nonpolar and hydrophobic channel surface by the conversion of carboxyl (–COOH) groups into terminated alkyl ($–C_3H_7$) groups. The channel surface becomes neutral due to the combined effect of nonpolar and hydrophobic behaviour of terminal propyl groups. Hence the *I-V* curve becomes linear, indicating that the channel no longer rectifies the ion current. Therefore, when the channel is exposed to BSA solution, the adsorption of protein molecules occurs readily on the hydrophobic channel surface. The adsorbed BSA molecules impart negative charge to the channel surface because these are negatively charged at pH 6.5. As a result, the channel starts rectifying (i.e. rectification characteristic of the channel was recovered) as expected for a negatively charged surface as shown in Figure 3.2.7.

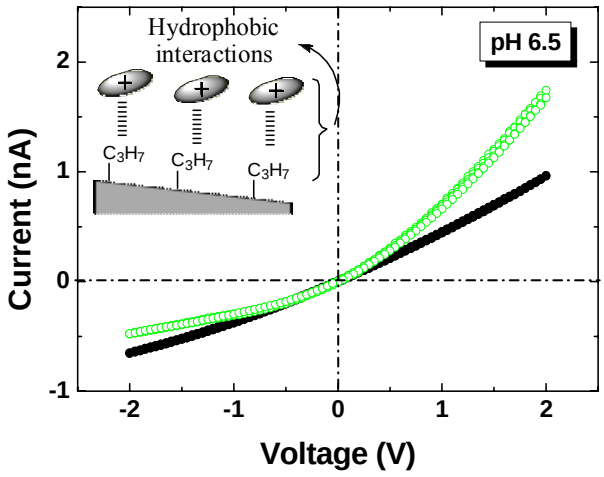

Figure 3.2.7: Current-voltage characteristics of a propylated PET nanochannel in 0.1 M KCl having d ~ 16 nm and D ~ 300 nm, prior to (●) and after (○) the addition of 100 nM BSA at pH 6.5.

For the experiments conducted here, separate polymer membranes with single asymmetric channels, were used for the above measurements before and after the chemical modification. It is

not possible to restore the original behaviour of the channel due to the adsorbed protein molecules on the channel surface even after several washings. As explained already above, the diameters can only be roughly estimated from the conductivity measurements based on the current flowing through the channels. Furthermore, the rectification of the ion current depends on the surface charge of the channel. However, the actual channel diameter does not play a crucial role in modification and electrochemical sensing experiments, since the success of the experiment can be derived from the comparison of the obtained *I-V* curves with those measured before using an unmodified channel. Yet, it is still difficult to make a quantitative statement regarding the current versus diameters of the nanochannels.

3.2.3 Conclusion

The etching method for the fabrication of asymmetric channels in PET has been refined. The new method yields channels with *I-V* characteristics similar to those produced with one-side etching, but is faster and more reproducible. Ion current fluctuations are neither observed during the etching process nor in the current-time traces of the final channel. The surface charge of the channel has been manipulated by chemical functionalization, and the success of the chemical reactions was proven by measuring both the rectification behaviour as well as the ion selectivity of the channel. The unmodified and modified channels were successfully subjected for electrochemical detection of BSA protein. This strategy constitutes a promising platform for the electrochemical sensing of biomolecules upon the variation of pH values.

3.3 Biosensing and Supramolecular Bioconjugation in Single Conical Polymer Nanochannels: Facile Incorporation of Biorecognition Elements into Nanoconfined Geometries.

3.3.1 Introduction

Ion channels are ubiquitous in nature and represent key elements in many important life processes, like energy production and storage or signal propagation and processing.[2,67,135] The generation of artificial ion channels have strong implications for developing new technologies related to materials and life sciences fields.[65,136] This explains the increasing interest in incorporating natural transport systems into artificial sensors, which could then exhibit the inherent sensitivity of biochemical systems.[137-139] However, maintaining a natural environment in an artificial device is such a difficult task, thus demanding the construction of fully and highly functional artificial systems[140-142] with the ability of mimicking natural systems. This challenging subject led to the creation of different strategies to obtain artificial architectures resembling the characteristics of ion channels or nanochannels commonly encountered in membranes of living systems.[22,63,97,143-148] These architectures, inspired by their biological counterparts, are commonly described as "solid-state nanochannels" and represent a valuable substitute to fragile lipid bilayer membranes in case of replacing the biological nanochannel with a fully *"abiotic"* equivalent.[31,34, 114,123,126,149] Recently, Siwy *et al.*[38] introduced a new type of protein nanobiosensor constituted of a single conical gold nanotube embedded in the polymeric membrane, thus creating an asymmetric nanochannel. The sensing read-out consisted of passing an ionic current through the nanochannels. Since the protein analyte and the channel mouth were comparable in size, binding of the protein led to the blocking of the nanochannel which was detected as a permanent blockage of the ion current.[38]

These experiments clearly revealed the critical role of the channel surface on achieving the desired functionality of the biomimetic system, thus considering that the chemical groups, incorporated on the inner channel walls, act as binding sites for different analytes as well as interact with molecules passing through the channel.

Nanoscale control over the surface properties of the channel wall plays a crucial role in the whole range of applications of solid-state nanochannels.[28,51,145,146] In order to achieve this goal, different methods to tailor nanochannel surfaces have been developed. One of the most widespread strategies applicable for track-etched channels in polymers was developed by Martin and co-workers and consists of covering the channel walls with gold by electroless deposition followed by the chemisorption of end-functionalized thiols.[150] This procedure enables the incorporation of molecular recognition elements into the inner channel wall of these nanotubes.[54] However, this gold plating step introduces another level of considerable complexity into the channel fabrication process. That is why it is highly desirable to design alternative strategies enabling the facile functionalization of the inner channel wall by directly exploiting the chemical functional groups already existing at the polymer nanochannel wall. For example, in the case of track-etched channels in polyethylene terephthalate (PET) films, the channel surface possesses carboxyl groups. It would also be very convenient if the method enables the incorporation of the chemical functionalities in the nanoconfined environment without requiring the use of solvents or chemicals that could be harmful or incompatible with the polymer channel or biological materials. In this context, considering the inherent surface charge of the channel wall, electrostatic assembly could be an extremely versatile route for incorporating chemical functionalities into the nanochannel without requiring complex chemical steps. In this work, we show that by using simple electrostatic self-assembly we can introduce binding sites into the nanochannel, which can then be used as recognition elements for creating a nanobiosensor. Moreover, the possibility of controlling the chemical functionalities and molecular recognition events inside the nanochannels, enabled us the facile construction of supramolecular bioconjugates inside the nanochannel.

3.3.2 Results and discussion

Single conical nanochannels were prepared by an asymmetric track-etching[30] process as described in chapter 2 (section 2.2.2) using heavy ion-irradiated polyethylene terephthalate (PET) foils. Track-etched channels on PET substrates possess carboxyl groups which are negatively charged under physiological pH conditions (pH 7.4). These moieties can act as sites for the electrostatic assembly of a positively charged building block. Considering that our goal was to electrostatically assemble the biorecognition elements on the channel wall, we created a

bifunctional macromolecular multivalent ligand[151-153], constituted of biotinylated poly(allylamine) (b-PAH), which was able to interact with the channel surface and expose the binding sites inside the nanochannel without hindering their recognition properties (Figure 3.3.1).

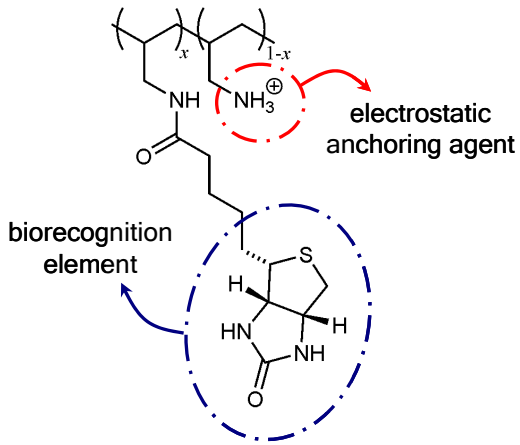

Figure 3.3.1: Chemical structure of the bifunctional polyvalent ligand used in this work to biotinylate the conical channel wall. $x = 0.21$.

The macromolecular characteristics of the bifunctional polyvalent ligand are due to the fact that having multiple sites, in the same molecule, to electrostatically interact with the channel wall, confers the system more stability enabling the facile functionalization of the channel surface. The nanochannels used in this work were single conical channels in PET, with an opening of only a few nanometres on one side, similar to those which have recently been used successfully for the detection of DNA molecules.[101,102] These channels were characterized by asymmetric current-potential (*I-V*) curves, which originate from the electrostatic interaction between the charged channel surface and the ions passing through them after setting up an electric field across the nanochannel-containing membrane.[70,154,155] In the case of PET, at neutral pH, the channel walls were negatively charged due to ionized carboxyl groups ($–COO^-$), (Figure 3.3.2), which in combination with the conical shape of the channel led to an asymmetric intrinsic electrostatic potential along the channel axis, causing different dependences of the anion and cation concentrations within the channel on the applied voltage.

This effect led to the rectification of the ionic current. As a consequence, the surface charges of the channel wall impacted on the rectifying characteristics of the nanochannel and provided insight into the nature of these charges. Figure 3.3.3 describes the rectifying characteristics of the PET nanochannel prior to and after assembling the bifunctional macromolecular ligand on the channel wall. The *I-V* curves for the carboxylated ($–COO^-$) channel surface described a well-defined rectifying behaviour, indicating that the nanochannel was acting as a rectifier of the ionic transport, which preferentially transports species of charges opposite to those on the channel walls.[70,154,155]

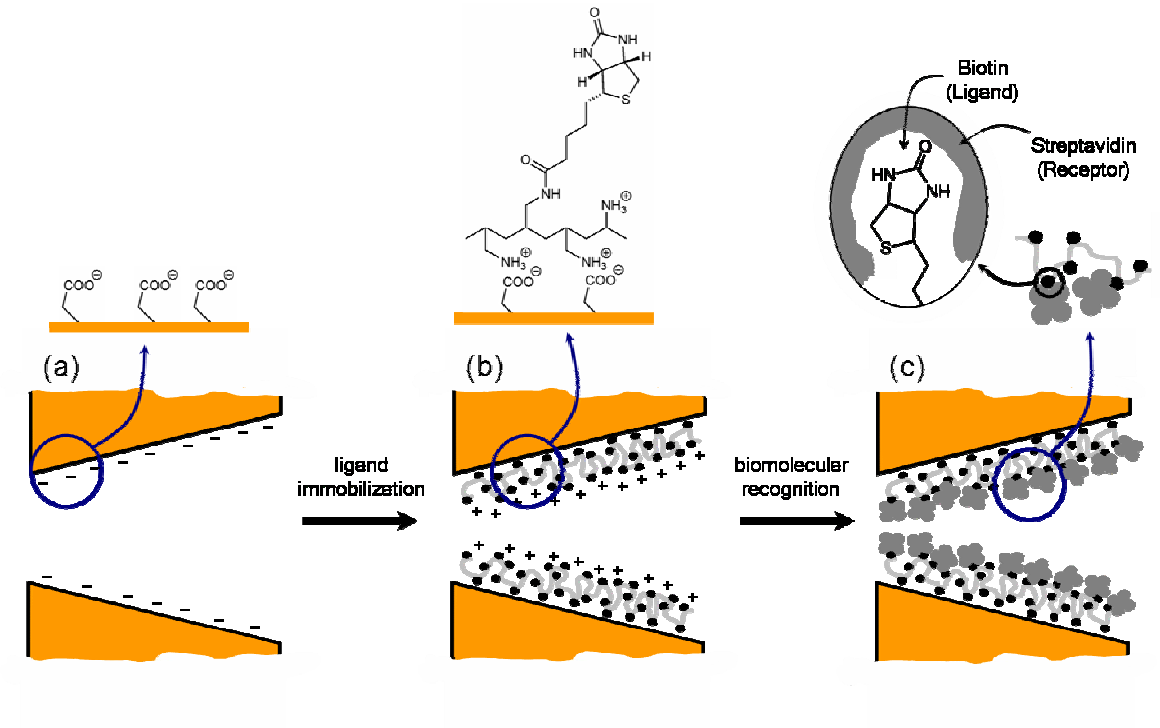

Figure 3.3.2: Simplified cartoon describing the incorporation of the biorecognition elements in the single conical nanochannel. The carboxylate-terminated nanochannel (a) is used as a platform for the electrostatic immobilization of the bifunctional macromolecular ligand, b-PAH (b). Then, the biorecognition event proceeds in the presence of the receptor (streptavidin) (c).

Assembling the b-PAH led to an immediate reversal of the rectifying characteristics (blue trace in Figure 3.3.3), indicating that the electrostatic anchoring promoted the reversal of the preferential direction of ionic transport. As is well-known, the direction of the rectification is an indicator of the polarity of the charges and the channel walls,[70,154,155] and its magnitude depends on the surface charge density. From Figure 3.3.3, it can be concluded that the assembly of b-PAH changed the polarity of the nanochannel from negative to positive.

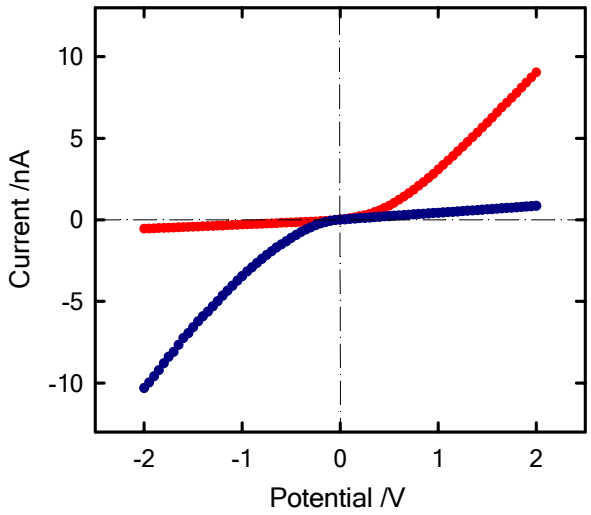

Figure 3.3.3: *I-V* characteristics of a single conical nanochannel in 0.1 M KCl prior to (●) and after (●) the electrostatic assembly of b-PAH.

Moreover, from the magnitude of the rectified currents at +2 and -2 V we can assume that the density of positive charges introduced on the channel surface is comparable to those originally encountered on the negatively-charged channel. This change in polarity can be interpreted as a result of the charge overcompensation originating from the assembly of the polycationic multivalent ligand on the negative surface.[156] This phenomenon plays a key role in the electrostatic assembly of polyelectrolyte multilayers, in which each polyelectrolyte layer reverses the surface charge of the assembly enabling the consecutive immobilization of polyelectrolytes bearing opposite charges.[157] The changes in the *I-V* characteristics prior to and after b-PAH assembly allowed the success of the ligand immobilization to be confirmed.

Once the channel was functionalized, we proceeded to study the biorecognition events inside the solid-state nanochannel. In principle, there are three major mechanisms governing the mass transport across nanochannels: a) volume exclusion principle,[63,158] b) hydrophobic interactions and c) electrostatic interactions. Regarding the hydrophobic interactions[55], we can mention the recent work by Vlassiouk *et al*.[49,55] in which surface-confined photochromic spyropyran molecules were applied to control the wettability of nanochannels in such a way of manipulating the admission of water into the membranes using light as triggering stimuli. A similar approach, in biological membranes, has been also reported by Feringa and co-workers.[159] In our case, we are dealing with the volume exclusion principle, in which the biorecognition event leads to the formation of a ligand-receptor bioconjugate which is supramolecularly confined in the nanochannel. This biorecognition process would affect the effective cross-section of the nanochannel and have an impact on the flux of the ions through the nanochannel. Consequently, the molecular recognition process would promote a sensitive change on the rectified current passing through the nanochannel. It is worth mentioning that the charge of the bioconjugated protein could also affect, to some extent, the electrostatics of the ion transport. However, the bioconjugated protein (~ 3nm) and the channel mouth dimension (~ 8nm) are comparable in size, thus indicating that volume exclusion (changes in effective cross-section) would be the major contribution governing the flux through the channel. This assumption is also supported by the recent work by Karnik et al.[145] on the interplay between the competing effect of charge and size of streptavidin on the nanochannel conductance. These authors demonstrated that the biomolecule charge dominates at low ionic concentrations, whereas at higher concentrations (as in our case) the volume exclusion effect dominates.[145] For detailed experimental procedure used

for electrostatic self-assembling of biotinylated poly(allylamine HCl), see chapter 2 (section 2.4.3)

Figure 3.3.4 describes the changes in the *I-V* plots upon putting into contact the biotin-modified nanochannel with streptavidin solutions of different concentrations. As expected, the presence of streptavidin, even at very low concentrations, led to a drastic change of the rectified current. The permselective transport of ions across the b-PAH-modified nanochannel, measured at -2V, was -10.3 nA. The presence of 1 pM streptavidin impacted a rectified current of -1.7 nA; this means that the blockage of the nanochannel due to the formation of the bioconjugate decreased the ionic flux across the nanochannel by ~85 %. This effect was even more pronounced when working with more concentrated SAv solutions. The presence of 100 pM SAv promoted a ~96 % decrease of the rectified current observed in the non-bioconjugated nanochannel. These experimental results provide clear evidence that the electrostatic assembly enables the anchoring of ligands which are able to biorecognize receptors inside the nanochannel, and this biorecognition can be transduced in an electronic signal provided by the ionic flux through the channel.

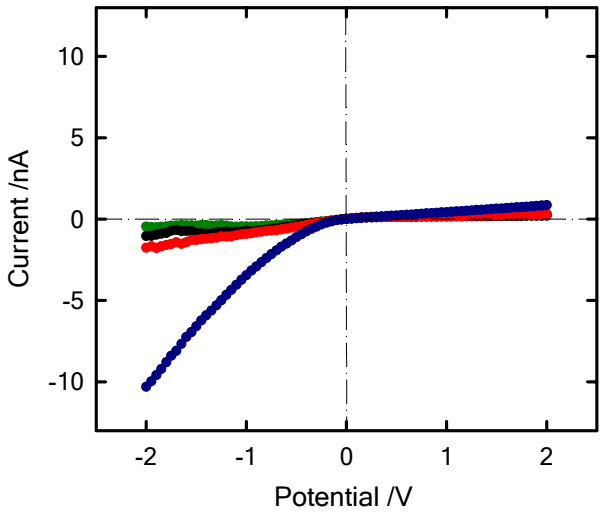

Figure 3.3.4: *I-V* characteristics of a b-PAH-modified single conical channel in 0.1 M KCl in the presence of different concentrations of streptavidin (SAv): (●) no SAv; (●) 1 pM; (●) 10 pM; and (●) 100 pM.

However, one important aspect of biosensing platforms relies on the selectivity for the detection and transduction of specific events. In other words, in order to show that this approach is valid to create biosensing platforms inside nanochannels, it is mandatory to demonstrate that the changes in the rectified current are solely due to the biorecognition event, and not to the simple blockage of the nanochannel due to the fouling of the protein on the b-PAH-modified PET surface. To verify the bioselectivity of the b-PAH-modified nanochannel, we repeated the same experiments using proteins that do not biorecognize biotin, like lysozyme and bovine serum albumin (BSA), under more concentrated conditions. Figure 3.3.5 shows the variations in the *I-V* plots of b-PAH-modified nanochannels in the presence of 100 nM lysozyme and BSA, respectively. From the

slight variations in the rectified current we can conclude that the electrostatically biotinylated nanochannels display a remarkable specificity towards streptavidin (Table 3.3.1).

These results, describing the versatility of the electrostatic assembly to create protein biosensors based on biofunctionalized solid-state nanochannels, also indicate that this strategy provides a friendly procedure to construct interfacial architectures in confined geometries. This constitutes a remaining challenge in materials science related to the creation of functional supramolecular nanostructures, derived from the construction of organized assemblies in nanoconstrained enviroments. Molecular level control of the chemical topology of nanoconfined interfacial architectures would be the key to enabling highly functional biomimetic molecular devices.

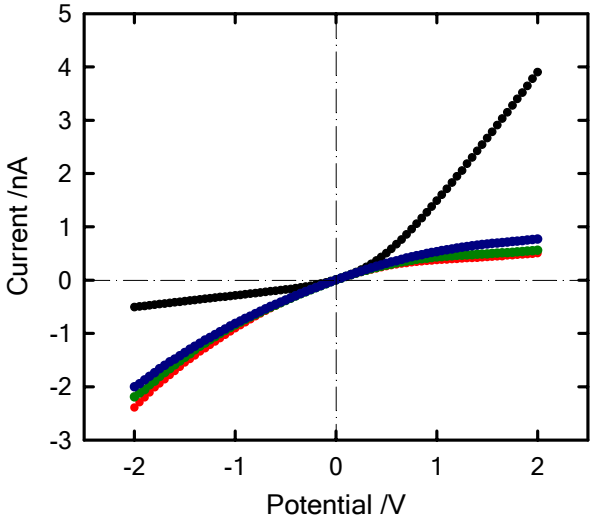

Figure 3.3.5: *I-V* characteristics of a single conical nanochannel in 0.1 M KCl prior to (●) and after (●) the electrostatic immobilization of b-PAH followed by the addition (separately) of 100 nM lysozyme (●) and 100 nM bovine serum albumin (●).

Table 3.3.1: Variations of the rectified ion flux in the presence of the different proteins.

Protein (Concentration)	**Decrease of the rectified current**
Streptavidin (1 pM)	~ 85 %
Streptavidin (10 pM)	~ 90 %
Streptavidin (100 pM)	~ 96 %
Bovine Serum Albumin (100 nM)	~ 14 %
Lysozyme (100 nM)	~ 9 %

At this point, we were able to functionalize the nanochannel by using a multivalent bifunctional ligand. After the bioconjugation with the tetravalent streptavidin protein, the channel surface is, in principle, functionalized with a protein which is able to biorecognize biotin centers. This indicates that the chemical/biochemical characteristics of the channel are given by the streptavidin, which could be used for the recognition-mediated spontaneous assembly of a "multivalent" building block, like the b-PAH. Multivalency is based on the interaction through multiple simultaneous molecular contacts[160,161] and has demonstrated to be a powerful and versatile self-assembly pathway.[162,163] Consequently, using the same (ligand-receptor) building blocks we proceeded to the assembly of the supramolecular bioconjugation inside the nanochannel in order to visualize the capabilities of our approach to manipulate the chemical functionalities and architectures in nanoconstrained environments (Figure 3.3.6).

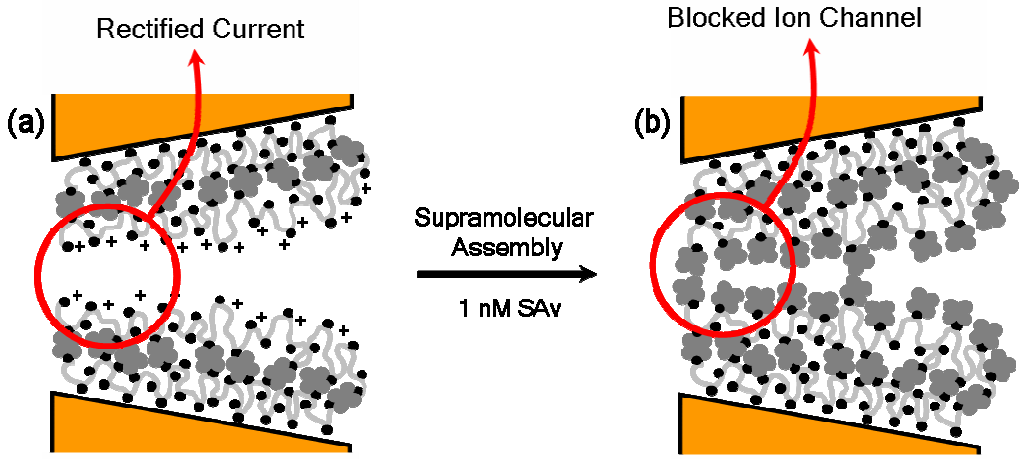

Figure 3.3.6: Simplified cartoon depicting the formation of a multilayered supramolecular bioconjugate inside the single conical nanochannel.

We followed the changes occurring in the nanochannel through the variations observed in the *I-V* plots (Figure 3.3.7). As described above, the conjugation of the streptavidin on the biotinylated channel led to a decrease of the rectified current. After assembling the polyvalent ligand onto the streptavidin-modified channel we observed an increase of the rectified current, but the magnitude of this current is still much lower than that detected in the absence of bioconjugation. From the well-defined rectifying characteristics of the *I-V* plot we conclude that the recognition-mediated

assembly of b-PAH rendered the channel surface positively charged, thus acting as a supramolecular permselective channel transporting preferentially anionic species.

It is worth mentioning that the occurrence of a rectified current can be probably attributed to a reorganization of the interfacial architecture after the b-PAH assembly affected the effective cross-section area of the nanochannel. Even though, subsequent SAv conjugation on the SAv/b-PAH led to an almost complete blockage of the nanochannel. This gives clear evidence that the multivalent character of b-PAH enables the creation of a biotinylated interface on top of the SAv layer where the protein is able to biorecognize the ligands without sensitively affecting the stability of the supramolecular architecture. More important, in close analogy to polyelectrolyte multilayers, where each polyion is responsible for the reversal of the surface charge, the multivalent character of building blocks is responsible for reversing the ligand-receptor characteristics of the nanochannel. This is an important feature of the supramolecular interfacial conjugate[164,165] in order to create stable and complex functional architectures[166] inside the nanochannel. This concept constitutes a toolbox to achieve actual molecular design of supramolecular systems[167-170] in nanoconfined environments using pre-designed molecular recognition interactions. Supramolecular assembly,[171-173] the cornerstone of the so-called *"soft nanotechnology"*,[174] occurs spontaneously and can lead to highly functional and controlled structures if selective and directional non-covalent interactions are exploited.[175] The experimental results described above demonstrate that controlling the supramolecular assembly and manipulating the directionality of the processes occur in the nanoconfined environment is completely feasible just by using very simple tools.

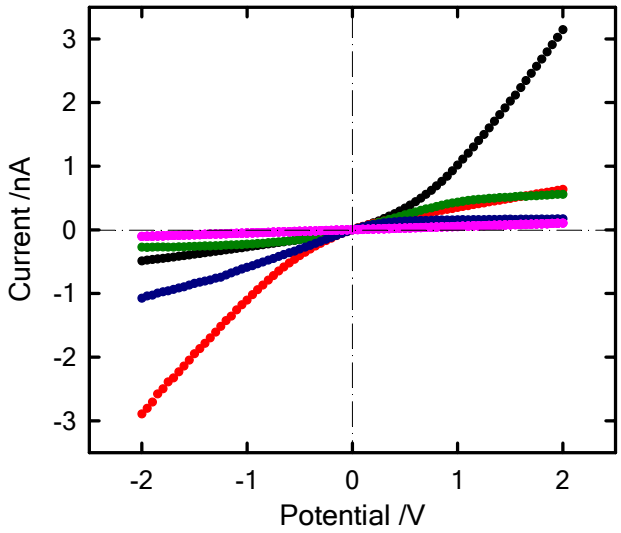

Figure 3.3.7: *I-V* curves of a surface-modified nanochannel in 0.1 M KCl corresponding to: (●) carboxylate-terminated channel; (●) b-PAH-modified channel; (●) (SAv)(b-PAH)-modified channel; (●) (SAv)(b-PAH)$_2$-modified channel; (●) (SAv)$_2$(b-PAH)$_2$-modified channel.

3.3.3 Conclusion

In summary, in this work we presented a simple and straightforward strategy to incorporate biorecognition elements in nanoconfined environments, as represented by single conical nanochannels. The approach is based on exploiting the ability of a bifunctional multivalent ligand to electrostatically assemble on the charged channel wall and expose the ligand to the inner environment of the nanochannel. The experimental results indicated that the electrostatically modified surfaces are very stable and suitable to be used as platforms in biorecognition processes, in which the bioconjugation of the protein does not lead to the removal of the ligands from the surface. Moreover, the electrostatically assembled channel surface displayed good biospecificity and non-fouling properties as observed in the control experiments using proteins that are not biorecognized by the ligands. Finally, we demonstrated that by using this approach it is possible to exploit the remarkable stability of systems created by ligand-receptor interactions to generate supramolecular interfacial architectures inside the nanochannel. In this context, we envision that the formation of multilayered supramolecular assemblies inside solid-state nanochannels could be turned into an enabling technology leading to the production of fully artificial biomimetic systems displaying tailor-made topology, shape and biochemical functionality.

3.4 A pH-Tunable Nanofluidic Diode with a Broad Range of Rectifying Properties

3.4.1 Introduction

Nanochannels, nanopipettes, and nanoelectrodes are based on a new generation of devices designed for single-molecule sensing, molecular separation, and energy storage.[28,89,117,120,126,136,176-179] In particular, nanochannels with fixed charges provide ionic selectivity and sensing, exploiting the fact that the internal channel volume is not much larger than the ionic analyte size.[96,114,120,151] The channel does not act simply as a mechanical filter because it displays also ionic selectivity due to the electrical charges attached to the surface. These charges favor the passage of counter-ions (ions with charge opposite to that of the channel) but hinder the passage of co-ions (ions with charge of the same sign as the channel).[71,89] The ionic selectivity is high when the surface potential is high and the radius of the channel is decreased down to the Debye length of the electrolyte, which is usually on the nanometer scale.[71,89,180]

The functionalization of chemical groups on the channel surface allows controlling the transport through the nanochannel, and a variety of different substrate-specific methods aimed at modifying the nanochannel surface have been reported. The use of fixed-charge nanochannels in practical applications may require tuning externally the electrostatic interaction between the surface charge groups and the ionic permeants. This would allow integrating a variety of functions on the same nanostructure, as is the case of biological membranes where both positive (amino) and negative (carboxylic) fixed charge groups coexist in the same ion channel.[181] However, the fact is that the external control of the fixed charges is severely limited in most cases. In particular, no charge reversal is possible, except for the very specific case of gold-coated nanotubule membranes[43,182] where the application of an electric potential to the internal metallic surface of the channels allows implementing cation and anion-exchange properties on a unique separation device. It constitutes a significant innovation to design, produce and characterize, theoretically and experimentally, a single-track amphoteric nanochannel containing both positively and negatively fixed charge groups whose properties are very sensitive to the

external pH. In fact, previous work with amphoteric crosslinked polymer networks has been carried out mainly on the macroscopic scale (two well-known examples are hydrogels[183,184] and porous membranes).[185,186] Nanometer-scaled amphoteric channels are of general interest because of their potential applications in drug delivery systems, ion-exchange membranes for separation of biomacromolecules, antifouling materials with reduced molecular adsorption, and biochemical sensors.

Nanofluidic diodes based on asymmetric nanochannels[37,63,187] and bipolar transistors[61,146] have recently been demonstrated. We go a step further here and demonstrate a nanofluidic diode with amphoteric chains (lysine or histidine) functionalized on the channel surface. This permits a broad set of rectification properties using the same nanodevice by changing simply the *pH* values in the external solutions. A definite plus is to functionalize the amphoteric chains on a conical nanochannel with well-defined, controlled structural asymmetry because this gives unique selectivity and rectification properties. Conical nanochannels have a small-diameter opening (tip), usually in the range 1-10 nm.[71,88,89,96,114,127,188] Selectivity and rectification are dictated by the tip because it is in this narrow, nanometer-sized region where the influence of the radial electrical double layer and the major part of the applied axial voltage drop act together to determine the final device performance.[71,127] We demonstrate also that the intrinsic (geometric and electrostatic) asymmetries of the device permit to obtain virtually every rectification characteristic that may be required in practical applications.

3.4.2 Results and Discussion

During the process of surfactant-controlled (chapter 2, section 2.2.3) asymmetric track-etching in a PET membrane, the carboxyl groups were generated on the channel surface. Polymeric membranes with single conical nanochannels incorporating L-lysine or L-histidine as amphoteric chains were obtained following the procedure described in chapter 2 (section 2.4.2.2.1). The lysine and histidine chains were attached onto these carboxyl groups according to the reaction schemes (Figure 3.4.1).

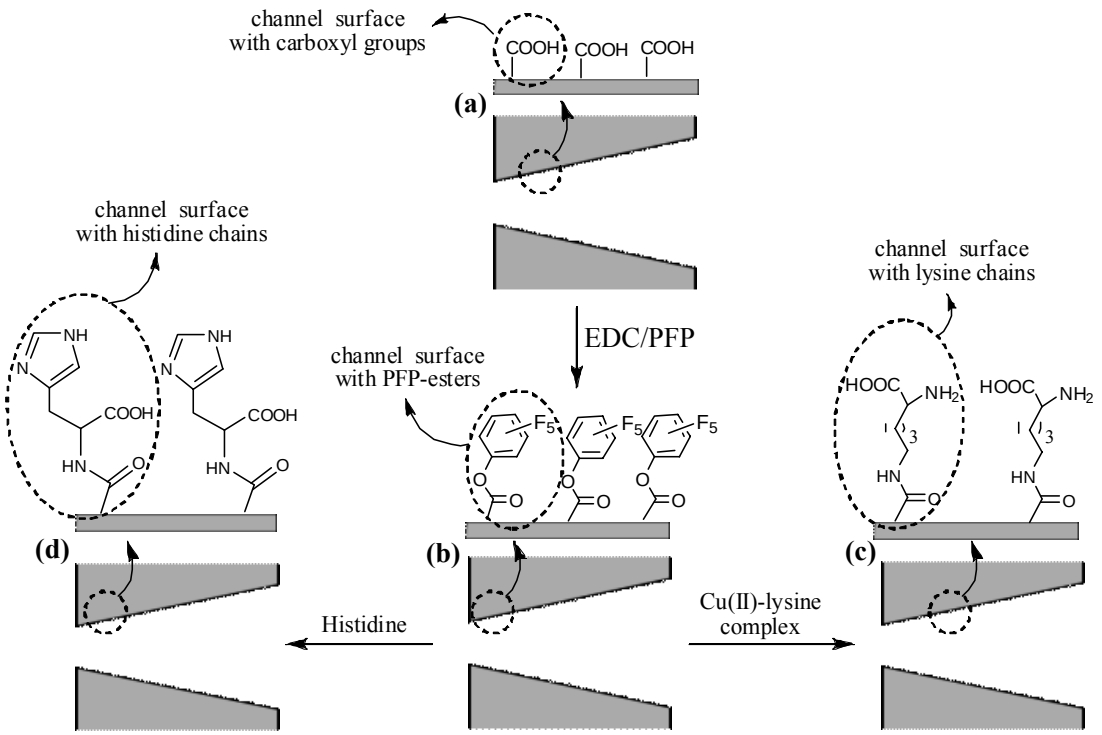

Figure 3.4.1: Scheme describing the functionalization of the channel surface carboxyl groups with (c) L-lysine chains, and (d) L-histidine chains, respectively.

The selective functionalization of lysine with surface carboxyl groups was accomplished by blocking the amino group and carboxyl group bounded to the α-carbon with Cu^{2+} ion to form a copper-chelate complex,[189] leaving an unprotected ε-amino group. The free ε-amino-terminator (-NH_2) of the copper(II)-lysine complex is covalently coupled with the carboxyl group created during track-etching. In order to break the complex, EDTA was used because it has a strong affinity to copper compared with amino acid (lysine) and forms a water-soluble copper chelate.[190] The resulting chain displays two ionizable residues: one α-carboxylic group (pK_a = 2.2) and one α-amino group (pK_a = 9.0).[191] Histidine contains an imidazole ring at the terminus of its side chain along with amino (–NH_2) and carboxyl (–COOH) groups bounded to α-carbon. The histidine was functionalized on the channel surface through the covalent bond between amino and activated carboxyl groups. The imidazole side chain ring is protonated at slightly acidic pH values (pK_a 6.7–7.1).[192]

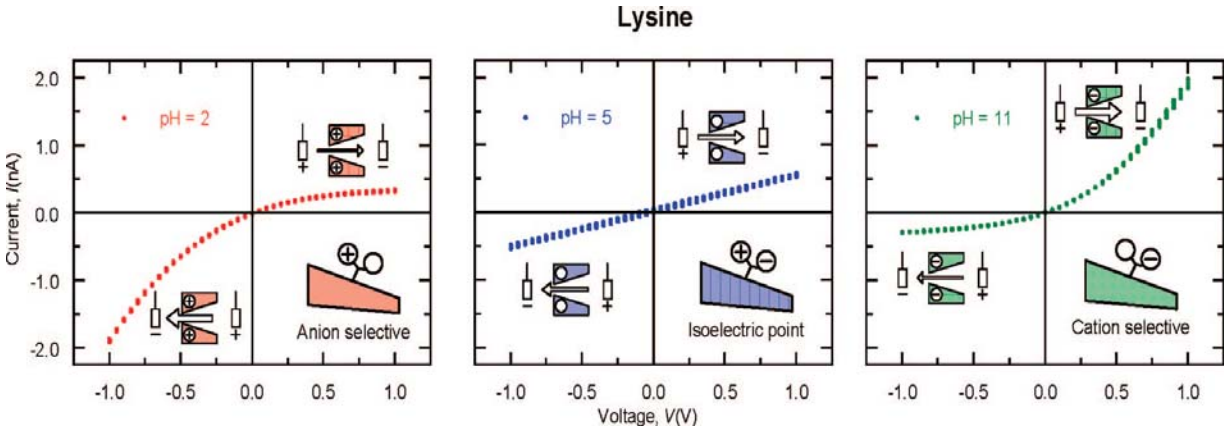

Figure 3.4.2: Current-voltage curves of the amphoteric (lysine) nanochannel at pH = 2 (left), pH = 5 (center), and pH = 11 (right).

Figure 3.4.2 shows the effect of pH on the *I-V* curves of an amphoteric nanochannel functionalized with lysine. At low pH values (left), the ionized amino groups ($–NH_3^+$) are positively charged due to protonation, while the protonated carboxylate groups (–COOH) are neutral. The nanochannel is then selective to anions and shows the rectification properties characteristic of conical channels with positive fixed charges:[37,72] a high conducting ("on") state for $V < 0$ and a low conducting ("off") state for $V > 0$. Conversely, at high pH values (right), the deprotonated amino groups ($–NH_2$) are in neutral form, while the carboxylate groups ($–COO^-$) are ionized. The net channel fixed charge is then negative and the nanochannel is now selective to cations. The nanochannel "on" and "off" states appear at $V > 0$ and $V < 0$, respectively. The transition between these two rectification regimes occurs at pH = 5 (center), which is close to the isoelectric point $pI = 5.6$ of the lysine chain attached to the channel surface, calculated from the pK_a values of the α-carboxylic and the α-amino groups.[191] At this pH value, the α-carboxylic and the α-amino groups are charged but the nanochannel net charge is zero, and the *I-V* curve shows a linear, ohmic behavior. The reversal of the nanochannel selectivity with increasing pH is further confirmed by independent reversal potential measurements, giving -10 mV (pH = 2), 0 mV (pH = 5), and +32 mv (pH = 11) for an external solution concentration ratio of 0.1 M / 0.01 M (0.1M KCl on the base side and 0.01 M KCl on the tip side of the channel).

The *I-V* curves obtained with the conical nanochannel modified with histidine (not shown) display similar characteristics as those of Figure 3.4.2. At pH = 2.0, the protonated carboxyl is neutral while the ionized imidazole group provides a net positive charge. The isoelectric point is

now pI = 4.2, leading to the linear I-V curve. The channel starts rectifying again at pH values above the isoelectric point because of the ionized carboxylate groups. At pH > 7.0, the unprotonated imidazole group (pK_a 6.7–7.1) becomes neutral and only the carboxylate groups are responsible for the negatively charged channel surface.

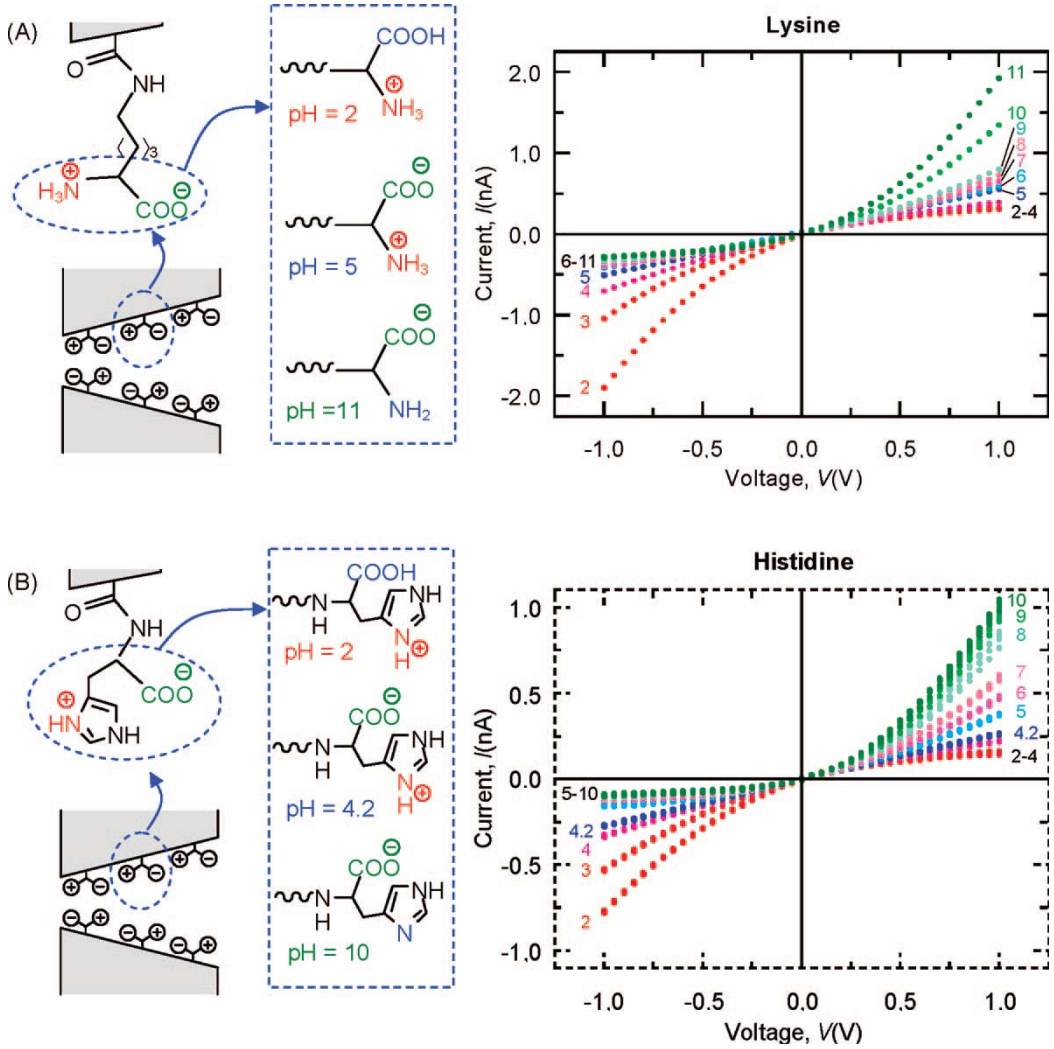

Figure 3.4.3: (A): Effect of pH on the I-V curves of the amphoteric (lysine) nanochannel. (B): Effect of pH on the I-V curves of the amphoteric (histidine) nanochannel. The numbers in the curves correspond to the pH values.

Figure 3.4.3 shows the effect of changing the pH on the I-V curves of the nanochannel functionalized with lysine (Figure 3.4.3A) and histidine (Figure 3.4.3B). The curves obtained with the two nanochannels give a progressive change of the nanochannel charge (and then of the current) between the two experimental limits of low pH (most α-amino groups are positively

charged) and high pH (most α-carboxylic groups are negatively charged). Comparison of the curves for the two samples shows higher currents for the lysine nanochannel than for the histidine nanochannel. The curves for pH = 2 and pH = 11 are almost perfectly symmetrical in the case of lysine. However, in the case of histidine, the electric currents are slightly higher for pH = 10 than for pH = 2. This could be ascribed tentatively to two effects: first, substitution of the carboxylic groups by the histidine chains could be less effective for histidine than for lysine; second, the interactions between the carboxylic and amino groups are likely to be different for lysine and histidine because of spatial constraints. These two effects may yield a net charge lower (in absolute value) at pH = 2 than that attained at pH = 10.

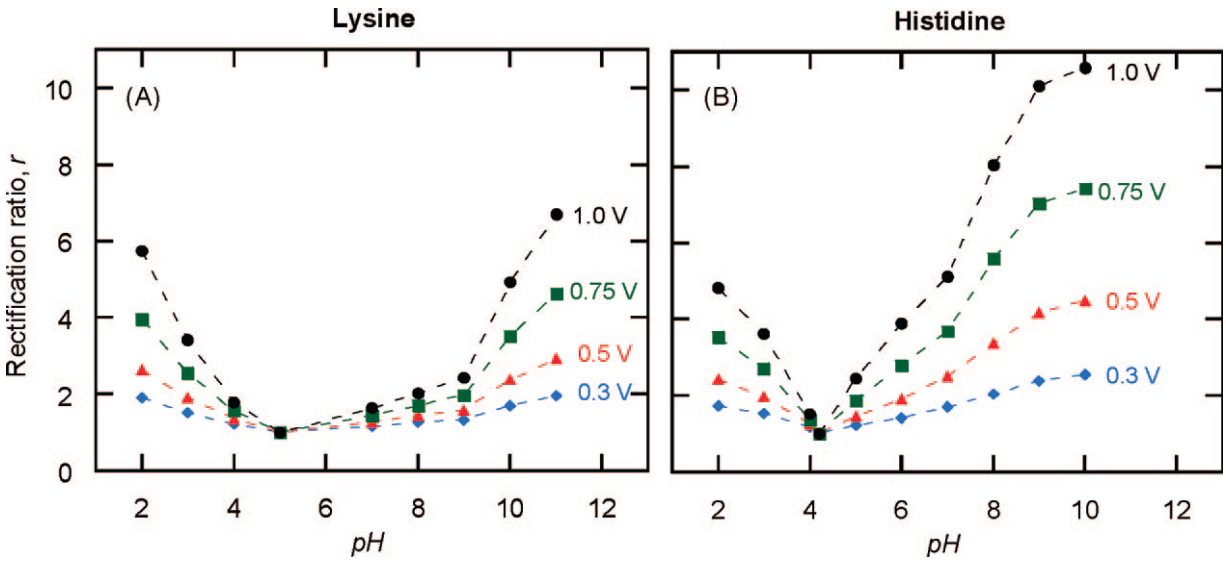

Figure 3.4.4: (A): Rectification ratio versus pH at different applied voltages (lysine). (B): Rectification ratio versus pH at different applied voltages (histidine). The numbers in the curves correspond to the on/off voltages for the rectification ratio.

Figure 3.4.4 shows the rectification ratio *r*, defined as the absolute value of the current ratio *I*(on state)/*I*(off state) at a given voltage, versus the pH value of the external solutions. As in the case of the *I-V* curves in Figure 3.4.4, the rectification characteristics are slightly different for the two nanochannels. The experiments indicate again a symmetry between the points measured at pH = 2 and pH = 11 in the case of lysine (Figure 3.4.4A). However, the nanochannel functionalized with histidine (Figure 3.4.4B) shows a *r* value significantly higher for pH = 10 than that for pH = 2, probably because of the reasons mentioned for the *I-V* curves of Figure 3.4.3. The results obtained with the two nanochannels reveal that the rectification ratio can be reversed simply by

changing the pH of the solutions. Therefore, the amphoteric nanochannel shows tunable ionic selectivity and rectification characteristics. In particular, a number of functions including diode rectification in nanofluidic circuits,[63,120,187] sensing,[54,96,114,117] separation,[43,182] electrophoretic capture/release of a charged species[178], and ion pumping against an external concentration gradient, could now be implemented on the basis of the nanostructure characteristics demonstrated in Figures 3.4.3 and 3.4.4.

The above experimental results can now be described theoretically in terms of a continuous model based on the Poisson and Nernst-Planck (PNP) equations[72]

$$\nabla^2\phi = \frac{F}{\varepsilon}\left(c_{Cl^-} - c_{K^+}\right) \qquad 3.4.1$$

$$\nabla \cdot \vec{J}_i = -\nabla \cdot \left[D_i\left(\nabla c_i + z_i c_i \nabla\phi\right)\right] = 0\,,\; i = K^+, Cl^- \qquad 3.4.2$$

where $\vec{J}_i$, c_i, D_i and z_i are the flux, the local concentration, the diffusion coefficient and the charge number of ion i (i = K^+ and Cl^-), with φ and ε the local electric potential and the dielectric permittivity of the solution within the channel, respectively. Despite the nanometer scales involved in the problem, the fact is that most models of selectivity are still based on the classical continuum theories because these are relatively simple and predict correctly the qualitative trends of the problem.[63,71,72,89,127,180,186,193-195] Comparison between theory and experiment reveals that the agreement between the PNP theory and the experiments is also quantitative for the two nanochannels (Figure 3.4.5A for lysine and 3.4.5B for histidine), and allows for the determination of the nanochannel surface charge by using the following procedure. First, the radius of the wide channel opening is determined by FESEM using a polymer foil containing approximately 10^7 channels cm^{-2} which was etched simultaneously with the sample containing the single channel under the same conditions. Second, the radius of the channel tip is calculated from the (linear) fitting of the *I–V* curve at the respective isoelectric points (Figure 3.4.2, center). Once the channel radii have been calculated, the only free parameter of the PNP model is the surface charge σ (in elementary charges per square nanometer). We emphasize finally that the values of σ in Figure 3.4.5 are in good agreement with those found previously for negatively charged conical nanochannels.[70]

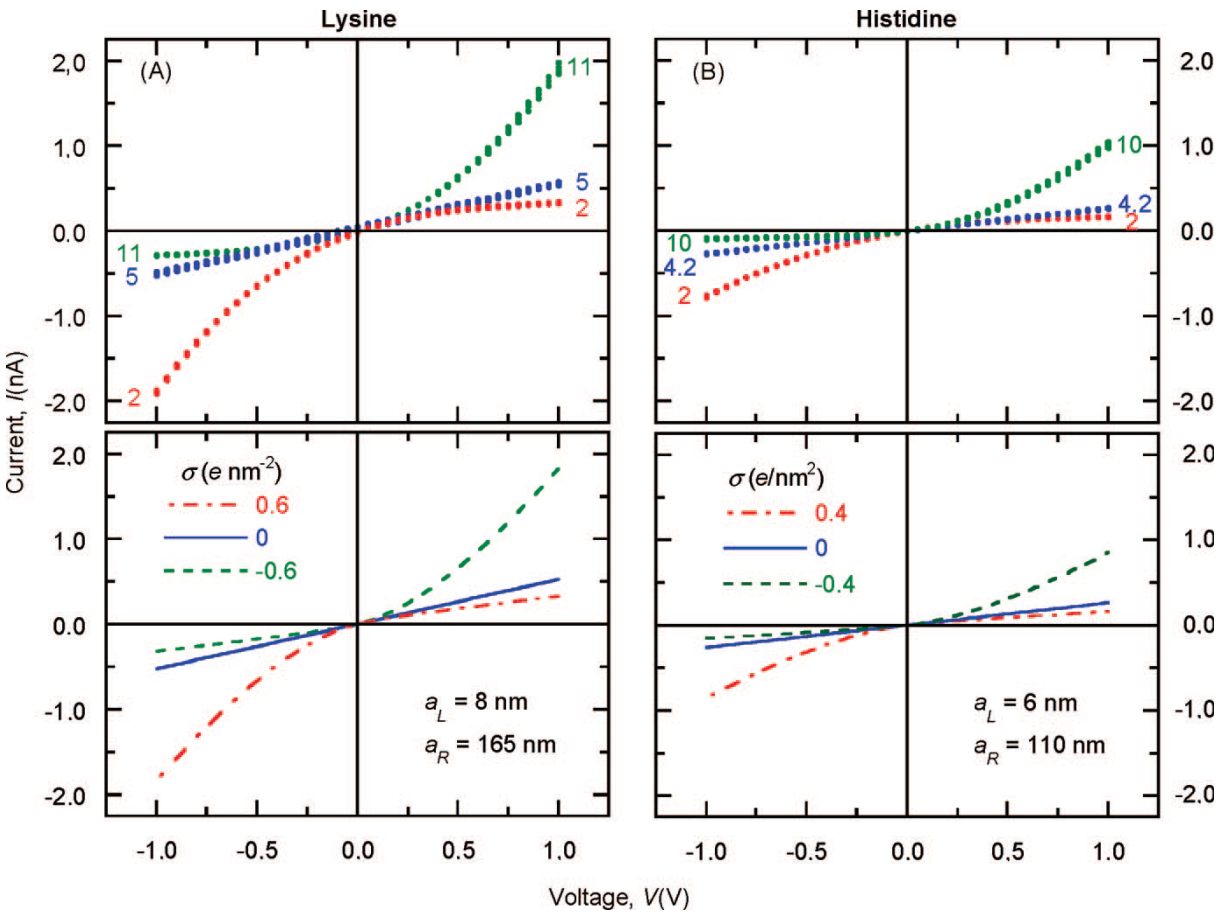

Figure 3.4.5: (A): Experimental *I-V* curves of the amphoteric nanochannel (lysine) at pH = 2, 5, and 11 (up) and theoretical results from a PNP model (down). (B): Experimental *I-V* curves of the amphoteric nanochannel (histidine) at pH = 2, 4.2, and 10 (up) and theoretical results from a PNP model (down).

3.4.3 Conclusion

In conclusion, the amphoteric chains functionalized on the conical nanochannel surface form the basis of a nanofluidic diode allowing pH-tunable rectification properties. The results demonstrate that virtually any characteristics required in practical applications can be accomplished with the same device by simply changing the pH of the external solutions. The conical nanochannel has a well-defined, controlled structural asymmetry, showing selectivity and rectification properties that are dictated by the nanometer-sized tip region. The intrinsic (geometric and electrostatic) asymmetries of the device permit to implement different functions on a unique nanostructure.

3.5 Single Conical Nanochannels displaying pH-Tunable Rectifying Characteristics. Manipulating Ionic Transport with Zwitterionic Polymer Brushes

3.5.1 Introduction

One of the remarkable aspects of the ever-growing field of nanotechnology relies on the creation of architectures with length scales and functional features comparable to biological machineries.[114,149] The progress in this field enabled the reproducible fabrication[188] of synthetic nanochannels displaying properties that mimic their biological counterparts.[141] Single conical nanochannels are able to rectify the ion transport flowing through them, which is in close resemblance to voltage-gated biological ion channels.[54,68,89,108] In this context, generating "fully synthetic" architectures with functionalities comparable to biological entities triggered the interest of the scientific community related to diverse research fields, including life sciences, chemistry and applied biophysics. One of the central features that determine the rectifying characteristics of the conical nanochannels is the nanoscale control over the surface properties of the channel walls.[38] It has been demonstrated, both theoretically[71,155] and experimentally,[54,68,89,108] that the rectifying characteristics of the nanochannels emerge due to a synergy of the driving force caused by the channel asymmetry and the electrostatic effects due to the fixed charges on the channel wall. As a consequence, finding new avenues to manipulate the surface charges of conical nanochannels is of paramount importance to further expand the potentialities of these nanosized systems.[38,51,61,63,123,143,146] The development of functionalized conical nanochannels with "smart" properties leading to the modulation of the fixed charges provides an exciting new approach to gain control over the ion transport through the nanochannels. Controlling the permeation through membranes with pH-tunable moieties has attracted considerable attention during recent years.[196] Seminal work of Martin and co-workers described the pH-switchable permselectivity of cylindrical cysteine-modified gold-coated nanotubules demonstrating the huge potential of zwitterionic moieties to tailor the surface charge properties of confined environments.[35] On the contrary, in spite of its relevance, little is known about the behaviour of rectifying conical nanochannels bearing tailorable surface charges. In addition, to the best of our

knowledge, the tailoring of the surface charge in single conical nanochannels has been exclusively performed using monolayer assemblies. Within this framework, we have to note that polymer brushes provide a versatile toolbox to molecularly design interfaces with nanoscale control being applicable to a plethora of "smart" chemical functionalities.[197,198] For example, this chemical methodology would enable the facile construction of multi-responsive nanochannels by simply using copolymer brushes incorporating predefined functionalities.[199] More important, considering that the degree of rectification is highly dependent on the surface charge density, polymer brushes provide a simple mean to sensitively increase the number of fixed charges on the nanochannel walls. These particular features of polymer brushes merged with the transport properties of conical nanochannels would open the door to completely new signal-responsive chemical nanodevices. It was demonstrated that the growth of zwitterionic polymer brushes provides a useful strategy to finely tune the rectifying characteristics of the nanochannel and, consequently, to manipulate the mass or ion transport through them by simply varying the environmental pH.

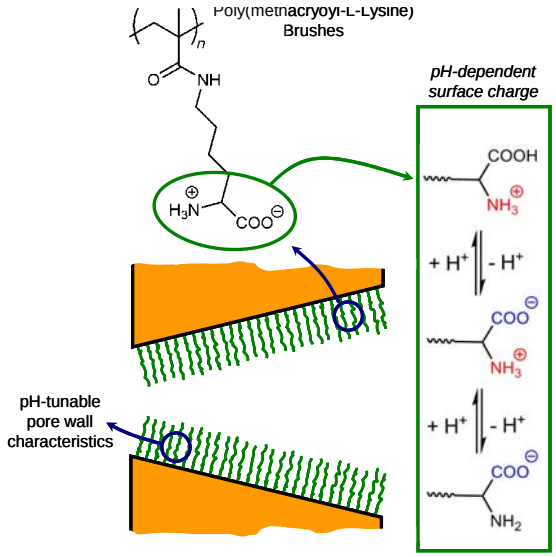

Figure 3.5.1: Schematic cartoon describing the polymer brush-modified conical nanochannel. The chemical structure of the polymer brush and the equilibrium associated with the pH-dependent behaviour of the zwitterions in monomer units are also indicated.

3.5.2 Results and discussion

Single conical nanochannels, with a tip diameter (*d*) of ~20 nm and a base diameter (*D*) of ~1.65 μm, were fabricated by tack-etching of polyimide membranes,[69] irradiated with single swift heavy ion as described in chapter 2 (section 2.2.2.1). Then, the single nanochannel-containing membrane was modified with 4,4′-azobis(4-cyanopentanoic acid) as the surface-initiated polymerization initiator.[128,200] Afterwards, the brush growth was accomplished by surface-initiated free radical polymerization of the zwitterionic monomer methacryloyl-L-lysine (Figure

3.5.1) by following the experimental procedure described in chapter 2, section 2.4.4.1. After a preset polymerization time, the membranes were thoroughly rinsed with deionized water and mounted in the conductivity cell.

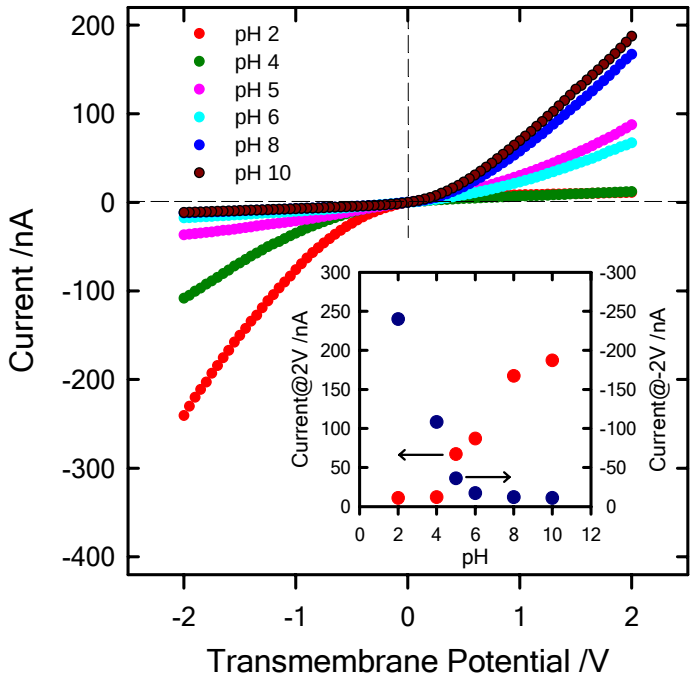

Figure 3.5.2: *I-V* curves corresponding to a single conical nanochannel modified with poly(methacryloyl-L-lysine) brushes measured at different pH values (using 1 M KCl as electrolyte). The different pHs are displayed using colored symbols as indicated in the Figure. The inset describes the changes in the rectified currents upon variation in the environmental pH. The red and blue dots refer to the rectified currents measured at -2 and +2 V, respectively.

Figure 3.5.2 depicts *I-V* curves of a single conical nanochannel in PI modified with polyzwitterionic brushes using 1 M KCl (at different pHs) as electrolyte solution in both half cells. Considering the zwitterionic nature of the monomer units (Figure 3.5.1) we can infer that at strongly acidic pHs the monomer units covalently tethered to the channel wall, will be bearing positively charged groups corresponding to $-NH_3^+$. As is well-known, the presence of rectification requires surface charges. In our case we observed that at pH 2 the *I-V* curve displayed a well-defined rectification behaviour which would imply the permselective transport of anionic species through the positively-charged nanochannel (Figure 3.5.2). The degree of rectification (f_{rec}),[61] defined as the ratio between currents measured at voltages of the same amplitude but opposite polarities, was 22. At this point, it is worth mentioning that these results

are similar to those previously reported in the literature using positively charged nanochannels except for the higher degree of rectification, as compared with typical values for conical nanochannels modified with monolayer assemblies, $f_{rec} \sim 5$.

The next goal was to achieve a fine tuning of the surface charges in order to manipulate the ionic transport through the channel. As described in Figure 3.5.1, the equilibrium of the zwitterionic units involves a variety of charged states that are thermodynamically controlled by the pH value. So, we modified the acidic pH from 2 to 4, where the population of charged "bipolar" monomer units grew at the expense of the $-NH_3^+$ species resulting in a "less positive" surface charge. The *I-V* curve indicated that at pH 4 the well-defined rectification behaviour was still observed, but in this case the rectified current had decreased. This variation in pH led to a significant decrease in f_{rec} from 22 to 9. This fact clearly indicates that the zwitterionic brush enables the tuning of the rectified current under the same permselective conditions. Then, increasing the pH to 5 resulted in a significant loss of rectification behaviour of the channel. At pH 5 we are close to the isoelectric point of the zwitterionic brush (*pI* ~4.7), where the net charges are zero. The estimation of the *pI* was carried out by determining, via interpolation, the pH at which the currents measured at +2V and -2V display the same magnitude (Figure 3.5.3). This particular condition refers to the scenario in which the positive and negative surface charges inside the nanochannel are the same and, consequently, no rectification should be observed.

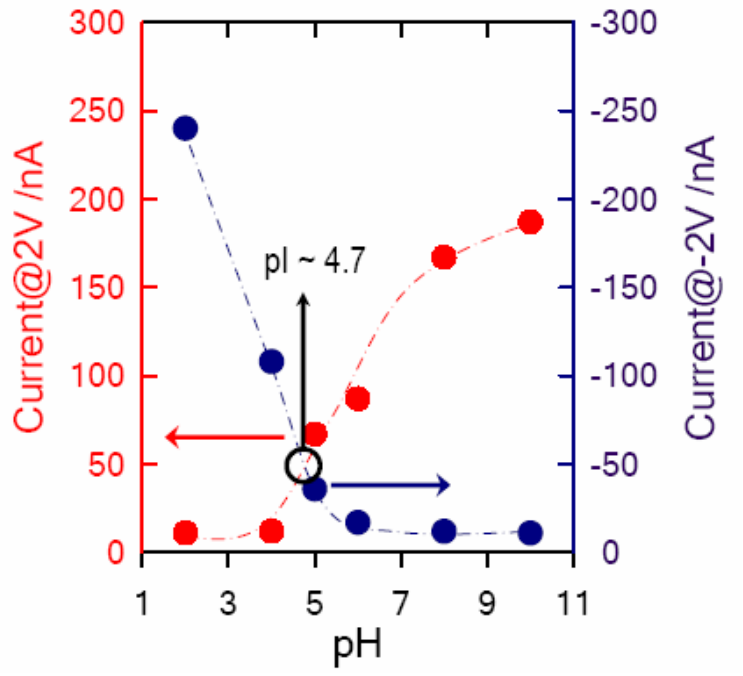

Figure 3.5.3: Changes in the rectified currents upon variation in the environmental pH. The red and blue dots refer to the rectified currents measured at +2 and -2 V, respectively. In the Figure *pI* is also indicated.

The significant decrease of net surface charges explains the poor rectifying behaviour displayed by the channel. However, at pH 5 we are slightly above the pI and the presence of some negative net charges gives rise to the rectifying characteristics depicted in Figure 3.5.2 (pink trace). Increasing the pH above 5 promoted further displacement of the zwitterionic equilibrium towards the formation of negatively charged species ($-COO^-$), thus reversing the permselectivity and rectification characteristics observed at acidic pHs. Changing the pH from 6 to 10 displayed a sensitive variation in the rectified current measured at +2 V from +87 to +187 nA, while the current sensed at –2 V remained almost the same. In terms of f_{rec} the pH variation promoted a change from 5 to 17 in the rectification efficiency. This observation further indicates that, even in reversed permselective conditions, variations in pH can lead to the fine tuning of the rectification characteristics.

3.5.3 Conclusion

In summary, we showed for the first time the integration of polymer brushes into conical single nanochannels in order to obtain highly functional chemical nanodevices. Our experimental evidences describing the use of zwitterionic brushes and exploiting the pH-dependent chemical equilibrium of their monomer units, demonstrate that the fine tuning of the ionic transport, by presetting the environmental pH, is achievable and enables a higher degree of control over the ion transport properties of the system. We envision that these results will pave the way to new "smart" nanodevices based on the interplay between the chemical richness of polymer brushes and the remarkable physical characteristics of conical nanochannels.

3.6 Ionic Transport through Single Solid-State Nanochannels Controlled with Thermally Nanoactuated Macromolecular Gates

3.6.1 Introduction

Biological nanochannels acting as membrane channels play a determinant role in all living systems. They operate as very sensitive devices in charge of regulating key functions as electric potential, ionic flow, and molecular transport through membranes.[2,135,201] Ion channels of biological membranes are formed by channel-like single proteins that span cell membranes and open and close in response to stimuli like changes in the transmembrane potential, binding of a ligand, or mechanical stress.[202] These stimuli-sensitive biological building blocks (like α-hemolysin) embedded into the membrane enable the modulation of ion transport through the protein channel due to passage of single molecules or proteins.[202] They are responsible for providing the conducting pathways for the ion species. When they are in open conformation, ions pass through the channel, and when they are resting in closed nonconducting conformations, ion transport is precluded.[64,203] This indicates that nanochannels change their conformations between different states in order to enable or prohibit the transport of species through the biological membrane, thus acting as a gate. In addition, the conformational transition between the states is usually referred to as gating. Hence, these biological channels work as nanodevices that control the molecular transport through a physical nanointerface. Biological nanochannels, such as α-hemolysin, provide unique features in regard to single molecule sensitivity;[8] however they are labile and difficult to handle in environments different from the lipid membrane and not fully compatible with nanodevice systems. This explains the growing interest in developing chemical devices that mimic the function of biological ion channels.[97,144] The possibility of creating fully artificial nanogating devices is one of the challenges in nanotechnology,[141,143,145,146,158] in which the generation of bioinspired switchable and easily controllable molecular gates would provide new tools for the creation of complex nanomachineries. In this context, solid-state nanochannels have demonstrated to be a robust alternative to biological nanochannels.[34,38,54,117,122,123,149,150] Besides, they also offer better control over channel geometry and compatibility with the

integration into functional systems.[54] They show huge potential in biomolecular recognition and also on creating gating functions, like rectification, in which the gating behaviour can be modulated by ionic strength or high-valent ions.[54] However, controlling the internal architecture and the chemical features of synthetic nanochannels, as precisely as α-hemolysin or other biological ion channels, is a non-trivial task.

This introduces a new nanotechnological demand focused on the quest for novel alternative switchable nanochannel machineries capable of being "nanoactuated" by external stimuli in a controllable manner. In this regard, one stimulus of particular interest in biological and non-biological systems is temperature.[204] Biological ionic channels activated by temperature changes transduce this information into conformational changes that open the channel. A typical example is thermosensation that is carried out by the direct activation of thermally-gated ion channels in the surface membranes of sensory neurones. This complex task is accomplished by temperature-sensitive ion channels which are members of the extensive TRP family (transient receptor potential channels).[205] An other good example concerns *N*-methyl-D-aspartate (NMDA) receptors which are glutamate-gated Ca^{2+} permeable ion channels constituted of heteromultimers involving NR1 and NR2 subunits activated by glutamate and glycine. Recently, Cais *et al.* demonstrated that these subunits undergo significant conformational transitions at 21.9–46.5 ^{o}C, which could have strong implications on the neuronal excitability at physiological temperatures.[103] With the inspiration of examples from nature, the scientific community started to build up biomimetic thermosensitive channels, as is the case of Movileanu and co-workers who created temperature-responsive protein channels containing elastin-like polypeptide (ELP) loops.[206] These ELP loops were placed within the cavity of the lumen of the α-hemolysin channel. Below the transition temperature the ELP loop is fully expanded and blocks the channel, above its transition temperature the ELP is dehydrated and the structure collapses, enabling a substantial flow of ions through the channel.

In this context, here we describe for the first time the application of solid-state nanochannels modified with thermoresponsive brushes as molecular gates nanoactuated by temperature-driven conformational transitions. We demonstrated the creation of "fully artificial" smart nanochannels with tunable diameters controlled by the temperature changes in the physiological range. These results demonstrate the huge potential of "soft nanotechnology"[174,207] to emulate and replicate complex biological functions using soft matter-based man-made systems.

3.6.2 Results and Discussion

Solid-state single conical nanochannels used in this study were fabricated in polyimide membranes by asymmetric chemical etching of the latent tracks of energetic heavy ions[69] as described in detail in chapter 2 section 2.2.2. After etching, carboxyl groups were generated on the nanochannel surface, which were then converted into amino groups by covalent linkage of diamine using conventional EDC/PFP coupling chemistry.[208] Next, we modified the membranes containing only a single channel with the thermo-responsive polymer brushes. This was easily accomplished by using aqueous surface-initiated atom transfer radical polymerization (SI-ATRP), leading to the formation of a dense polymer layer (brush) covalently tethered at one end to the nanochannel sidewall (Figure 3.6.1) by following the procedure described in chapter 2, section 2.4.4.2. Even though it is well-known that polymer brushes can be grown by a number of different polymerization techniques,[209] ATRP resulted in a very attractive alternative due to its simplicity to synthesize different polymer architectures in aqueous environments.[197,210] The solvents used in the aqueous ATRP are fully compatible with the membrane material, thus avoiding any detrimental effect on the single channel characteristics, i.e. closure, due to the swelling of the PI. Firstly, we modified the membranes having single aminated channels with the initiator groups. Secondly, we proceeded to the polymer brush growth (Figure 3.6.1) by immersing the initiator-modified membrane into the corresponding polymerization solution under conditions described elsewhere.[211] The choice of a *N*-isopropylacrylamide-based thermoresponsive system was due to the fact that it requires a simple and widely available monomer whose temperature-driven conformational changes are well-documented in the literature.[212,213] After polymerization, the brushes were extensively rinsed with water and methanol for removing the polymerization solution and kept under water prior to perform the thermoactuated gating experiments.

The track-etching technique allows control over the shape of the nanochannels, and in our experiments the etched single nanochannel was conical. Its large opening (base) was usually ~ 1.0 to 1.5 micrometer, and the narrow opening a few tens of nanometers. Diameter measurements of single conical nanochannels were conducted with a commonly used electrochemical technique.[30]

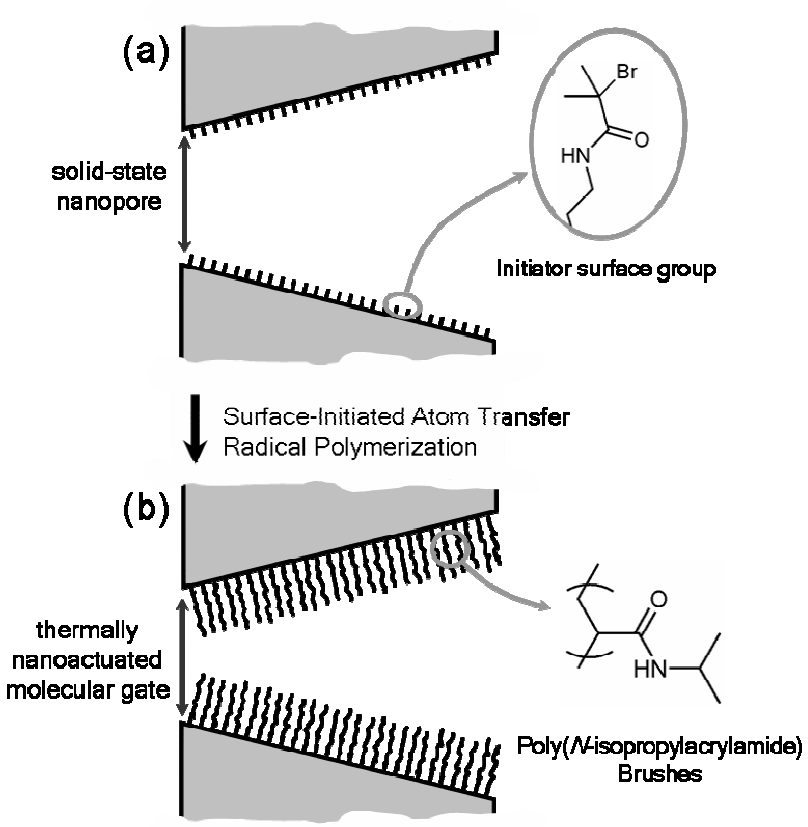

Figure 3.6.1: Scheme illustrating the surface modification of the nanochannel by the polymerization of polyNIPAM brushes. Firstly, the aminated channel wall is modified with the initiator groups (a). Then, the aqueous atom transfer radical polymerization (ATRP) is carried out (b). The Figure also desplaces the chemical structures of the ATRP initiator and the polyNIPAM brushes.

An electrochemical method described by Apel *et al.*[30] was used to calculate the tip diameter, *d*, of the single conical nanochannels. Briefly, this method implies mounting the membrane containing the conical nanochannel in a cell setup. The membrane divides the cell in two halves, where each half-cell was filled with 1 M KCl, and a Ag/AgCl electrode was immersed into each half-cell solution. A current–voltage (*I-V*) curve for the electrolyte-filled nanochannel was then obtained. The slope of this *I-V* curve is equal to the ionic conductance, *G* (in Siemens, S), of the nanochannel. The diameter of the small opening (*d*) was estimated from the conductivity by the following equation:

$$d = \frac{4LI}{\pi\kappa UD} \qquad 3.6.1$$

Here L is the length of the channel, D is the diameter of the large opening, κ is the specific conductivity of the electrolyte, U is the voltage applied across the membrane, and I is the measured current.

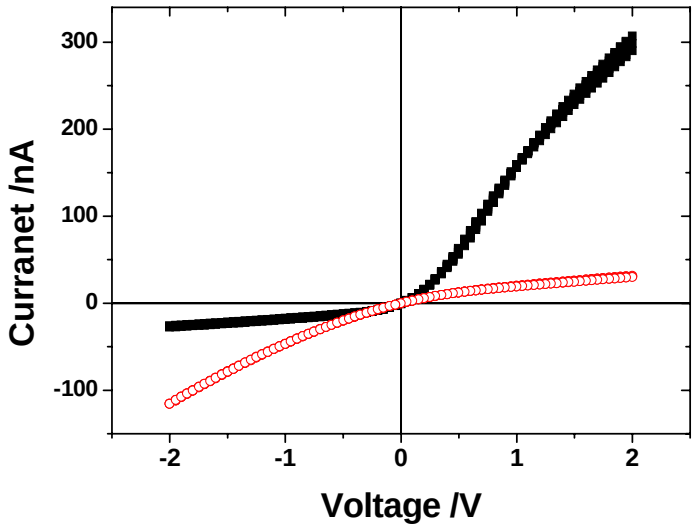

Figure 3.6.2: Current-voltage characteristics of a polyimide single conical nanochannel in 1 M KCl having d ~ 48 nm and D ~ 1.45 µm, prior to (●) and after (○) the modification with ethylenediamine. The terms d and D refer to the diameter of the small and large opening of the channel, respectively.

At neutral pH, the carboxylated conical nanochannels rectify the ion current due to the presence of negative charges on the channel surface. After modification with ethylenediamine, the channel walls were positively charged (due to the protonated amino groups) which resulted in the inversion of rectification as shown in Figure 3.6.2.

Figure 3.6.3 shows the *I-V* curves of a single PI nanochannel modified with PNIPAM brushes recorded at different temperatures. PNIPAM brushes neutralize the surface charge of the channels resulting in the loss of rectifying behaviour and, consequently, the channel exhibits a linear *I-V* characteristic (Figure 3.6.3). At room

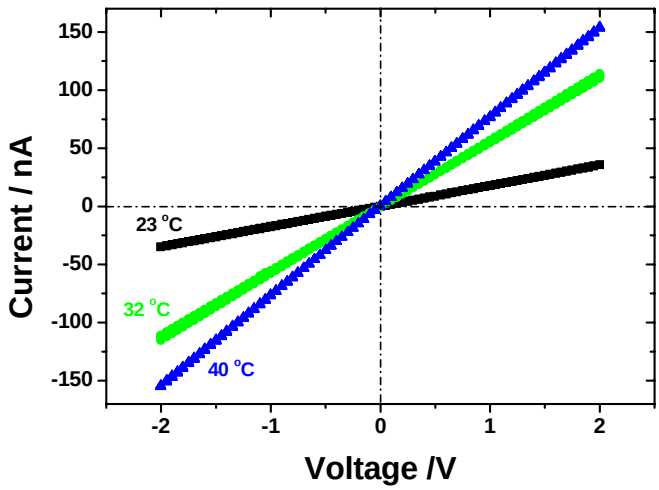

Figure 3.6.3: *I-V* curves in 1 M KCl for a polyimide single conical nanochannel after modification with polyNIPAM brushes at different temperatures.

temperature (23 °C) PNIPAM brushes remain swollen, thus decreasing the effective cross-section of the nanochannel. This is described by the low slope of the *I-V* curve which is associated with a low conductance of the nanochannel of 17 nS. Raising the temperature above the lower critical solubility temperature (LCST) promotes drastic changes of the conformational state of the NIPAM brushes. In this case, the brushes undergo a transition into a collapsed state[212,213] which has also an impact on the effective diameter on the nanochannel (Figure 3.6.4).

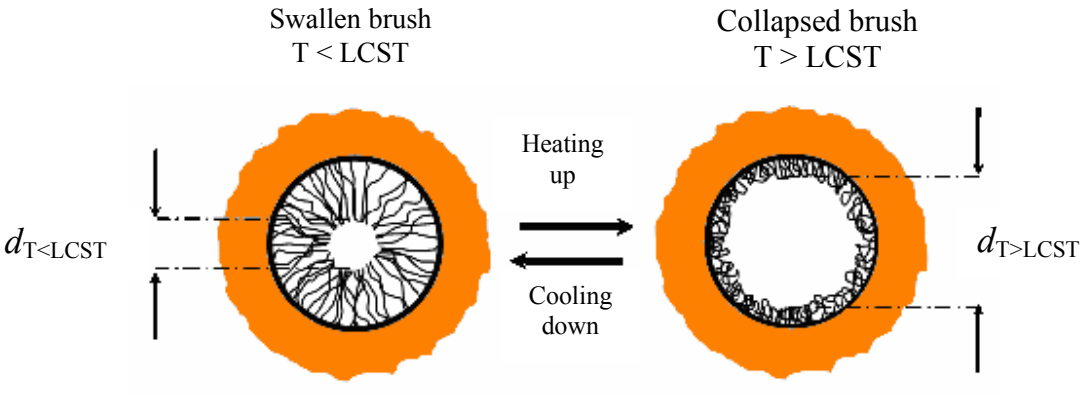

Figure 3.6.4: Cartoon describing the thermally-driven nanoactuation of the polyNIPAM brushes in the nanochannel.

The conformational transition into a more compact state promotes the widening of the nanochannel, which is evidenced as an increase in conductance as derived from the slope of the *I-V* plots at 40 °C. Regarding this latter, it is worth mentioning that the slope increase of the *I-V* plots could also be attributed to changes in the specific conductivity of the electrolyte.[30] In order to estimate the contributions to the conductance, coming from the specific conductivity changes due to temperature variations,[214] we proceeded to estimate the nanochannel conductance considering the corrected values of specific conductivity (Table 3.6.I).

$$G^{T} = \frac{\kappa^{T} \pi D d^{T}}{4L} \qquad 3.6.2$$

The superscript T indicates the parameters estimated at temperature *T*. In expression 3.6.2, we are assuming that the effective diameter of the large opening (base) and the thickness of the membrane film are not sensitively affected by the conformational changes of the PNIPAM brushes. In this context, a more realistic estimation of the variation of the effective nanochannel cross-section is given by:

$$\frac{G^{23^{o}C}}{G^{40^{o}C}} = \frac{\kappa^{23^{o}C} d^{23^{o}C}}{\kappa^{40^{o}C} d^{40^{o}C}} = \frac{17\,\text{nS}}{76\,\text{nS}} \qquad 3.6.3$$

Considering that the specific conductivity of 1 M KCl at 23 and 40 °C is 0.1073 and 0.1417 S·cm, respectively, from the electrochemical measurements we estimated that the effective diameter of the nanochannel changed in accordance to:

$$\frac{d^{40^oC}}{d^{23^oC}} \sim 3.4 \qquad 3.6.4$$

These results clearly evidence the nanoactuating behaviour of the PNIPAM brush that above the LCST undergoes a sharp change in the conformational state, leading to a 3-fold increase of the effective cross-section of the nanochannel. The thermoresponsive brush is acting as a thermally driven macromolecular gate controlling the ionic flow through the nanochannel.

Table 3.6.1: Changes in conductance (G), specific conductivity (κ), channel opening and channel diameter (d) upon variations in temperature.

T /°C	G /nS	κ/ S·cm^{-1}	$\frac{d^{T}}{d^{23^oC}}$	d (nm)
23	17	0.1073	1	~ 8
32	56	0.1252	2.8	~ 22
40	76	0.1417	3.4	~ 27

The very sensitive nature of the thermoactuated nanochannel is also evidenced when studied at temperatures near the LCST. Figure 3.6.3 depicts the *I-V* plots for the PNIPAM-modified channel measured at 32 °C. In that case, we recorded a very stable *I-V* curve with a slope corresponding to a nanochannel conductance of 56 nS, which is between 17 nS (23 °C) and 76 nS (40 °C). This fact further evidences the molecular-level control of the gating process in the nanoconfined environment driven by the fine-tuning of the temperature. In other

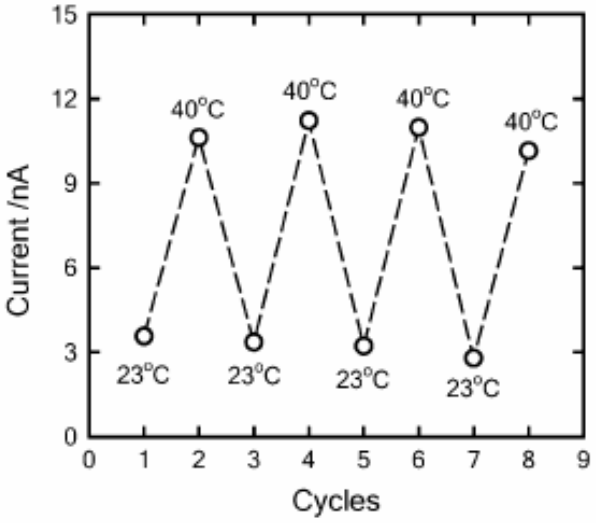

Figure 3.6.5: Temperature cycling between 23 and 40 °C corresponding to a nanochannel modified with PNIPAM brushes. D = 1.26 μm, $d_{23\,^oC}$ ~ 1.2 nm, $d_{40\,^oC}$ ~ 4.8 nm.

words, temperature variations in the physiological range (23 - 40 ^{o}C) can lead to the accurate control of the macromolecular nanogate through temperature-driven intermediate conformational states (Table 3.6.1).

Another important aspect of these thermoresponsive nanoarchitectures relies on the reversibility of the conformational changes, which are evidenced as reversible changes in the ionic current through the nanochannel. Figure 3.6.5 displays the temperature cycling between 23 and 40^{o}C of a PNIPAM brush-modified single nanochannel with d < 5 nm. It can be clearly seen that the variations in the ionic flux, originated from the thermally triggered conformational changes of the PNIPAM brush, are completely reversible. This fact further illustrates the versatility of the polymer brushes to achieve an accurate and reversible control of the topological characteristics of the nanoconfined environments with the dimension comparable to the biological ion channels.

3.6.3 Conclusion

In summary, in this work it was described for the first time the combined use of thermoresponsive polymer brushes together with single solid-state nanochannels to create fully artificial stimuli-responsive nanochannels which resemble those commonly encountered in nature. We demonstrated that the PNIPAM-modified nanochannels act as thermally driven molecular gates with closure stages that can be remotely controlled by simply tuning the working temperature in the 23 – 40^{o}C range. Achieving a delicate control of the nanoactuating characteristics of this molecular device in the physiological temperature range is an interesting feature that could be of much interest for the implementation of artificial nanosystems propelled and/or controlled by temperature variations in living systems, like human beings. In this context, one interesting application could be in the area of biomedical science and nanomedicine through the implementation of these fully *"abiotic"* nanogating devices as "intelligent" channels enabling the temperature-tuned release of drugs.

3.7 Synthetic Proton-Gated Ion Channels via Single Solid-State Nanochannels Modified with Responsive Polymer Brushes.

3.7.1 Introduction

During the last few years, the scientific community witnessed great interest in the study and application of nanoscale fluidic architectures in order to control and manipulate the transport of chemical and biochemical species in close resemblance to the biological nanochannels.[54,66,89,110,114,149] This endeavor together with the remarkable advances in nanofabrication techniques gave rise to different routes to construct in a reproducible manner fully "abiotic" nanochannels in organic polymeric and also inorganic materials with dimensions comparable to biological molecules.[188] Furthermore, synthetic solid-state nanochannels display several important advantages over their biological counterparts such as robustness, stability, control over channel geometry, amenable integration into devices and tailorable surface properties.[51,114] It is worthwhile mentioning that appealing effects arise when the channel surface is charged, with dimensions comparable to the range of the electrostatic interactions in solution.[37, 63,215] In case of having a channel size with dimensions smaller than the Debye length, the nanoconfined environment becomes a "unipolar solution" of counterions in order to neutralize the immobilized surface charge.[143,145] This implies that by controlling the surface charge density along the confined environment the channel conductance and, as a consequence, the ion current can be modulated. A key goal of nanotechnology relies on the design and construction of functional systems having properties which are specific to their size.[117] These fascinating physicochemical properties, displayed by charged nanochannels provided the scenario to create new functional and addressable architectures and also led to the birth of a whole new area of research concerning the design of nanochannel-based devices resting on surface-charge – governed ionic transport, e.g.: nanofluidic diode[89,108] bipolar diode.[61] Regulation of nanochannel surface charge is a most important principle that nature also exploits to create molecular gates enabling the controlled passage of ions through the membranes. However, in biological channels, the mechanisms for activating the transport of ions can be more complicated and triggered by environmental conditions.[202] In the presence of specific chemical stimuli, the channel can be

switched from an "off" state, in which blockage or low ionic current passes through the channels, to an "on" state that is evidenced by a high transmembrane ionic current. This gives rise to a molecular gate that is activated by an external chemical stimulus, like pH. For example, the tetrameric M2 protein from influenza A, one of the simplest pH-gated ion channels known, suffers a conformational switch upon protonation of its histidine residues.[216] The structural switch, from a uniprotonated to a biprotonated channel, causes an electrostatic repulsion between the charged histidine moieties that pushes the helices apart. More important, the pH required to activate the channel is close to the pKa of the histidine groups, indicating that the protonation change is responsible for the channel gating.[217] This example illustrates how the nanochannel environment adapts the external changes to tune its electrostatic characteristics. Recently, we have demonstrated that polymer brushes represent a valuable alternative to modify the electrostatic environment of nanochannels and to significantly increase the surface density of functional groups.[218] These macromolecular films make it possible to achieve molecularly designed interfaces in order to control surface charge, hydrophobicity, and chemical functionality in an accurate manner.[197,198] In few words, they provide unique new avenues to incorporate "smart" or "responsive" chemical functionalities into confined geometries.

Within this framework, the integration of environmental stimuli-responsive brushes into solid-state nanochannels would lead to the creation of robust signal-responsive devices mimicking the function of proton-gated ion channels commonly encountered in biological membranes, i.e., the nanochannel can be switched from an "off" state to an "on" state in response to a pH drop.

Here, we report the construction of a nanochannel-based chemical device whose transmembrane ion current can be accurately controlled by manipulating the proton concentration in the surrounding environment. In this context, pH-responsive poly(4-vinyl pyridine) brushes were incorporated into single solid-state nanochannels in such a fashion that leads to a nanodevice whose electronic readout can be switched between "on" and "off" states. In close resemblance to biological channels, the pH required to activate the "abiotic" ion channel is close to the pKa of the pyridine groups. The electrostatic changes arising from the protonation/deprotonation of these groups are responsible for tuning the channel conductance that leads to the channel gating. More important, it was also demonstrated that the pH can tune and amplify the electronic readout in the "on" configuration. The use of "responsive" macromolecular architectures to manipulate the ion transport through nanochannels provides an attractive strategy to create electronic nanodevices

with environmental responsive characteristics to be implemented as robust "smart" nanochannel sensors.

3.7.2 Results and Discussion

Single cylindrical nanochannels, with diameter (*d*) of ~ 15 nm and length (*L*) of ~12 μm, were fabricated by symmetrical etching of ion-tracked polyethylene terephthalate (PET) films, irradiated with single swift heavy ions (chapter 2, section 2.2.1). Then, the single nanochannel-containing membranes were modified with 4,4´-azobis(4-cyanopentanoic acid) as a surface-initiated polymerization initiator.[128,200] Afterwards, the polyvinylpyridine (PVP) brush growth was accomplished by surface-initiated free radical polymerization of the pH-responsive monomer 4-vinyl pyridine (Figure. 3.7.1).

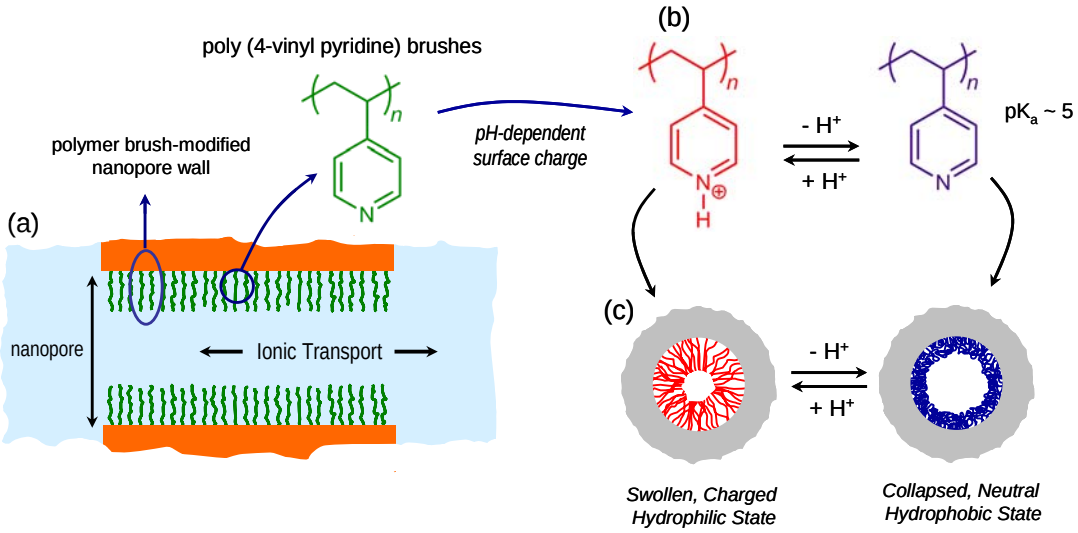

Figure 3.7.1. (a) Schematic description of the brush-modified cylindrical nanochannel. In the scheme is also indicated the chemical structure of poly(4-vinyl pyridine) brushes. (b) pH-dependent pyridine-pyridinium equilibrium taking place in the brush environment. (c) Simplified illustration indicating the conformational changes occurring in the brush layer upon variations in the environmental pH.

After a preset polymerization time, the membranes were thoroughly rinsed with deionized water and mounted between the two halves of the conductivity cell. Figure 3.7.2 depicts the *I-V* curves of a single nanochannel modified with PVP brushes using 0.1 M KCl (at different pHs) as an electrolyte solution in both half cells. By increasing the pH from 2 to 4, and finally to 10, a significant decrease in the transmembrane ionic current was observed under the same applied

bias. The pH-dependent *I-V* response is correlated to the channel conductance values of 0.27, 0.12, and 0.033 nS for pHs 2, 4, and 10, respectively. The conductance values of the nanochannel were determined by fitting the slope of the transmembrane current as a function of the applied voltage[110]. These results reveal that by changing the pH from 2 to 10 can lead to an eight-fold decrease in transmembrane ionic current, from 0.52 to 0.065 nA, passing through the nanochannel.

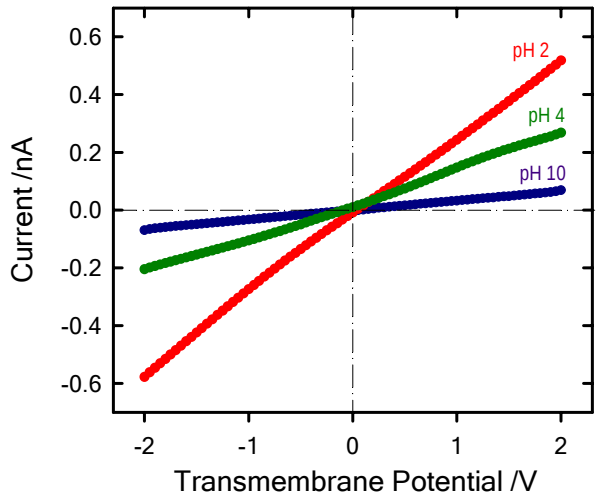

Figure 3.7.2: Current-voltage characteristics of a single cylindrical PVP brush-modified nanochannel in 0.1 M KCl at different pH s (red circles) 2, (green circles) 4, (blue circles) 10.

In close resemblance to the biological channel of the M2 protein, the interpretation of these results requires considering the chemical equilibrium associated to the protonation of the pyridine moieties in the brush layer. The pyridine-pyridinium equilibrium is responsible for setting the electrostatic characteristics of the molecular film covering the inner walls of the nanochannel (Figure 3.7.1). As is well known, surface charges induce electrostatic screening and electrokinetic effects that may have large effects on the channel conductance.[215] In highly confined environments, with dimensions comparable to the Debye length, the surface charge density (σ) determines the local ionic concentration within the nanochannel and in this way controls the nanochannel conductance (G). The charged surface attracts the mobile counterions from the ionic solution and builds up a charged layer that screens the surface-confined charges. As a result, surface charges proportionally raise the nanochannel conductance by mediating the transport of counter ions near the surface, $G \propto \sigma$. Therefore, we can infer that at strongly acidic pH values the pyridine moieties in the brush are protonated, thus conferring a well-defined cationic character to the surface charges immobilized in the inner environment of the nanochannel. As described in Figure 3.7.1, the equilibrium of the pyridine moieties, which in turn determines the population of pyridinium species, is thermodynamically controlled by the pH value. The p*K*a of the pyridine-pyridinium equilibrium is 5.2.[219] So, by changing the acidic pH from 2 to 4 the population of neutral pyridine moieties grew at the

expense of the pyridinium species, resulting in a "less positive" nanochannel surface. This pH-induced variation in surface charges proportionally affects the channel conductance, *i.e.* the channel conductance decreases as the pH increases. Figure 3.7.3 shows that the displacement of the protonation equilibrium enables the modulation of the transmembrane ionic current by changes in the proton concentration in the range $2 \leq$ pH ≤ 5.

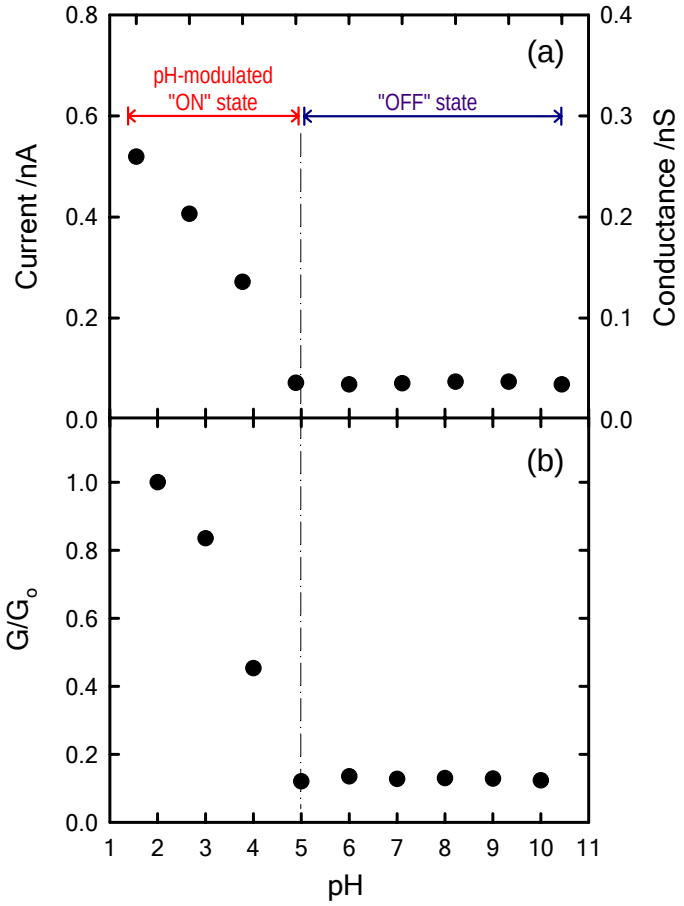

Figure 3.7.3: Representation of the transmembrane ionic current (measured at 2 V of applied bias voltage) (panel a), the nanochannel conductance (panel a) and the nanochannel conductance normalized to the maximal conductance of the "fully" open channel at pH 2 (G/G_o) (panel b) as a function of the environmental pH for a PVP brush-modified cylindrical nanochannel. In the plot are also indicated the regions corresponding to the "ON" and "OFF" states of the nanogate. The dotted vertical line at pH 5 (~ p$Ka_{Py\text{-}Py+}$) was introduced to guide the eye.

The decreasing variation in transmembrane current is 0.147 nA/pH-unit. This indicates that the pH-controlled pyridine/pyridinium equilibrium provides a facile chemical tool to easily tune the electronic readout originating from the ionic transport through the nanochannel. The magnitude

of the transmembrane ion currents and channel conductivities at different pHs are highly reproducible, indicating the fidelity and robustness of the PVP brush to control the ion transport through the nanochannel. After that, increasing the pH above p*K*a caused no further changes in the transmembrane current values. As is evident from Figure 3.7.3, the transmembrane current decreases with increasing proton concentration until reaching the condition pH ~ p*K*a, in which the nanochannel displays the lowest conductance value, 33 pS. Then, a constant low conductance value in the range $5 \leq$ pH ≤ 10 was observed. This can be interpreted considering that the equilibrium of the PVP brush has been fully displaced towards the formation of uncharged pyridine and, consequently, the surface charges which mediated the transport of counterions near the surface, and boosted the channel conductance, were removed from the channel. The full deprotonation of the PVP brush led to the "off" state (low conductance) of the nanochannel. In our experimental scenario, the transmembrane ion currents in the "off" and "on" states differ by nearly one, an order of magnitude, thus indicating that the pH-induced physicochemical changes, undergone by the brush, enable the opening and closure of the gate. Figure 3.7.3b shows the channel conductance normalized to the maximal conductance of the "fully" open channel at pH 2, G/G_o, plotted against the applied pH. The chemical actuation of the ionic gate from the "on" to the "off" state promotes a 90 % decrease in channel conductance. It is worthwhile noticing that these relative changes in channel conductance measured in the PVP brush-modified nanochannel are comparable to that observed in many biological systems, as evidenced from the proton-gated Na^+ current in patch-clamped Calu-3 cells, which display ~ 90 % decrease in ion current upon closing their channels.[220]

Nevertheless, it should also be kept in mind that deprotonation of PVP not only promotes the removal of the surface charges but also leads to a sharp transition of the swollen hydrophilic brush into a collapsed hydrophobic state.[221] In principle, the structural reorganization into a collapsed state would change the effective cross section of the channel which would lead to a slight increase in channel conductivity. As can be seen in Figure 3.7.3, collapsing the brush above pH 5 does not reflect any increase in conductivity. This indicates that the cross-sectional changes which can occur as a result of the brush collapse are not significant when compared with the major electrostatic changes promoted by the deprotonation of the pyridinium moieties. Furthermore, the collapse of the PVP brushes promotes major changes in the hydrophobicity of the surface. Recently, Lindqvist *et al.* reported that the wettability of surfaces modified with PVP brushes can be switched from 0^o to 120^o upon variations in pH from 3 to 9.[222] This indicates that

increasing the pH above p*K*a switches the inner environment of the nanochannel from a hydrophilic conducting "on" state to a hydrophobic nonconducting "off" state. It was hypothesized that decreasing the polarity of the channel wall, i.e., increasing its hydrophobicity, could act as an effective mechanism to hinder the formation of the mobile electrolyte layer which mediates the ionic transport in the boundaries of the channel wall.[49] In addition, we have to note that water in very confined geometries can exhibit different dynamics not seen in the bulk system, including the wet–dry transition due to confinement.[223] Recent experimental work reported by Dekker and co-workers described the anomalous conductance behaviour of nanochannels ~ 10 nm in diameter.[224] This behavior was attributed to the presence of air nanobubbles trapped inside the nanochannels. In a similar fashion, Russo *et al.* suggested that the bubbles can act as bistable hydrophobic gates responsible for the on-off transitions of single channel currents.[225] In our case, we did not observe any fluctuations in the channel conductivity at any fixed pH, which might indicate that no nanobubbles are present. Reversing the pH of the solution reflects highly reproducible and reversible changes in the transmembrane ion currents flowing through the macromolecular gate operating in the "on" and "off" states. The difference in amplitude between the higher conductance state and the lower one is remarkably constant.

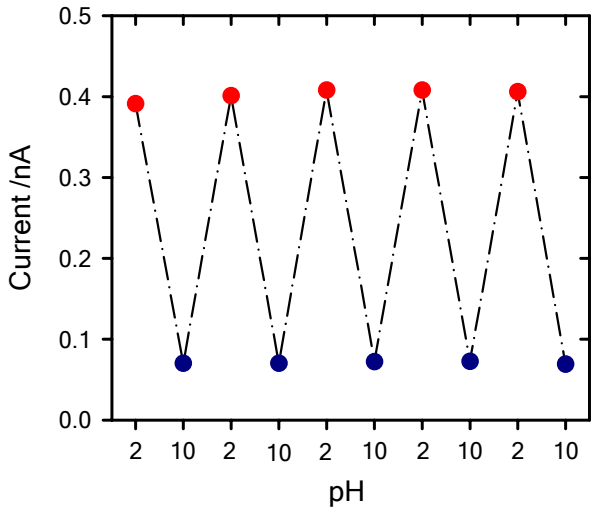

Figure 3.7.4: Reversible variation of the transmembrane ionic current passing through the PVP brush-modified nanochannel upon alternating the environmental pH between 2 (red circles. "on" state) and 10 (blue circles "off" state).

3.7.3 Conclusion

In summary, it was described here the construction of a fully "abiotic" nanodevice displaying the ionic-current switching behaviour typical of that observed in many biological channels that fulfil key pH-dependent transport functions in living organisms. Construction of such a nanodevice required the integration of stable and ductile macromolecular building blocks with the

appropriate responsiveness that could act as gate-keepers managing and constraining the flow of ionic species through the confined environment. Our approach employs dressing of the inner walls of PET-made single nanochannels with pH-responsive poly (4-vinyl pyridine) brushes. The "on/off" switching is based on the manipulation of the surface charges of the channel walls via the protonation of the brush layer, which in turn control the channel conductivity. The externally controllable switch is chemically actuated through environmental pH changes with which the gate is opened or closed. In the range $2 \leq$ pH ≤ 5, the measurable electronic readout is modulated with gradual changes in the proton concentration, thus leading to a pH-tunable transmembrane ionic current. Increasing the pH above the p*K*a of the pyridine moieties lead to the full deprotonation of the nanochannel which gives rise to the closure of the ionic gate.

The development of chemically actuated nanovalves with tunable properties resulting from charge and macromolecular changes provides an attracting avenue to design and construct robust nanoscale systems resembling the functions of sophisticated biological structures, like channel-forming proteins. In this context, the use of responsive polymer bushes, incorporated into solid-state single nanochannels, represents an exciting approach to create tailor-made nanovalves to be implemented in sensoring, dosing, signal transduction or nanofluidic systems.

4. SUMMARY AND OUTLOOK

There is a growing quest for tailorable nanochannels having dimensions comparable to the size of biological molecules and mimicking the function of biological ion channels. This interest is based on the use of nanochannels as extremely sensitive single-molecule biosensors. The biosensing and stimuli-responsive capabilities of these nanochannels depend sensitively on the surface characteristics of their inner walls in order to achieve the desired functionality of the biomimetic system. Nanoscale control over the surface properties of the nanochannel plays a crucial role in the biosensing and stimuli-responsive performance due to the chemical groups incorporated on the inner channel walls which act as binding sites for different analytes as well as interact with molecules passing through the channel.

This work deals with the functionalization and application of synthetic nanochannels fabricated in ion-tracked polymer (PET and PI) membranes. Single conical nanochannels in PET were fabricated by asymmetric etching with 9 M NaOH at room temperature, using a stopping solution of 1 M KCl + 1 M HCOOH. For Kapton, NaOCl was used as an etchant while 1 M KI acts as a stopping solution at 50 ºC. The etching procedure for the fabrication of asymmetric nanochannels in PET was further improved and refined by using surfactant in the etchant. The surfactant-controlled etching technique reduces the etching time from one hour to a few minutes and is more reproducible as compared to the traditional asymmetric (one-sided) etching method.

The surface of ion track-etched nanochannels in polymer membranes bears carboxyl (-COOH) groups which were chemically reacted with a variety of different molecules having variable size and polarity. Firstly, these carboxyl groups were activated into NHS-esters or PFP-esters by using EDC/NHS or EDC/PFP coupling chemistry, respectively. Subsequently, these reactive esters were covalently coupled with primary amino groups of the reacting molecules. It was also found that the reactive intermediate PFP-ester is more active than the corresponding NHS-ester, which leads to higher efficiency of the modification reaction.The success of these chemical modification reactions were confirmed by measuring *I-V* curves and permselectivity of the channel after functionalization. The nanochannels with variable surface charge were successfully used for the electrochemical detection of proteins. For example, the electrostatic/hydrophobic association of

bovine serum albumin on the channel surface (before and after functionalization) was monitored via the changes in the ionic current flowing through the channel upon the variation of pH values.
The surface carboxyl groups were also used for the electrostatical self-assemblies of bifunctional macromolecular ligands. The biorecognition elements were incorporated into the single conical nanochannels by using biotinylated-poly(allylamine HCl) for constructing a nano-biosensor. The experimental results demonstrated that the ligand-functionalized nanochannels are very stable and the biorecognition event (protein i.e. streptavidin conjugation) does not promote the removal of the ligands from the channel surface. In addition, control experiments indicated that the electrostatically assembled nanochannel surface displays good biospecificity and non-fouling properties. This approach also enables the creation of supramolecular multilayered architectures inside the nanochannel which are stabilized by strong ligand-receptor (biotin-streptavidin) interactions.
Single PET conical nanochannels were selectively functionalized with monolayers of lysine and histidine chains, respectively. The positive and negative charges at the terminus of these chains are very sensitive to the external pH. This nanofluidic diode, with amphoteric chains attached to the channel surface allows for a broad set of rectification properties supported by a single nanodevice. A definite plus is to functionalize these groups on a conical nanochannel with well-defined, controlled structural asymmetry which gives virtually every rectification characteristic that may be required in practical applications. Nanometer-scaled amphoteric channels are of general interest because of the potential applications in drug delivery systems, ion-exchange membranes for separation of bio-macromolecules, antifouling materials with reduced molecular adsorption, and biochemical sensors.
Single conical nanochannels fabricated in PI, were functionalized with poly(methacryloyl-L-lysine) brushes, in order to obtain a new highly functional signal-responsive chemical nanodevice. The responsive brushes were constituted of zwitterionic monomers (methacryloyl-L-lysine) whose charge is regulated via pH changes in the environmental conditions. The pH-dependent chemical equilibrium of the monomer units provides a fine-tuning of the ion transport through the nanochannel by simply presetting the pH of the electrolyte solution. It was demonstrated that this strategy enables a higher degree of control over the rectification properties when compared to the nanochannels modified with charged monolayer assemblies.
These conical nanochannels in polyimide were also functionalized with thermo-responsive polyNIPAM brushes. The PNIPAM-functionalized nanochannels were acting as a thermally

driven macromolecular gate, with tunable diameter, controlled by the temperature changes in the physiological range. At lower temperature (23 ºC), the PNIPAM brushes remained in swollen state which leads to a decrease in the effective cross-section of the channel. When the temperature of the external environment was increased above the lower critical temperature (> 32 ºC), the PNIPAM brushes were in collapsed state, leading to an increase in the effective diameter of the channel and thus allowed the ion transport through the nanochannel.

PET membranes containing single cylindrical nanochannels were also decorated with pH-responsive poly(4-vinyl pyridine) brushes. The transport properties of PVP-funtionalized nanochannels was controlled by manipulating the proton concentration in the surrounding environment, that is, the nanochannel can be switched from an "off" state to an "on" state in repose to a pH drop. The "on/off" switching is based on the manipulation of the surface charges of the channel walls via the protonation of the brush layer, which in turn control the channel conductivity.

In the context of future activities, it is planned to explore in more detail the possibilities to chemically functionalize the surface of track-etched nanochannels in different polymer membranes. These nanochannels, functionalized with a variety of different molecular recognition elements, will be used for the detection of a specific type of biomolecules. By manipulating the surface properties (charge and hydrophobicity), the single polymer nanochannels could also be used for the detection and analysis of single molecules, e.g., DNA analytes.

It would be an interesting task to functionalize these nanochannels with specific type of polypeptides or enzymes, which will be used for the complexation of metal ions and catalysis of a specific type of reagents, respectively.

In near future, it is also planned to modify the surface charge of multi-channel polymer membranes for the controlled transport of charged organic molecules and dyes through them. It would also be possible to immobilize specific enzymes on the multi-channel membranes for the separation of enantiomers.

Concerning the extraordinary stability of PI and polyetheretherketone (PEEK), with respect to mechanical stress and high temperature, these track-etched porous membranes would also be useful for the fuel cell applications. In this context, the nanochannels in these membranes can be filled with a specific polyelectrolyte, which conducts protons selectively through them.

5. REFERENCES

1. Hille, B., *Ionic channels of excitable membranes*. Second ed.; Sinauer Associates Inc.: Sunderland, Massachusetts, 1992.
2. Voet, D.; Voet, J. G., *Biochemistry*. Third ed.; John Wiley and Sons: New York, 2004.
3. Gouaux, E.; MacKinnon, R., Principles of selective ion transport in channels and pumps. *Science* **2005,** 310, (5753), 1461-1465.
4. Hodgkin, A. L.; Huxley, A. F., Currents carried by sodium and potassium ions through the membrane of the giant axon of Loligo. *The Journal of Physiology* **1952,** 116, 449-472.
5. Katz, B., *Nerve, Muscle, Synapse*. McGraw-Hill: New York, 1966.
6. Henry, J. P.; Chich, J. F.; Goldschmidt, D.; Thieffry, M., Blockade of a mitochondrial cationic channel by an addressing peptide - An electrophysiological study. *Journal of Membrane Biology* **1989,** 112, (2), 139-147.
7. Simon, S. M.; Blobel, G., A protein-conducting channel in the endoplasmic-reticulum *Cell* **1991,** 65, (3), 371-380.
8. Bayley, H.; Cremer, P. S., Stochastic sensors inspired by biology. *Nature* **2001,** 413, (6852), 226-230.
9. Mathe, J.; Aksimentiev, A.; Nelson, D. R.; Schulten, K.; Meller, A., Orientation discrimination of single-stranded DNA inside the alpha-hemolysin membrane channel. *Proceedings of the National Academy of Sciences of the United States of America* **2005,** 102, (35), 12377-12382.
10. Ashkenasy, N.; Sanchez-Quesada, J.; Bayley, H.; Ghadiri, M. R., Recognizing a single base in an individual DNA strand: A step toward DNA sequencing in nanopores. *Angewandte Chemie-International Edition* **2005,** 44, (9), 1401-1404.
11. Butler, T. Z.; Gundlach, J. H.; Troll, M., Ionic current blockades from DNA and RNA molecules in the alpha-hemolysin nanopore. *Biophysical Journal* **2007,** 93, (9), 3229-3240.
12. Howorka, S.; Cheley, S.; Bayley, H., Sequence-specific detection of individual DNA strands using engineered nanopores. *Nature Biotechnology* **2001,** 19, (7), 636-639.
13. Astier, Y.; Braha, O.; Bayley, H., Toward single molecule DNA sequencing: Direct identification of ribonucleoside and deoxyribonucleoside 5 '-monophosphates by using an engineered protein nanopore equipped with a molecular adapter. *Journal of the American Chemical Society* **2006,** 128, (5), 1705-1710.
14. Henrickson, S. E.; Misakian, M.; Robertson, B.; Kasianowicz, J. J., Driven DNA transport into an asymmetric nanometer-scale pore. *Physical Review Letters* **2000,** 85, (14), 3057-3060.
15. Braha, O.; Gu, L. Q.; Zhou, L.; Lu, X. F.; Cheley, S.; Bayley, H., Simultaneous stochastic sensing of divalent metal ions. *Nature Biotechnology* **2000,** 18, (9), 1005-1007.
16. Kasianowicz, J. J.; Burden, D. L.; Han, L. C.; Cheley, S.; Bayley, H., Genetically engineered metal ion binding sites on the outside of a channel's transmembrane beta-barrel. *Biophysical Journal* **1999,** 76, (2), 837-845.

17. Kang, X. F.; Cheley, S.; Guan, X. Y.; Bayley, H., Stochastic detection of enantiomers. *Journal of the American Chemical Society* **2006,** 128, (33), 10684-10685.
18. Howorka, S.; Nam, J.; Bayley, H.; Kahne, D., Stochastic detection of monovalent and bivalent protein-ligand interactions. *Angewandte Chemie-International Edition* **2004,** 43, (7), 842-846.
19. Movileanu, L.; Howorka, S.; Braha, O.; Bayley, H., Detecting protein analytes that modulate transmembrane movement of a polymer chain within a single protein pore. *Nature Biotechnology* **2000,** 18, (10), 1091-1095.
20. Gu, L. Q.; Braha, O.; Conlan, S.; Cheley, S.; Bayley, H., Stochastic sensing of organic analytes by a pore-forming protein containing a molecular adapter. *Nature* **1999,** 398, (6729), 686-690.
21. Guan, X. Y.; Gu, L. Q.; Cheley, S.; Braha, O.; Bayley, H., Stochastic sensing of TNT with a genetically engineered pore. *Chembiochem* **2005,** 6, (10), 1875-1881.
22. Li, J.; Stein, D.; McMullan, C.; Branton, D.; Aziz, M. J.; Golovchenko, J. A., Ion-beam sculpting at nanometre length scales. *Nature* **2001,** 412, (6843), 166-169.
23. Storm, A. J.; Chen, J. H.; Ling, X. S.; Zandbergen, H. W.; Dekker, C., Fabrication of solid-state nanopores with single-nanometre precision. *Nature Materials* **2003,** 2, (8), 537-540.
24. Ho, C.; Qiao, R.; Heng, J. B.; Chatterjee, A.; Timp, R. J.; Aluru, N. R.; Timp, G., Electrolytic transport through a synthetic nanometer-diameter pore. *Proceedings of the National Academy of Sciences of the United States of America* **2005,** 102, (30), 10445-10450.
25. Wu, S. S.; Park, S. R.; Ling, X. S., Lithography-free formation of nanopores in plastic membranes using laser heating. *Nano Letters* **2006,** 6, (11), 2571-2576.
26. Danelon, C.; Santschi, C.; Brugger, J.; Vogel, H., Fabrication and functionalization of nanochannels by electron-beam-induced silicon oxide deposition. *Langmuir* **2006,** 22, (25), 10711-10715.
27. Biance, A. L.; Gierak, J.; Bourhis, E.; Madouri, A.; Lafosse, X.; Patriarche, G.; Oukhaled, G.; Ulysse, C.; Galas, J. C.; Chen, Y.; Auvray, L. Focused ion beam sculpted membranes for nanoscience tooling. *Microelectronic Engineering* **2006,** 83, (4-9), 1474-1477.
28. Umehara, S.; Pourmand, N.; Webb, C. D.; Davis, R. W.; Yasuda, K.; Karhanek, M., Current rectification with poly-L-lysine-coated quartz nanopipettes. *Nano Letters* **2006,** 6, (11), 2486-2492.
29. Wang, G. L.; Zhang, B.; Wayment, J. R.; Harris, J. M.; White, H. S., Electrostatic-gated transport in chemically modified glass nanopore electrodes. *Journal of the American Chemical Society* **2006,** 128, (23), 7679-7686.
30. Apel, P. Y.; Korchev, Y. E.; Siwy, Z.; Spohr, R.; Yoshida, M., Diode-like single-ion track membrane prepared by electro-stopping. *Nucl. Instrum. Methods Phys. Res. B* **2001,** 184, (3), 337-346.
31. Harrell, C. C.; Siwy, Z. S.; Martin, C. R., Conical nanopore membranes: Controlling the nanopore shape. *Small* **2006,** 2, (2), 194-198.
32. Siwy, Z.; Apel, P.; Dobrev, D.; Neumann, R.; Spohr, R.; Trautmann, C.; Voss, K., Ion transport through asymmetric nanopores prepared by ion track etching. *Nucl. Instrum. Methods Phys. Res. B* **2003,** 208, 143-148.
33. Siwy, Z.; Gu, Y.; Spohr, H. A.; Baur, D.; Wolf-Reber, A.; Spohr, R.; Apel, P.; Korchev, Y. E., Rectification and voltage gating of ion currents in a nanofabricated pore. *Europhysics Letters* **2002,** 60, (3), 349-355.

34. Harrell, C. C.; Kohli, P.; Siwy, Z.; Martin, C. R., DNA - Nanotube artificial ion channels. *Journal of the American Chemical Society* **2004,** 126, (48), 15646-15647.
35. Lee, S. B.; Martin, C. R., pH-switchable, ion-permselective gold nanotubule membrane based on chemisorbed cysteine. *Analytical Chemistry* **2001,** 73, (4), 768-775.
36. Martin, C. R.; Nishizawa, M.; Jirage, K.; Kang, M. S.; Lee, S. B., Controlling ion-transport selectivity in gold nanotubule membranes. *Advanced Materials* **2001,** 13, (18), 1351-1362.
37. Siwy, Z.; Heins, E.; Harrell, C. C.; Kohli, P.; Martin, C. R., Conical-nanotube ion-current rectifiers: The role of surface charge. *Journal of the American Chemical Society* **2004,** 126, (35), 10850-10851.
38. Siwy, Z.; Trofin, L.; Kohli, P.; Baker, L. A.; Trautmann, C.; Martin, C. R., Protein biosensors based on biofunctionalized conical gold nanotubes. *Journal of the American Chemical Society* **2005,** 127, (14), 5000-5001.
39. Braha, O.; Walker, B.; Cheley, S.; Kasianowicz, J. J.; Song, L. Z.; Gouaux, J. E.; Bayley, H., Designed protein pores as components for biosensors. *Chemistry & Biology* **1997,** 4, (7), 497-505.
40. Cheley, S.; Gu, L. Q.; Bayley, H., Stochastic sensing of nanomolar inositol 1,4,5-trisphosphate with an engineered pore. *Chemistry & Biology* **2002,** 9, (7), 829-838.
41. Howorka, S.; Movileanu, L.; Braha, O.; Bayley, H., Kinetics of duplex formation for individual DNA strands within a single protein nanopore. *Proceedings of the National Academy of Sciences of the United States of America* **2001,** 98, (23), 12996-13001.
42. Gu, L. Q.; Bayley, H., Interaction of the noncovalent molecular adapter, beta-cyclodextrin, with the staphylococcal alpha-hemolysin pore. *Biophysical Journal* **2000,** 79, (4), 1967-1975.
43. Nishizawa, M.; Menon, V. P.; Martin, C. R., Metal nanotubule membranes with electrochemically switchable ion-transport selectivity *Science* **1995,** 268, (5211), 700-702.
44. Alem, H.; Blondeau, F.; Glinel, K.; Demoustier-Champagne, S.; Jonas, A. M., Layer-by-layer assembly of polyelectrolytes in nanopores. *Macromolecules* **2007,** 40, (9), 3366-3372.
45. Hou, Z. Z.; Abbott, N. L.; Stroeve, P., Self-assembled monolayers on electroless gold impart pH-responsive transport of ions in porous membranes. *Langmuir* **2000,** 16, (5), 2401-2404.
46. Love, J. C.; Estroff, L. A.; Kriebel, J. K.; Nuzzo, R. G.; Whitesides, G. M., Self-assembled monolayers of thiolates on metals as a form of nanotechnology. *Chemical Reviews* **2005,** 105, (4), 1103-1169.
47. Nilsson, J.; Lee, J. R. I.; Ratto, T. V.; Letant, S. E., Localized functionalization of single nanopores. *Advanced Materials* **2006,** 18, (4), 427-431.
48. Odom, D. J.; Baker, L. A.; Martin, C. R., Solvent-extraction and Langmuir-adsorption-based transport in chemically functionalized nanopore membranes. *Journal of Physical Chemistry B* **2005,** 109, (44), 20887-20894.
49. Vlassiouk, I.; Park, C. D.; Vail, S. A.; Gust, D.; Smirnov, S., Control of nanopore wetting by a photochromic spiropyran: A light-controlled valve and electrical switch. *Nano Letters* **2006,** 6, (5), 1013-1017.
50. Vlassiouk, I.; Rios, F.; Vail, S. A.; Gust, D.; Smirnov, S., Electrical conductance of hydrophobic membranes or what happens below the surface. *Langmuir* **2007,** 23, (14), 7784-7792.

51. Wanunu, M.; Meller, A., Chemically modified solid-state nanopores. *Nano Letters* **2007,** 7, (6), 1580-1585.
52. Kohli, P.; Harrell, C. C.; Cao, Z. H.; Gasparac, R.; Tan, W. H.; Martin, C. R., DNA-functionalized nanotube membranes with single-base mismatch selectivity. *Science* **2004,** 305, (5686), 984-986.
53. Vlassiouk, I.; Krasnoslobodtsev, A.; Smirnov, S.; Germann, M., "Direct" detection and separation of DNA using nanoporous alumina filters. *Langmuir* **2004,** 20, (23), 9913-9915.
54. Sexton, L. T.; Horne, L. P.; Martin, C. R., Developing synthetic conical nanopores for biosensing applications. *Molecular Biosystems* **2007,** 3, (10), 667-685.
55. Savariar, E. N.; Krishnamoorthy, K.; Thayumanavan, S., Molecular discrimination inside polymer nanotubules. *Nature Nanotechnology* **2008,** 3, (2), 112-117.
56. Li, J.; Maekawa, Y.; Yamaki, T.; Yoshida, M., Chemical modification of a poly(ethylene terephthalate) surface by the selective alkylation of acid salts. *Macromolecular Chemistry and Physics* **2002,** 203, (17), 2470-2474.
57. Maekawa, Y.; Suzuki, Y.; Maeyama, K.; Yonezawa, N.; Yoshida, M., Visualization of chemical modification of pore internal surfaces using fluorescence microscopy. *Chemistry Letters* **2004,** 33, (2), 150-151.
58. Maekawa, Y.; Suzuki, Y.; Maeyama, K.; Yonezawa, N.; Yoshida, M., Chemical modification of the internal surfaces of cylindrical pores of submicrometer size in poly(ethylene terephthalate). *Langmuir* **2006,** 22, (6), 2832-2837.
59. Marchandbrynaert, J.; Deldime, M.; Dupont, I.; Dewez, J. L.; Schneider, Y. J., Surface functionalization of poly(ethylene terephthalate) film and membrane by controlled wet chemistry: chemical characterization of carboxylated surfaces. *Journal of Colloid and Interface Science* **1995,** 173, (1), 236-244.
60. Papra, A.; Hicke, H. G.; Paul, D., Synthesis of peptides onto the surface of poly(ethylene terephthalate) particle track membranes. *Journal of Applied Polymer Science* **1999,** 74, (7), 1669-1674.
61. Kalman, E. B.; Vlassiouk, I.; Siwy, Z. S., Nanofluidic bipolar transistors. *Advanced Materials* **2008,** 20, (2), 293-297.
62. Kececi, K.; Sexton, L. T.; Buyukserin, F.; Martin, C. R., Resistive-pulse detection of short dsDNAs using a chemically functionalized conical nanopore sensor. *Nanomedicine* **2008,** 3, (6), 787-796.
63. Vlassiouk, I.; Siwy, Z. S., Nanofluidic diode. *Nano Letters* **2007,** 7, (3), 552-556.
64. Xia, F.; Guo, W.; Mao, Y. D.; Hou, X.; Xue, J. M.; Xia, H. W.; Wang, L.; Song, Y. L.; Ji, H.; Qi, O. Y.; Wang, Y. G.; Jiang, L., Gating of single synthetic nanopores by proton-driven DNA molecular motors. *Journal of the American Chemical Society* **2008,** 130, (26), 8345-8350.
65. Kasianowicz, J. J.; Robertson, J. W. F.; Chan, E. R.; Reiner, J. E.; M., S. V., Nanoscopic porous sensors. *Annual review of Analytical Chemistry* **2008,** 1, 737-766.
66. Gyurcsanyi, R. E., Chemically-modified nanopores for sensing. *Trac-Trends in Analytical Chemistry* **2008,** 27, (7), 627-639.
67. Rhee, M.; Burns, M. A., Nanopore sequencing technology: nanopore preparations. *Trends in Biotechnology* **2007,** 25, (4), 174-181.
68. Siwy, Z. S., Ion-current rectification in nanopores and nanotubes with broken symmetry. *Advanced Functional Materials* **2006,** 16, (6), 735-746.

69. Siwy, Z.; Dobrev, D.; Neumann, R.; Trautmann, C.; Voss, K., Electro-responsive asymmetric nanopores in polyimide with stable ion-current signal. *Applied Physics a-Materials Science & Processing* **2003,** 76, (5), 781-785.
70. Cervera, J.; Alcaraz, A.; Schiedt, B.; Neumann, R.; Ramirez, P., Asymmetric selectivity of synthetic conical nanopores probed by reversal potential measurements. *Journal of Physical Chemistry C* **2007,** 111, (33), 12265-12273.
71. Cervera, J.; Schiedt, B.; Neumann, R.; Mafe, S.; Ramirez, P., Ionic conduction, rectification, and selectivity in single conical nanopores. *Journal of Chemical Physics* **2006,** 124, (10), 104706.
72. Cervera, J.; Schiedt, B.; Ramirez, P., A Poisson/Nernst-Planck model for ionic transport through synthetic conical nanopores. *Europhysics Letters* **2005,** 71, (1), 35-41.
73. Siwy, Z.; Fulinski, A., A nanodevice for rectification and pumping ions. *American Journal of Physics* **2004,** 72, (5), 567-574.
74. Siwy, Z.; Kosinska, I. D.; Fulinski, A.; Martin, C. R., Asymmetric diffusion through synthetic nanopores. *Physical Review Letters* **2005,** 94, (4), 048102.
75. Doupnik, C. A.; Davidson, N.; Lester, H. A., The inward rectifier potassium channel family. *Current Opinion in Neurobiology* **1995,** 5, (3), 268-277.
76. Reimann, F.; Ashcroft, F. M., Inwardly rectifying potassium channels. *Current Opinion in Cell Biology* **1999,** 11, (4), 503-508.
77. Fischer, B. E.; Spohr, R., Production and use of nuclear tracks-imprinting structure on solids. *Reviews of Modern Physics* **1983,** 55, (4), 907-948.
78. Zeigler, J. F.; Biersack, J. P.; Ziegler, M. D., *SRIM: The Stopping and Range of Ions in Matter.*Lulu Press Co., Morrisville, NC, USA: 2008.
79. Trautmann, C.; Bouffard, S.; Spohr, R., Etching threshold for ion tracks in polyimide. *Nucl. Instrum. Methods Phys. Res. B* **1996**, 429-433.
80. Spohr, R., Real-time control of track etching and recent experiments relevant to micro and nano fabrication. *Radiation and Measurements* **2008,** 43, S560-S570.
81. DeSorbo, W., Ultraviolet effects and aging effects on etching characteristics of fission tracks in polycarbonate film. *Nuclear Tracks* **1979,** 3, 13-32.
82. Zhu, Z.; Maekawa, Y.; Liu, Q.; Yoshida, M., Influence of UV light illumination on latent track structure in PET. *Nucl. Instrum. Methods Phys. Res. B* **2005**, 61-67.
83. Dobrev, D.; Trautmann, C.; Neumann, R., Novel two-step etching process for ion tracks in polyimide. *GSI Scientific Report* **2006**, 321.
84. Apel, P. Y.; Blonskaya, I. V.; Oganessian, V. R.; Orelovitch, O. L.; Trautmann, C., Morphology of latent and etched heavy ion tracks in radiation resistant polymers polyimide and poly(ethylene naphthalate). *Nucl. Instr. & Method. B* **2001,** 185, 216-221.
85. Schiedt, B. Charactarization and application of ion track-etched nanopores. Ph.D. Thesis, University of Heidelberg, Heidelberg, 2007.
86. Ghosh, M. K.; Mittal, k. L., *Polyimides: fundamentals and applications*. Marcel Dekker, Inc: New York, 1996.
87. Apel, P. Y.; Blonskaya, I. V.; Dmitriev, S. N.; Mamonova, T. I.; Orelovitch, O. L.; Sartowska, B.; Yamauchi, Y., Surfactant-controlled etching of ion track nanopores and its practical applications in membrane technology. *Radiation and Measurements* **2008,** 43, S552-S559.
88. Apel, P. Y.; Blonskaya, I. V.; Dmitriev, S. N.; Orelovitch, O. L.; Presz, A.; Sartowska, B. A., Fabrication of nanopores in polymer foils with surfactant-controlled longitudinal profiles. *Nanotechnology* **2007,** 18, (30), 305302.

89. Siwy, Z.; Fulinski, A., Fabrication of a synthetic nanopore ion pump. *Physical Review Letters* **2002,** 89, (19), 198103.
90. Healy, K., Nanopore-based single-molecule DNA analysis. *Nanomedicine* **2007,** 2, (4), 459-481.
91. Heins, E. A.; Siwy, Z. S.; Baker, L. A.; Martin, C. R., Detecting single porphyrin molecules in a conically shaped synthetic nanopore. *Nano Letters* **2005,** 5, (9), 1824-1829.
92. Krasilnikov, O. V.; Rodrigues, C. G.; Bezrukov, S. M., Single polymer molecules in a protein nanopore in the limit of a strong polymer-pore attraction. *Physical Review Letters* **2006,** 97, (1), 018301.
93. Stefureac, R.; Long, Y. T.; Kraatz, H. B.; Howard, P.; Lee, J. S., Transport of alpha-helical peptides through alpha-hemolysin and aerolysin pores. *Biochemistry* **2006,** 45, (30), 9172-9179.
94. Kim, Y. R.; Min, J.; Lee, I. H.; Kim, S.; Kim, A. G.; Kim, K.; Namkoong, K.; Ko, C., Nanopore sensor for fast label-free detection of short double-stranded DNAs. *Biosensors & Bioelectronics* **2007,** 22, (12), 2926-2931.
95. Meller, A.; Nivon, L.; Brandin, E.; Golovchenko, J.; Branton, D., Rapid nanopore discrimination between single polynucleotide molecules. *Proceedings of the National Academy of Sciences of the United States of America* **2000,** 97, (3), 1079-1084.
96. Healy, K.; Schiedt, B.; Morrison, A. P., Solid-state nanopore technologies for nanopore-based DNA analysis. *Nanomedicine* **2007,** 2, (6), 875-897.
97. Iqbal, S. M.; Akin, D.; Bashir, R., Solid-state nanopore channels with DNA selectivity. *Nature Nanotechnology* **2007,** 2, (4), 243-248.
98. Martin, C. R.; Nishizawa, M.; Jirage, K.; Kang, M., Investigations of the transport properties of gold nanotubule membranes. *Journal of Physical Chemistry B* **2001,** 105, (10), 1925-1934.
99. Pasternak, C. A.; Alder, G. M.; Apel, P. Y.; Bashford, C. L.; Edmonds, D. T.; Korchev, Y. E.; Lev, A. A.; Lowe, G.; Milovanovich, M.; Pitt, C. W.; Rostovtseva, T. K.; Zhitariuk, N. I. In *Nuclear track-etched filters as model pores for biological membranes*, 1995; 1995; pp 675-683.
100. Marchand-Brynaert, J.; Deldime, M.; Dupont, I.; Dewez, J. L.; Schneider, Y. J., Surface functionalization of poly(ethylene terephthalate) film and membrane by controlled wet chemistry: chemical characterization of carboxylated surfaces. *Journal of Colloid and Interface Science* **1995,** 173, (1), 236-244.
101. Mara, A.; Siwy, Z.; Trautmann, C.; Wan, J.; Kamme, F., An asymmetric polymer nanopore for single molecule detection. *Nano Letters* **2004,** 4, (3), 497-501.
102. Schiedt, B.; Healy, K.; Morrison, A. P.; Neumann, R.; Siwy, Z., Transport of ions and biomolecules through single asymmetric nanopores in polymer films. *Nucl. Instrum. Methods Phys. Res. B* **2005,** 236, 109-116.
103. Cais, O.; Sedlacek, M.; Horak, M.; Dittert, I.; Vyklicky, L., Temperature dependence of NR1/NR2B NMDA receptor channels. *Neuroscience* **2008,** 151, (2), 428-438.
104. Kosinska, I. D., How the asymmetry of internal potential influences the shape of I-V characteristic of nanochannels. *Journal of Chemical Physics* **2006,** 124, (24), 244707.
105. Lahiri, J.; Isaacs, L.; Tien, J.; Whitesides, G. M., A strategy for the generation of surfaces presenting ligands for studies of binding based on an active ester as a common reactive intermediate: A surface plasmon resonance study. *Analytical Chemistry* **1999,** 71, (4), 777-790.

106. Williams, A.; Ibrahim, I. T., Carbodiimide chemistry: Recent advances. *Chemical Reviews* **1981,** 81, (6), 589-636.
107. Qhobosheane, M.; Santra, S.; Zhang, P.; Tan, W. H., Biochemically functionalized silica nanoparticles. *Analyst* **2001,** 126, (8), 1274-1278.
108. Wei, C.; Bard, A. J.; Feldberg, S. W., Current rectification at quartz nanopipet electrodes. *Analytical Chemistry* **1997,** 69, (22), 4627-4633.
109. Korchev, Y. E.; Bashford, C. L.; Alder, G. M.; Apel, P. Y.; Edmonds, D. T.; Lev, A. A.; Nandi, K.; Zima, A. V.; Pasternak, C. A., A novel explanation for fluctuations of ion current through narrow pores. *Faseb Journal* **1997,** 11, (7), 600-608.
110. Lev, A. A.; Korchev, Y. E.; Rostovtseva, T. K.; Bashford, C. L.; Edmonds, D. T.; Pasternak, C. A., Rapid switching of ion current in narrow pores - implications for biological ion channels. *Proceedings of the Royal Society of London Series B-Biological Sciences* **1993,** 252, (1335), 187-192.
111. Choi, Y.; Baker, L. A.; Hillebrenner, H.; Martin, C. R., Biosensing with conically shaped nanopores and nanotubes. *Physical Chemistry Chemical Physics* **2006,** 8, (43), 4976-4988.
112. Fologea, D.; Ledden, B.; McNabb, D. S.; Li, J. L., Electrical characterization of protein molecules by a solid-state nanopore. *Applied Physics Letters* **2007,** 91, (5), 053901.
113. Han, A. P.; Schurmann, G.; Mondin, G.; Bitterli, R. A.; Hegelbach, N. G.; de Rooij, N. F.; Staufer, U., Sensing protein molecules using nanofabricated poresn. *Applied Physics Letters* **2006,** 88, (9), 093901.
114. Martin, C. R.; Siwy, Z. S., Learning nature's way: Biosensing with synthetic nanopores. *Science* **2007,** 317, (5836), 331-332.
115. Chang, H.; Kosari, F.; Andreadakis, G.; Alam, M. A.; Vasmatzis, G.; Bashir, R., DNA-mediated fluctuations in ionic current through silicon oxide nanopore channels. *Nano Letters* **2004,** 4, (8), 1551-1556.
116. Chen, P.; Gu, J. J.; Brandin, E.; Kim, Y. R.; Wang, Q.; Branton, D., Probing single DNA molecule transport using fabricated nanopores. *Nano Letters* **2004,** 4, (11), 2293-2298.
117. Dekker, C., Solid-state nanopores. *Nature Nanotechnology* **2007,** 2, (4), 209-215.
118. Fologea, D.; Gershow, M.; Ledden, B.; McNabb, D. S.; Golovchenko, J. A.; Li, J. L., Detecting single stranded DNA with a solid state nanopore. *Nano Letters* **2005,** 5, (10), 1905-1909.
119. Rhee, M.; Burns, M. A., Nanopore sequencing technology: research trends and applications. *Trends in Biotechnology* **2006,** 24, (12), 580-586.
120. Schoch, R. B.; Han, J. Y.; Renaud, P., Transport phenomena in nanofluidics. *Reviews of Modern Physics* **2008,** 80, (3), 839-883.
121. Jirage, K. B.; Hulteen, J. C.; Martin, C. R., Nanotubule-based molecular-filtration membranes. *Science* **1997,** 278, (5338), 655-658.
122. Sexton, L. T.; Horne, L. P.; Sherrill, S. A.; Bishop, G. W.; Baker, L. A.; Martin, C. R., Resistive-pulse studies of proteins and protein/antibody complexes using a conical nanotube sensor. *Journal of the American Chemical Society* **2007,** 129, (43), 13144-13152.
123. Ali, M.; Schiedt, B.; Healy, K.; Neumann, R.; Ensinger, W., Modifying the surface charge of single track-etched conical nanopores in polyimide. *Nanotechnology* **2008,** 19, (8), 085713 (1-6).
124. Chaiyasut, C.; Tsuda, T., Isoelectric points estimation of proteins by electroosmotic flow: pH relationship using physically adsorbed proteins on silica gel. *Chromatography* **2001,** 22, 91–95.

125. Shang, L.; Wang, Y. Z.; Jiang, J. G.; Dong, S. J., pH-dependent protein conformational changes in albumin : gold nanoparticle bioconjugates: A spectroscopic study. *Langmuir* **2007,** 23, (5), 2714-2721.
126. Wharton, J. E.; Jin, P.; Sexton, L. T.; Horne, L. P.; Sherrill, S. A.; Mino, W. K.; Martin, C. R., A method for reproducibly preparing synthetic nanopores for resistive-pulse biosensors. *Small* **2007,** 3, (8), 1424-1430.
127. Ramirez, P.; Apel, P. Y.; Cervera, J.; Mafe, S., Pore structure and function of synthetic nanopores with fixed charges: tip shape and rectification properties. *Nanotechnology* **2008,** 19, (31), 315707.
128. Huang, W. X.; Skanth, G.; Baker, G. L.; Bruening, M. L., Surface-initiated thermal radical polymerization on gold. *Langmuir* **2001,** 17, (5), 1731-1736.
129. Lee, K. B.; Kim, D. J.; Lee, Z. W.; Woo, S. I.; Choi, I. S., Pattern generation of biological ligands on a biodegradable poly(glycolic acid) film. *Langmuir* **2004,** 20, (7), 2531-2535.
130. Hyun, J.; Chilkoti, A., Surface-initiated free radical polymerization of polystyrene micropatterns on a self-assembled monolayer on gold. *Macromolecules* **2001,** 34, (16), 5644-5652.
131. Kovacs, J.; Mayers, G. L.; Johnson, R. H.; Cover, R. E.; Ghatak, U. R., Racemization of amino acid derivatives. Rate of racemization and peptide bond formation of cysteine active esters. *Journal of Organic Chemistry* **1970,** 35, 1810-1815.
132. Ermakova, L. E.; Sidorova, M. P.; Bezrukova, M. E., Filtration and electrokinetic characteristics of track membranes. *Colloid Journal* **1998,** 60, (6), 705-712.
133. Drelich, J.; Payne, T.; Kim, J. H.; Miller, J. D., Selective froth flotation of PVC from PVC/PET mixtures for the plastics recycling industry. *Polymer Engineering and Science* **1998,** 38, (9), 1378-1386.
134. Deval, J.; Umali, T. A.; Lan, E. H.; Dunn, B.; Ho, C. M., Reconfigurable hydrophobic/hydrophilic surfaces in microelectromechanical systems (MEMS). *Journal of Micromechanics and Microengineering* **2004,** 14, (1), 91-95.
135. Perozo, E.; Cortes, D. M.; Sompornpisut, P.; Kloda, A.; Martinac, B., Open channel structure of MscL and the gating mechanism of mechanosensitive channels. *Nature* **2002,** 418, (6901), 942-948.
136. Griffiths, J., The realm of the nanopore. *Analytical Chemistry* **2008,** 80, (1), 23-27.
137. Castellana, E. T.; Cremer, P. S., Solid supported lipid bilayers: From biophysical studies to sensor design. *Surface Science Reports* **2006,** 61, (10), 429-444.
138. Knoll, W.; Koper, I.; Naumann, R.; Sinner, E. K., Tethered bimolecular lipid membranes - A novel model membrane platform. *Electrochimica Acta* **2008,** 53, 6680-6689.
139. Sinner, E. K.; Knoll, W., Functional tethered membranes. *Current Opinion in Chemical Biology* **2001,** 5, (6), 705-711.
140. Jeon, Y. J.; Kim, H.; Jon, S.; Selvapalam, N.; Oh, D. H.; Seo, I.; Park, C. S.; Jung, S. R.; Koh, D. S.; Kim, K., Artificial ion channel formed by cucurbit[n]uril derivatives with a carbonyl group fringed portal reminiscent of the selectivity filter of K+ channels. *Journal of the American Chemical Society* **2004,** 126, (49), 15944-15945.
141. Sisson, A. L.; Shah, M. R.; Bhosale, S.; Matile, S., Synthetic ion channels and pores (2004-2005). *Chemical Society Reviews* **2006,** 35, (12), 1269-1286.
142. Talukdar, P.; Bollot, G.; Mareda, J.; Sakai, N.; Matile, S., Synthetic ion channels with rigid-rod pi-stack architecture that open in response to charge-transfer complex formation. *Journal of the American Chemical Society* **2005,** 127, (18), 6528-6529.
143. Daiguji, H.; Yang, P. D.; Majumdar, A., Ion transport in nanofluidic channels. *Nano Letters* **2004,** 4, (1), 137-142.

144. Gershow, M.; Golovchenko, J. A., Recapturing and trapping single molecules with a solid-state nanopore. *Nature Nanotechnology* **2007,** 2, (12), 775-779.
145. Karnik, R.; Castelino, K.; Fan, R.; Yang, P.; Majumdar, A., Effects of biological reactions and modifications on conductance of nanofluidic channels. *Nano Letters* **2005,** 5, (9), 1638-1642.
146. Karnik, R.; Fan, R.; Yue, M.; Li, D. Y.; Yang, P. D.; Majumdar, A., Electrostatic control of ions and molecules in nanofluidic transistors. *Nano Letters* **2005,** 5, (5), 943-948.
147. Miedema, H.; Vrouenraets, M.; Wierenga, J.; Meijberg, W.; Robillard, G.; Eisenberg, B., A biological porin engineered into a molecular, nanofluidic diode. *Nano Letters* **2007,** 7, (9), 2886-2891.
148. White, H. S.; Bund, A., Ion current rectification at nanopores in glass membranes. *Langmuir* **2008,** 24, (5), 2212-2218.
149. Baker, L. A.; Bird, S. P., Nanopores - A makeover for membranes. *Nature Nanotechnology* **2008,** 3, (2), 73-74.
150. Hulteen, J. C.; Jirage, K. B.; Martin, C. R., Introducing chemical transport selectivity into gold nanotubule membranes. *Journal of the American Chemical Society* **1998,** 120, (26), 6603-6604.
151. Anzai, J.; Kobayashi, Y.; Nakamura, N.; Nishimura, M.; Hoshi, T., Layer-by-layer construction of multilayer thin films composed of avidin and biotin-labeled poly(amine)s. *Langmuir* **1999,** 15, (1), 221-226.
152. Cassier, T.; Lowack, K.; Decher, G., Layer-by-layer assembled protein/polymer hybrid films: nanoconstruction via specific recognition. *Supramolecular Science* **1998,** 5, (3-4), 309-315.
153. Lindegren, S.; Andersson, H.; Jacobsson, L.; Back, T.; Skarnemark, G.; Karlsson, B., Synthesis and biodistribution of At-211-labeled, biotinylated, and charge-modified poly-L-lysine: Evaluation for use as an effector molecule in pretargeted intraperitoneal tumor therapy. *Bioconjugate Chemistry* **2002,** 13, (3), 502-509.
154. Constantin, D.; Siwy, Z. S., Poisson-Nernst-Planck model of ion current rectification through a nanofluidic diode. *Physical Review E* **2007,** 76, (4), 041202.
155. Kosinska, I. D.; Goychuk, I.; Kostur, M.; Schmid, G.; Hänggi, P., Rectification in synthetic conical nanopores: A one-dimensional Poisson-Nernst-Planck model. *Physical Review E* **2008,** 77, (3), 031131.
156. Decher, G., Fuzzy nanoassemblies: Toward layered polymeric multicomposites. *Science* **1997,** 277, (5330), 1232-1237.
157. Bertrand, P.; Jonas, A.; Laschewsky, A.; Legras, R., Ultrathin polymer coatings by complexation of polyelectrolytes at interfaces: suitable materials, structure and properties. *Macromolecular Rapid Communications* **2000,** 21, (7), 319-348.
158. van der Heyden, F. H. J.; Bonthuis, D. J.; Stein, D.; Meyer, C.; Dekker, C., Power generation by pressure-driven transport of ions in nanofluidic channels. *Nano Letters* **2007,** 7, (4), 1022-1025.
159. Kocer, A.; Walko, M.; Meijberg, W.; Feringa, B. L., A light-actuated nanovalve derived from a channel protein. *Science* **2005,** 309, (5735), 755-758.
160. Kane, R. S., Polyvalency: Recent developments and new opportunities for chemical engineers. *Aiche Journal* **2006,** 52, (11), 3638-3644.
161. Kiessling, L. L.; Gestwicki, J. E.; Strong, L. E., Synthetic multivalent ligands as probes of signal transduction. *Angewandte Chemie-International Edition* **2006,** 45, (15), 2348-2368.

162. Crespo-Biel, O.; Ravoo, B. J.; Reinhoudt, D. N.; Huskens, J., Noncovalent nanoarchitectures on surfaces: from 2D to 3D nanostructures. *Journal of Materials Chemistry* **2006,** 16, (41), 3997-4021.
163. Mulder, A.; Huskens, J.; Reinhoudt, D. N., Multivalency in supramolecular chemistry and nanofabrication. *Organic & Biomolecular Chemistry* **2004,** 2, (23), 3409-3424.
164. Azzaroni, O.; Mir, M.; Alvarez, M.; Tiefenauer, L.; Knoll, W., Electrochemical rectification by redox-labeled bioconjugates: Molecular building blocks for the construction of biodiodes. *Langmuir* **2008,** 24, (6), 2878-2883.
165. Azzaroni, O.; Mir, M.; Knoll, W., Supramolecular architectures of streptavidin on biotinylated self-assembled monolayers. Tracking biomolecular reorganization after bioconjugation. *Journal of Physical Chemistry B* **2007,** 111, (48), 13499-13503.
166. Schmittel, M.; Kalsani, V., Functional, discrete, nanoscale supramolecular assemblies. In *Functional Molecular Nanostructures*, 2005; Vol. 245, pp 1-53.
167. Knoll, W.; Park, H.; Sinner, E. K.; Yao, D. F.; Yu, F., Supramolecular interfacial architectures for optical biosensing with surface plasmons. *Surface Science* **2004,** 570, 30-42.
168. Muller, W.; Ringsdorf, H.; Rump, E.; Wildburg, G.; Zhang, X.; Angermaier, L.; Knoll, W.; Liley, M.; Spinke, J., Attemps to mimic docking processes of the immune-system-recognition-induced formation of protein multilayers *Science* **1993,** 262, (5140), 1706-1708.
169. Ringsdorf, H.; Wustefeld, R. In *Molecular engineering of liquid-crystalline polymers - Architecture and functionalization* 1990; 1990; pp 95-108.
170. Steinbeck, M.; Ringsdorf, H., Model systems for molecular recognition at interfaces: Synthesis and characterisation of functionalised disulfides with hydrogen-bonding properties. *Chemical Communications* **1996**, (10), 1193-1194.
171. Hartgerink, J. D.; Beniash, E.; Stupp, S. I., Self-assembly and mineralization of peptide-amphiphile nanofibers. *Science* **2001,** 294, (5547), 1684-1688.
172. Liu, G. Y.; Amro, N. A., Positioning protein molecules on surfaces: A nanoengineering approach to supramolecular chemistry. *Proceedings of the National Academy of Sciences of the United States of America* **2002,** 99, (8), 5165-5170.
173. Martin, T.; Obst, U.; Rebek, J., Molecular assembly and encapsulation directed by hydrogen-bonding preferences and the filling of space. *Science* **1998,** 281, (5384), 1842-1845.
174. Huck, W. T. S., Responsive polymers for nanoscale actuation. *Materials Today* **2008,** 11, (7-8), 24-32.
175. Yokoyama, T.; Yokoyama, S.; Kamikado, T.; Okuno, Y.; Mashiko, S., Selective assembly on a surface of supramolecular aggregates with controlled size and shape. *Nature* **2001,** 413, (6856), 619-621.
176. Ali, M.; Yameen, B.; Neumann, R.; Ensinger, W.; Knoll, W.; Azzaroni, O., Biosensing and supramolecular bioconjugation in single conical polymer nanochannels. Facile incorporation of biorecognition elements into nanoconfined geometries. *Journal of the American Chemical Society* **2008,** 130, (48), 16351-16357.
177. Ku, J. R.; Lai, S. M.; Ileri, N.; Ramirez, P.; Mafe, S.; Stroeve, P., pH and ionic strength effects on amino acid transport through Au-nanotubule membranes charged with self-assembled monolayers. *Journal of Physical Chemistry C* **2007,** 111, (7), 2965-2973.
178. Lee, S.; Zhang, Y. H.; White, H. S.; Harrell, C. C.; Martin, C. R., Electrophoretic capture and detection of nanoparticles at the opening of a membrane pore using scanning electrochemical microscopy. *Analytical Chemistry* **2004,** 76, (20), 6108-6115.

179. Zhang, Y. H.; Zhang, B.; White, H. S., Electrochemistry of nanopore electrodes in low ionic strength solutions. *Journal of Physical Chemistry B* **2006,** 110, (4), 1768-1774.
180. Mafe, S.; Manzanares, J. A.; Pellicer, J., On the introduction of the pore wall charge in the space-charge model for microporous membranes. *Journal of Membrane Science* **1990,** 51, (1-2), 161-168.
181. Alcaraz, A.; Ramirez, P.; Garcia-Gimenez, E.; Lopez, M. L.; Andrio, A.; Aguilella, V. M., A pH-tunable nanofluidic diode: Electrochemical rectification in a reconstituted single ion channel. *Journal of Physical Chemistry B* **2006,** 110, (42), 21205-21209.
182. Chun, K. Y.; Mafe, S.; Ramirez, P.; Stroeve, P., Protein transport through gold-coated, charged nanopores: Effects of applied voltage. *Chemical Physics Letters* **2006,** 418, (4-6), 561-564.
183. English, A. E.; Mafe, S.; Manzanares, J. A.; Yu, X. H.; Grosberg, A. Y.; Tanaka, T., Equilibrium swelling properties of polyampholytic hydrogels. *Journal of Chemical Physics* **1996,** 104, (21), 8713-8720.
184. Mafe, S.; Manzanares, J. A.; English, A. E.; Tanaka, T., Multiple phases in ionic copolymer gels. *Physical Review Letters* **1997,** 79, (16), 3086-3089.
185. Jimbo, T.; Ramirez, P.; Tanioka, A.; Mafe, S.; Minoura, N., Passive transport of ionic drugs through membranes with pH-dependent fixed charges. *Journal of Colloid and Interface Science* **2000,** 225, (2), 447-454.
186. Ramirez, P.; Mafe, S.; Tanioka, A.; Saito, K., Modelling of membrane potential and ionic flux in weak amphoteric polymer membranes. *Polymer* **1997,** 38, (19), 4931-4934.
187. Karnik, R.; Duan, C. H.; Castelino, K.; Daiguji, H.; Majumdar, A., Rectification of ionic current in a nanofluidic diode. *Nano Letters* **2007,** 7, (3), 547-551.
188. Spohr, R., Status of ion track technology - Prospects of single tracks. *Radiation and Measurements* **2005,** 40, (2-6), 191-202.
189. Wolf, D. E.; Valiant, J.; Peck, R. L.; Folkers, K., Synthesis of Biocytin. *Journal of the American Chemical Society* **1952,** 74, 2002-2003.
190. Kuwata, S.; Watanabe, H., Removal of Copper from Copper Complex of Omega-Acylamino Acid with EDTA. *Bulletin of the Chemical Society of Japan* **1965,** 38, 676-677.
191. Mathews, C. K.; van Holde, K. E., *Biochemistry*. Benjamin/Cummings: Redwood City, 1990.
192. Hermanson, G. T., *Bioconjugate Techniques*. Academic Press: San Diego, 1996.
193. Ramirez, P.; Gomez, V.; Cervera, J.; Schiedt, B.; Mafe, S., Ion transport and selectivity in nanopores with spatially inhomogeneous fixed charge distributions. *Journal of Chemical Physics* **2007,** 126, (19), 194703.
194. Ramirez, P.; Mafe, S.; Aguilella, V. M.; Alcaraz, A., Synthetic nanopores with fixed charges: An electrodiffusion model for ionic transport. *Physical Review E* **2003,** 68, (1), 011910.
195. Ramirez, P.; Mafe, S.; Alcaraz, A.; Cervera, J., Modeling of pH-switchable ion transport and selectivity in nanopore membranes with fixed charges. *Journal of Physical Chemistry B* **2003,** 107, (47), 13178-13187.
196. Ramirez, P.; Aguilella-Arzo, M.; Alcaraz, A.; Cervera, J.; Aguilella, V. M., Theoretical description of the ion transport across nanopores with titratable fixed charges. *Cell Biochemistry and Biophysics* **2006,** 44, (2), 287-312.
197. Azzaroni, O.; Brown, A. A.; Huck, W. T. S., UCST wetting transitions of polyzwitterionic brushes driven by self-association. *Angewandte Chemie-International Edition* **2006,** 45, (11), 1770-1774.

198. Azzaroni, O.; Brown, A. A.; Huck, W. T. S., Tunable wettability by clicking into polyelectrolyte brushes. *Advanced Materials* **2007,** 19, (1), 151-154.
199. Minko, S., *Responsive Polymer Materials: Design and Applications*. Blackwell Publishing: Ames, IA: 2006.
200. Prucker, O.; Ruhe, J., Polymer layers through self-assembled monolayers of initiators. *Langmuir* **1998,** 14, (24), 6893-6898.
201. Banghart, M. R.; Volgraf, M.; Trauner, D., Engineering light-gated ion channels. *Biochemistry* **2006,** 45, (51), 15129-15141.
202. Bayley, H.; Braha, O.; Cheley, S.; Gu, L. Q., Engineered Nanopores. In *Nanobiotechnology: Concepts, Applications and Perspectives.* Niemeyer, C. M.; Mirkin, C. A., Eds. Wiley-VCH: Weinheim, Germany, 2004; pp 93-112.
203. Goychuk, I.; Hänggi, P., Ion channel gating: A first-passage time analysis of the Kramers type. *Proceedings of the National Academy of Sciences of the United States of America* **2002,** 99, (6), 3552-3556.
204. Urry, D. W., Molecular machines - How motion and other functions of living organisms can result from reversible chemical-changes. *Angewandte Chemie-International Edition in English* **1993,** 32, (6), 819-841.
205. Latorre, R.; Brauchi, S.; Orta, G.; Zaelzer, C.; Vargas, G., Thermo TRP channels as modular proteins with allosteric gating. *Cell Calcium* **2007,** 42, (4-5), 427-438.
206. Jung, Y.; Bayley, H.; Movileanu, L., Temperature-responsive protein pores. *Journal of the American Chemical Society* **2006,** 128, (47), 15332-15340.
207. Reber, N.; Kuchel, A.; Spohr, R.; Wolf, A.; Yoshida, M., Transport properties of thermo-responsive ion track membranes. *Journal of Membrane Science* **2001,** 193, (1), 49-58.
208. Ali, M.; Bayer, V.; Schiedt, B.; Neumann, R.; Ensinger, W., Fabrication and functionalization of single asymmetric nanochannels for electrostatic / hydrophobic association of protein molecules. *Nanotechnology* **2008,** 19, (48), 485711 (1-9).
209. Avidincula, A., Polymer Brushes by Anionic and Cationic Surface-Initiated Polymerization. In *Surface-Initiated Polymerization*, Jardon, R., Ed. Springer-Verlag: Heidelberg, 2006; pp 107-136.
210. Yameen, B.; Kaltbeitzel, A.; Langner, A.; Duran, H.; Müller, F.; Gösele, U.; Azzaroni, O.; Knoll, W., Facile large-scale fabrication of proton conducting channels. *Journal of the American Chemical Society* **2008,** 130, (39), 13140-13144.
211. Cui, Y.; Tao, C.; Zheng, S. P.; He, Q.; Ai, S. F.; Li, J. B., Synthesis of thermosensitive PNIPAM-co-MBAA nanotubes by atom transfer radical polymerization within a porous membrane. *Macromolecular Rapid Communications* **2005,** 26, (19), 1552-1556.
212. Jones, D. M.; Smith, J. R.; Huck, W. T. S.; Alexander, C., Variable adhesion of micropatterned thermoresponsive polymer brushes: AFM investigations of poly (N-isopropylacrylamide) brushes prepared by surface-initiated polymerizations. *Advanced Materials* **2002,** 14, (16), 1130-1134.
213. Weissman, J. M.; Sunkara, H. B.; Tse, A. S.; Asher, S. A., Thermally switchable periodicities and diffraction from mesoscopically ordered materials. *Science* **1996,** 274, (5289), 959-960.
214. Wu, Y. C.; Koch, W. F.; Hamer, W. J.; Kay, R. L., Review of electrolytic conductance standards. *Journal of Solution Chemistry* **1987,** 16, (12), 985-997.
215. Stein, D.; Kruithof, M.; Dekker, C., Surface-charge-governed ion transport in nanofluidic channels. *Physical Review Letters* **2004,** 93, (3).
216. Pinto, L. H.; Holsinger, L. J.; Lamb, R. A., Influenza-virus M2 protein has ion channel activity. *Cell* **1992,** 69, (3), 517-528.

217. Okada, A.; Miura, T.; Takeuchi, H., Protonation of histidine and histidine-tryptophan interaction in the activation of the M2 ion channel from influenza A virus. *Biochemistry* **2001,** 40, (20), 6053-6060.
218. Yameen, B.; Ali, M.; Neumann, R.; Ensinger, W.; Knoll, W.; Azzaroni, O., Single conical nanopores displaying pH-tunable rectifying characteristics. Manipulating ionic transport with zwitterionic polymer brushes. *Journal of the American Chemical Society* **2009,** 131, (6), 2070-2071.
219. Xu, Y. L.; Shi, L. Q.; Ma, R. J.; Zhang, W. Q.; An, Y. L.; Zhu, X. X., Synthesis and micellization of thermo- and pH-responsive block copolymer of poly (N-isopropylacrylamide)-block-poly(4-vinylpyridine). *Polymer* **2007,** 48, (6), 1711-1717.
220. Su, X.; Lodhi, I. J.; Saltiel, A. R.; Stahl, P. D., Insulin-stimulated interaction between insulin receptor substrate 1 and p85 alpha and activation of protein kinase B/Akt require Rab5. *Journal of Biological Chemistry* **2006,** 281, (38), 27982-27990.
221. Tam, T. K.; Ornatska, M.; Pita, M.; Minko, S.; Katz, E., Polymer brush-modified electrode with switchable and tunable redox activity for bioelectronic applications. *Journal of Physical Chemistry C* **2008,** 112, (22), 8438-8445.
222. Lindqvist, J.; Nystrom, D.; Ostmark, E.; Antoni, P.; Carlmark, A.; Johansson, M.; Hult, A.; Malmstrom, E., Intelligent dual-responsive cellulose surfaces via surface-initiated ATRP. *Biomacromolecules* **2008,** 9, (8), 2139-2145.
223. Roth, R.; Gillespie, D.; Nonner, W.; Eisenberg, R. E., Bubbles, gating, and anesthetics in ion channels. *Biophysical Journal* **2008,** 94, (11), 4282-4298.
224. Smeets, R. M. M.; Keyser, U. F.; Wu, M. Y.; Dekker, N. H.; Dekker, C., Nanobubbles in solid-state nanopores. *Physical Review Letters* **2006,** 97, (8).
225. Russo, J.; Melchionna, S.; De Luca, F.; Casieri, C., Water confined in nanopores: Spontaneous formation of microcavities. *Physical Review B* **2007,** 76, (19).

6. APPENDIX

6.1: List of Figures

Figure 2.15: FESEM images of (a) the small (surfactant-protected), (b) the large (UV-treated) side, (c) the side view of channels in a polymer membrane containing $1x10^8$ ion/cm^2 and etched by the method described above.

Figure 2.16: Scheme illustrating the geometrical parameters of conical (left) and cylindrical (right) nanochannels.

Figure 2.17: FESEM images of base opening of a single channel (left) and 10^7 channels cm^{-2} (right) of polyimide foils which were etched simultaneously in a conductivity cell.

Figure 2.18: *I-V* measurements for single a conical PET channel (a) triangle sweeps of voltage (black) and current (red), (b) corresponding *I-V* curve.

Figure 2.19: pH dependent *I-V* curves of a track-etched single conical nanochannel in polyimide.

Figure 2.20: Scheme describing the generation of carboxyl species on the channel surface.

Figure 2.21: Reaction scheme for the attachment of amino-terminators to surface carboxyl groups, and the subsequent attachment of carboxyl-terminated species.

Figure 2.22: Reaction scheme for the conversion of carboxyl groups into terminated amino groups (III) and propyl groups (IV), respectively.

Figure 2.23: Functionalization of the channel surface with L-lysine (II) and L-histidine (III), respectively.

Figure 3.1.1: Schematic representation of chemical modification of the channel surface (a) carboxyl groups into (b) amine- reactive NHS-esters, (c) terminated amino groups, and (d) re-termination of amino groups into carboxyl moieties.

Figure 3.1.2: pH dependence of the *I-V* curve with 0.1 M KCl of a polyimide channel with $d \sim$ 64 nm and $D \sim 1.57$ μm, where *d* and *D* are the diameters of the small and large openings of the conical channel respectively. (a) Before and (b) after the modification with ethylenediamine and (c) after the modification with succinic anhydride.

Figure 3.1.3: Degree of rectification calculated from the data shown in Figure 3.1.2. After modification with EDA, the channel shows a much lower degree of rectification for pH 7 and reverse rectification (values below 1) at pH 2. Treatment with succinic anhydride essentially restored the initial behaviour.

Figure 3.1.4: Sections of *I-V* curves recorded under a tenfold concentration gradient with 0.1 M KCl on the large and 0.01 M KCl on the small side of the channel, before and after modification with EDA, for pH 7 and pH 2. The dimensions of the channel were $d \sim$

30 nm and D ~ 1.4 µm. The reversal potential (potential for zero current) is reduced by the modification from 45 mV to 18 mV for pH 7 and changed its sign after the modification for pH 2 (-14 mV), indicating a significant change in the surface charge, which is now slightly positive.

Figure 3.2.1: Current fluctuations in a single nanochannel in PET in dependence on the applied voltage, measured with 0.1 M KCl (a.u. refers to arbitrary units). (a) One-side etching, tip diameter ~ 2 nm, (b) surfactant-controlled etching, tip diameter ~ 8 nm.

Figure 3.2.2: Representation of (a) applied voltage and ion current record, (b) current-voltage characteristic of a single PET channel with d ~ 8 nm and D ~ 320 nm in 0.1 M KCl solution.

Figure 3.2.3: Schematic representation of the conversion of channel surface carboxyl groups (a) into amine-reactive PFP-esters (b), which were further converted into, terminated amino (c) and terminated alkyl groups (d), respectively.

Figure 3.2.4: *I-V* characteristics of PET single asymmetric channels in 0.1 M KCl at pH 6.5, before (●) and after modification**,** (a) with ethylenediamine (○) having d ~ 18 nm, and (b) with propylamine (○) having d ~ 16 nm, respectively.

Figure 3.2.5: Current-voltage characteristics of a carboxylated PET channel in 0.1 M KCl having d ~ 10 nm and D ~ 288 nm, prior to (●) and after (○) the addition of 100 nM BSA, (a) at pH 6.5, (b) at pH 3.5.

Figure 3.2.6: Current-voltage characteristics of a aminated PET channel in 0.1 M KCl having d ~ 25 nm and D ~ 315 nm, prior to (●) and after (○) the addition of 100 nM BSA, (a) at pH 6.5, (b) at pH 3.5.

Figure 3.2.7: Current-voltage characteristics of a propylated PET nanochannel in 0.1 M KCl having d ~ 16 nm and D ~ 300 nm, prior to (●) and after (○) the addition of 100 nM BSA at pH 6.5.

Figure 3.3.1: Chemical structure of the bifunctional polyvalent ligand used in this work to biotinylate the conical channel wall. x = 0.21.

Figure 3.3.2: Simplified cartoon describing the incorporation of the biorecognition elements in the single conical nanochannel. The carboxylate-terminated nanochannel (a) is used as a platform for the electrostatic immobilization of the bifunctional macromolecular

ligand, b-PAH (b). Then, the biorecognition event proceeds in the presence of the receptor (streptavidin) (c).

Figure 3.3.3: *I-V* characteristics of a single conical nanochannel in 0.1 M KCl prior to (●) and after (●) the electrostatic assembly of b-PAH.

Figure 3.3.4: *I-V* characteristics of a b-PAH-modified single conical channel in 0.1 M KCl in the presence of different concentrations of streptavidin (SAv): (●) no SAv; (●) 1 pM; (●) 10 pM; (●) 100 pM.

Figure 3.3.5: *I-V* characteristics of a single conical nanochannel in 0.1 M KCl prior to (●) and after (●) the electrostatic immobilization of b-PAH followed by the addition (separately) of 100 nM lysozyme (●) and 100 nM bovine serum albumin (●).

Figure 3.3.6: Simplified cartoon depicting the formation of a multilayered supramolecular bioconjugate inside the single conical nanochannel.

Figure 3.3.7: *I-V* curves of a surface-modified single conical nanochannel in 0.1 M KCl corresponding to: (●) carboxylate-terminated channel; (●) b-PAH-modified channel; (●) (SAv)(b-PAH)-modified channel; (●) (SAv)(b-PAH)$_2$-modified channel; (●) (SAv)$_2$(b-PAH)$_2$-modified channel.

Figure 3.4.1: Scheme describing the functionalization of the channel surface carboxyl groups with (c) L-lysine chains, and (d) L-histidine chains, respectively.

Figure 3.4.2: Current-voltage curves of the amphoteric (lysine) nanochannel at pH = 2 (left), pH = 5 (center), and pH = 11 (right).

Figure 3.4.3: (A): Effect of pH on the *I-V* curves of the amphoteric (lysine) nanochannel. (B): Effect of pH on the *I-V* curves of the amphoteric (histidine) nanochannel. The numbers in the curves correspond to the pH values.

Figure 3.4.4: (A): Rectification ratio versus pH at different applied voltages (lysine). (B): Rectification ratio versus pH at different applied voltages (histidine). The numbers in the curves correspond to the on/off voltages for the rectification ratio.

Figure 3.4.5: (A): Experimental *I-V* curves of the amphoteric nanochannel (lysine) at pH = 2, 5, and 11 (up) and theoretical results from a PNP model (down). (B): Experimental *I-V* curves of the amphoteric nanochannel (histidine) at pH = 2, 4.2, and 10 (up) and theoretical results from a PNP model (down).

Figure 3.5.1: Schematic cartoon describing the polymer brush-modified conical nanochannel. The chemical structure of the polymer brush and the equilibrium associated to the pH-dependent behaviour of the zwitterion in monomer units are also indicated.

Figure 3.5.2: *I-V* curves corresponding to a single conical nanochannel modified with poly(methacryloyl-L-lysine) brushes measured at different pH values (using 1 M KCl as electrolyte). The different pHs are displayed using colored symbols as indicated in the Figure. The inset describes the changes in the rectified currents upon variation in the environmental pH. The red and blue dots refer to the rectified currents measured at -2 and +2 V, respectively.

Figure 3.5.3: Changes in the rectified currents upon variation in the environmental pH. The red and blue dots refer to the rectified currents measured at +2 and -2 V, respectively. In the Figure *pI* is also indicated.

Figure 3.6.1: Scheme illustrating the surface modification of the nanochannel by the polymerization of polyNIPAM brushes. Firstly, the aminated channel wall is modified with the initiator groups (a). Then, the aqueous atom transfer radical polymerization (ATRP) is carried out (b). The Figure also desplaces the chemical structures of the ATRP initiator and the polyNIPAM brushes.

Figure 3.6.2: Current-voltage characteristics of a polyimide single conical nanochannel in 1 M KCl having $d \sim 48$ nm and $D \sim 1.45$ μm, prior to (●) and after (○) the modification with ethylenediamine. The terms *d* and *D* refer to the diameter of the small and large opening of the channel, respectively.

Figure 3.6.3: *I-V* curves in 1 M KCl for a polyimide single conical nanochannel after modification with polyNIPAM brushes at different temperatures.

Figure 3.6.4: Cartoon describing the thermally-driven nanoactuation of the polyNIPAM brushes in the nanochannel.

Figure 3.6.5: Temperature cycling between 23 and 40 ^{o}C corresponding to a nanochannel modified with PNIPAM brushes. $D \sim 1.26$ μm, $d_{23\,^{o}C} \sim 1.2$ nm, $d_{40\,^{o}C} \sim 4.8$ nm.

Figure 3.7.1. (a) Schematic description of the brush-modified cylindrical nanochannel. In the scheme is also indicated the chemical structure of poly(4-vinyl pyridine) brushes. (b) pH-dependent pyridine-pyridinium equilibrium taking place in the brush environment. (c) Simplified illustration indicating the conformational changes occurring in the brush layer upon variations in the environmental pH.

6.2: List of Tables

6.3 List of Publications

The following articles in peer-reviewed journals have been derived from the material presented in this thesis;

1. Mubarak Ali, Birgitta Schiedt, Ken Healy, Reinhard Neumann and Wolfgang Ensinger, "Modifying the surface charge of single track-etched conical nanopores in polyimide" *Nanotechnology* **2008,** 19, (8), 085713.

2. Mubarak Ali, Basit Yameen, Reinhard Neumann, Wolfgang Ensinger, Wolfgang Knoll and Omar Azzaroni, "Biosensing and supramolecular bioconjugation in single conical polymer nanochannels. Facile incorporation of biorecognition elements into nanoconfined geometries" *Journal of the American Chemical Society* **2008,** 130, (48), 16351-16357.

3. Mubarak Ali, Veronika Bayer, Birgitta Schiedt, Reinhard Neumann and Wolfgang Ensinger, "Fabrication and functionalization of single asymmetric nanochannels for electrostatic / hydrophobic association of protein molecules" *Nanotechnology* **2008,** 19, (48), 485711.

4. Mubarak Ali, Patricio Ramirez, Salvador Mafé, Reinhard Neumann and Wolfgang Ensinger, "A pH-tunable nanofluidic diode with a broad range of rectifying properties" *ACS Nano* **2009,** 3, (3), 603-608.

5. Basit Yameen, Mubarak Ali, Reinhard Neumann, Wolfgang Ensinger, Wolfgang Knoll and Omar Azzaroni, "Single conical nanopores displaying pH-tunable rectifying characteristics. Manipulating ionic transport with zwitterionic polymer brushes" *Journal of the American Chemical Society* **2009,** 131, (6), 2070-2071.

6. Basit Yameen, Mubarak Ali, Reinhard Neumann, Wolfgang Ensinger, Wolfgang Knoll and Omar Azzaroni, "Ionic transport through single solid-state nanopores controlled with thermally nanoactuated macromolecular gate" *Small* **2009,** 5, (11), 1287-1291.

7. Basit Yameen, Mubarak Ali, Reinhard Neumann, Wolfgang Ensinger, Wolfgang Knoll and Omar Azzaroni, "Synthetic proton-gated ion channels via single solid-state nanochannels modified with responsive polymer brushes"
Nano Letters **2009,** 9, (7), 2788-2793.

8. Mubarak Ali, Salvador Mafé, Patricio Ramirez, Reinhard Neumann and Wolfgang Ensinger, "Logic gates using nanofluidic diodes based on conical nanopores functionalized with polyprotic acid chains" *Langmuir* **2009**, 25, (20), 11993-11997.

9. Mubarak Ali, Birgitta Schiedt, Reinhard Neumann and Wolfgang Ensinger, "Biosensing with functionalized single asymmetric polymer nanochannels"
Macromolecular Bioscience **2009, DOI:** 10.1002/mabi.200900198.

10. Basit Yameen, Mubarak Ali, Marta Álvarez, Reinhard Neumann, Wolfgang Ensinger, Wolfgang Knoll and Omar Azzaroni, "A facile rout for the preparation of azide-terminated polymers. “Clicking” macromolecular building blocks on planar surfaces and nanochannels" *Polymer Chemistry* **2009,** accepted.

Curriculum Vitae

Name:	Mubarak Ali
Date of birth:	10th September 1975
Palce of birth:	Narowal, Pakistan.
Nationality:	Pakistani.
Marital status:	Married.
Present address:	In den Wingerten 39, 64291 Darmstadt, Germany.
Permanent address:	Post office Dhabli Wala, Teh. & Distt. Narowal, Pakistan.

Academic Career

1994 – 1998	**B.S.Ed.** in Chemistry, Botany, Zoology and Education. Institution: Punjab University Lahore, Pakistan.
1998 – 2000	**M.Sc.** in Chemistry. Institution: Govt. College Lahore, Pakistan.
2001 – 2003	**M.Phil.** Specialization in Organic Chemistry. Institution: Quaid-i-Azam University Islamabad, Pakistan.
Since February 2006	**Doctoral thesis** under the supervision of Prof. Dr. Wolfgang Ensinger at Darmstadt University of Technology, Darmstadt, Germany.

Industrial Experience

Worked as a "Senior Analyst" in quality control department at Wilson's Pharmaceutical, Islamabad, Pakistan, from 02nd May 2003 to 06th February 2006.

Name, Adresse Datum: 20-07-2009

Mubarak Ali,
In den Wingerten 39,
64291 Darmstadt

Erklärung

Ich erkläre hiermit, noch keinen Promotionsversuch unternommen zu haben

Unterschrift

Name, Adresse Datum: 20-07-2009

Mubarak Ali,
In den Wingerten 39,
64291 Darmstadt

Eidesstattliche Erklärung

Ich erkläre hiermit an Eides Statt, daß ich meine Dissertation selbständig und mit den angegebenen Hilfsmitteln angefertigt habe.

Unterschrift